



AN ABSTRACT OF THE THESIS OF

Tian Qin for the degree of Master of Science in Chemical Engineering presented on November 25, 2008.

Title: Photoluminescence Properties Investigation of Germanium Inserted Biosilica Generated by Bioreactor Culture of Marine Diatom *Nitzschia frustulum*

Abstract approved:

---

Gregory L. Rorrer

The purpose of this research was to investigate the optoelectronic properties of the Ge doped biosilica, mainly focused on the photoluminescence (PL) properties of diatom frustules of *N. frustulum* that contain metabolically inserted germanium oxide produced by a two-stage photobioreactor cultivation process. In order to explain the observed PL intensity and peak change due to germanium incorporation, the effect of Ge insertion on growth of *N. frustulum* was studied first. It was found that Ge inhibited diatom growth and silicon uptake rate when the Ge to Si molar ratio was increased to 0.14 although this inhibition was not observed when the ratio was less than 0.07. Ge uptake rate was also decreased from  $0.458 \pm 0.018$  mL/ $10^7$ cells-hr to  $0.183 \pm 0.017$  mL/ $10^7$ cells-hr as initial soluble Ge concentration in the nutrients in stage II increased from 12  $\mu$ M to 85  $\mu$ M. This Ge uptake inhibition at high initial Ge concentration suggested that the amount of Ge incorporated in frustules will increase to a maximum value, which

was found in our experiment as  $1.20 \pm 0.22$  wt%Ge in biosilica at Ge concentration level of 30.4  $\mu$ M.

The effect of germanium insertion on PL emission of frustules of diatom *N. frustulum* was studied. The PL peak intensity of Ge inserted frustules was much lower compared to frustules without Ge (controls). As the level of Ge incorporated into the frustules increased, the PL peak intensity decreased. The peak wavelength of frustules was shifted from 524 nm to 457 nm when Ge was inserted. However, the wavelength shift was not very sensitive to the Ge concentration incorporated into the silica frustules.

Finally, TEM images of the submicron morphology of diatom frustule with and without Ge incorporation were studied. It was found that the pore structure of diatom frustule was altered to a slit-like structure due to Ge incorporation. The possible origin of the observed PL emission due to Ge insertion was proposed. It was suggested that the PL peak intensity decrease and peak wavelength shift were caused by the pore structure alternation.

©Copyright by Tian Qin  
November 25, 2008  
All Rights Reserved

Photoluminescence Properties Investigation of Germanium Inserted Biosilica  
Generated by Bioreactor Culture of Marine Diatom *Nitzschia frustulum*

by  
Tian Qin

A THESIS

Submitted to

Oregon State University

In partial fulfillment of  
the requirements for the  
degree of

Master of Science

Presented November 25, 2008

Commencement June 2009

Master of Science thesis of Tian Qin presented on November 25, 2008.

APPROVED:

---

Major Professor, representing Chemical Engineering

---

Head of the School of Chemical, Biological and Environmental Engineering

---

Dean of the Graduate School

I understand that my thesis will become part of the permanent collection of Oregon State University libraries. My signature below authorizes release of my thesis to any reader upon request.

---

Tian Qin, Author

## ACKNOWLEDGEMENTS

I would like to thank my advisor Dr. Gregory L. Rorrer, who provided me tremendous support and patience in helping me complete this project. His generous advice helped guide me to the success both in my academic field and my life.

I would like to thank Dr. Chih-hung Chang, the Co-PI of this project. He always generously shared his brilliant ideas with me and offered many helpful suggestions to me. I would like to thank Dr. Thomas K. Plant in the school of Electrical Engineering and Computer Science, who helped me a lot in setting up the photoluminescence measurement system.

I would like to thank all my lab mates, Debra Gale, Clayton Jeffryes, and Aaron Goodwin for their help and encouragement whenever I met a problem. I also want to thank them for creating such a friendly laboratory ambient. It has been a great experience working with these nice and smart people.

Finally, I would like to thank National Science Foundation for supporting this project.

## TABLE OF CONTENTS

	<u>Page</u>
Introduction .....	2
Photoluminescence of Ge-doped SiO <sub>2</sub> and its mechanism .....	2
Photoluminescence of other Ge-related materials .....	4
Methods of Ge-related materials fabrication .....	5
Germanium doped biosilica .....	6
Objectives of our work .....	7
Materials and Methods .....	8
Bioreactor Cultivation .....	8
Culture Maintenance .....	8
Nitrate LDM Seawater Medium Preparation .....	8
Bioreactor Operation .....	10
Bioreactor Inoculation .....	13
Sampling .....	14
Experimental Design for Bioreactor Experiments .....	14
Bioreactor Shutdown .....	16
Analytical Techniques .....	16
Soluble silicon concentration assay .....	16
Soluble germanium concentration assay .....	17
Nitrate Assay .....	19
Cell Counting via Hemocytometer .....	20
Cell mass density determination .....	20
Frustules isolation via H <sub>2</sub> O <sub>2</sub> treatment.....	21
Frustules isolation for imaging .....	22
Germanium and silicon concentration in solid biomass .....	23
Germanium and silicon concentration in frustules .....	24
Thermal Annealing .....	25
TEM sample preparation .....	25

TABLE OF CONTENTS (Continued)

	<u>Page</u>
Photoluminescence (PL) measurement .....	25
Results .....	27
Bioreactor Cultivation .....	27
Effect of initial germanium concentration in stage II on growth of <i>N. frustulum</i> .....	27
Effect of initial germanium concentration in stage II on incorporation of germanium into biomass of <i>N. frustulum</i> .....	38
Effect of nitrogen limitation in stage II on growth of <i>N. frustulum</i> .....	41
Photoluminescence of diatoms .....	47
Effect of germanium insertion in silica frustules on photoluminescence (PL) emission .....	47
Effect of germanium concentration incorporated in silica frustules on photoluminescence (PL) emission .....	51
Effect of nitrate limitation on photoluminescence (PL) of frustules .....	53
TEM analysis of submicron morphology .....	55
FT-IR Analysis .....	58
Discussion .....	60
Effect of germanium insertion on growth of <i>N. frustulum</i> .....	60
Effect of germanium insertion on PL emission of <i>N. frustulum</i> .....	63
Conclusions and Recommendations .....	66
Conclusions .....	66
Recommendations .....	66
References .....	67
Appendices .....	74

## LIST OF FIGURES

<u>Figure</u>	<u>Page</u>
1a Schematic of bioreactor setup .....	12
1b Picture of bioreactor setup .....	13
2 Schematic of PL system setup .....	26
3a The cell number density and Si concentration in liquid phase versus time $C_{Si,0} = 0.6$ mM (Ge / Si = 0 mol Ge / mol Si) .....	28
3b The cell number density and Si concentration in liquid phase versus time $C_{Si,0} = 0.6$ mM (Ge / Si = 0.02 mol Ge / mol Si) .....	28
3c The cell number density and Si concentration in liquid phase versus time $C_{Si,0} = 0.6$ mM (Ge / Si = 0.14 mol Ge / mol Si) .....	29
4a The Ge and Si concentration in liquid phase versus time $C_{Si,0} = 0.6$ mM (Ge / Si = 0.02 molGe / mol Si) .....	30
4b The Ge and Si concentration in liquid phase versus time $C_{Si,0} = 0.6$ mM (Ge / Si = 0.04 molGe / mol Si) .....	30
4c The Ge and Si concentration in liquid phase versus time $C_{Si,0} = 0.6$ mM (Ge / Si = 0.14 molGe / mol Si) .....	31
5a Effect of initial Ge concentration on growth parameter specific growth rate $\mu'$ in stage I and II.....	32
5b Effect of initial Ge concentration on growth parameter cell number yield $Y_{Xn/Si}$ in stage I and II .....	33
5c Effect of initial Ge concentration on growth parameter cell mass yield $Y_{X/Si}$ in stage I and II .....	33
5d Effect of initial Ge concentration on growth parameter uptake rate of Si $k'_{Si}$ in stage II .....	34
5e Effect of initial Ge concentration on growth parameter uptake rate of Ge $k'_{Ge}$ in stage II .....	34
6a Effect of initial Ge concentration on Si concentration in biomass $Y_{Si}$ in stage II .....	40
6b Effect of initial Ge concentration on Ge concentration in biomass $Y_{Ge}$ in stage II .....	40
6c Effect of initial Ge concentration on Ge concentration in silica frustules wt % Ge in stage II .....	41

## LIST OF FIGURES (Continued)

<u>Figure</u>	<u>Page</u>
7a	Effect of initial nitrate concentration on Si uptake $C_{N,O} = 4.00$ mmol/L .....42
7b	Effect of initial nitrate concentration on Si uptake $C_{N,O} = 8.00$ mmol/L .....43
7c	Nitrate concentration in liquid phase versus time during stage I and stage II .....43
8a	Effect of nitrate limitation on growth parameters specific growth rate $\mu'$ in stage I .....45
8b	Effect of nitrate limitation on growth parameters specific growth rate $\mu'$ in stage II .....45
8c	Effect of nitrate limitation on growth parameters cell number yield $Y_{Xn/Si}$ in stage II .....46
8d	Effect of nitrate limitation on growth parameters uptake rate of Si $k'_{Si}$ in the first 5 hours in stage II .....46
9a	Comparison of PL spectrum of frustules that contains no Ge (40) with that of 0.14 wt% Ge contained frustules (41) .....48
9b	Comparison of PL spectrum of frustules that contains no Ge (44) with that of 0.36 wt% Ge contained frustules (45) .....48
9c	Comparison of PL spectrum of Ge inserted frustules (0.14 wt%) before and after annealing (800 °C in air) .....49
10a	PL peak intensity comparison of frustules containing no Ge (40) with that of frustules containing 0.14 wt% Ge (41) .....49
10b	PL peak intensity comparison of frustules containing no Ge (44) with that of frustules containing 0.36 wt% Ge (45) .....50
10c	PL peak wavelength comparison along cultivation time in stage II 0 wt% Ge (40) and 0.14 wt% Ge (41) .....50
10d	PL peak wavelength comparison along cultivation time in stage II 0 wt% Ge (44) and 0.36 wt% Ge (45) .....51
11a	Comparison of PL spectrum of 0 wt% Ge inserted frustules with 1.20 wt% Ge inserted frustules in stage II .....52

## LIST OF FIGURES (Continued)

<u>Figure</u>	<u>Page</u>
11b	Effect of Ge concentration in biosilica in stage II on PL peak intensity of the frustules in stage II .....52
11c	Effect of Ge concentration in biosilica in stage II on PL peak wavelength of the frustules in stage II .....53
12a	PL peak intensity of frustules along cultivation time in stage II with nitrate limitation in stage II .....54
12b	PL peak wavelength of frustules along cultivation time in stage II with nitrate limitation in stage II .....54
13a	TEM images of intact silica frustules at micron scale with 0 $\mu\text{mol Ge/L}$ (control) being added in stage II .....55
13b	TEM images of intact silica frustules at submicron scale with 0 $\mu\text{mol Ge/L}$ (control) being added in stage II .....56
13c	TEM images of intact silica frustules at nano scale with 0 $\mu\text{mol Ge/L}$ (control) being added in stage II .....56
13d	TEM images of intact silica frustules at micron scale with 50.4 $\mu\text{mol Ge/L}$ being added in stage II .....57
13e	TEM images of intact silica frustules at submicron scale with 50.4 $\mu\text{mol Ge/L}$ being added in stage II .....57
13f	TEM images of intact silica frustules at nano scale with 50.4 $\mu\text{mol Ge/L}$ being added in stage II .....58
14	FT-IR spectra of <i>N. frustulum</i> frustules before and after annealing .....59
15a	A representative spectrum of STEM line scans of frustule with Ge incorporation (sample Ni-BC-45) .....61
15b	The blowup of spectrum of STEM line scans from figure 15a .....62

## LIST OF TABLES

<u>Table</u>		<u>Page</u>
1	Summary of process conditions for two-stage photobioreactor cultivation of <i>Nitzschia frustulum</i> .....	11
2	Comparison of growth parameters of <i>Nitzschia frustulum</i> with Ge addition .....	35
3	Spectroscopy analysis of Ge content in silica frustules isolated by hydrogen peroxide treatment of <i>Nitzschia frustulum</i> cell mass containing metabolically inserted germanium .....	39
4	Comparison of growth parameters of <i>Nitzschia frustulum</i> with nitrogen limitation .....	44

## LIST OF APPENDICES

	<u>Page</u>
Appendices .....	74
Appendix A: Calculations .....	75
Specific growth rate calculation .....	75
Germanium and silicon uptake rate calculation .....	77
Cell number and cell mass yield coefficient calculation .....	80
Materials balance in stage I and stage II .....	81
Appendix B: Calibrations .....	83
Soluble Ge concentration assay calibration at 525 nm .....	83
Soluble Si concentration assay calibration at 410 nm .....	87
Soluble Nitrate concentration assay calibration at 530 nm .....	91
Appendix C: PL Spectra .....	92

## LIST OF APPENDICES FIGURES

<u>Figure</u>	<u>Page</u>
A.1	The natural log of cell number density versus time for experiment Ni-BC-32, and the specific growth rate $0.0213 \text{ h}^{-1}$ .....76
A.2	The natural log of Si concentration and Ge concentration versus time for experiment Ni-BC-32, and the maximum specific uptake rate constants $0.242 \text{ mL}/10^7 \text{ cells-hr}$ for Si uptake and $0.296 \text{ mL}/10^7 \text{ cells-hr}$ for Ge uptake .....79
B.1	Soluble Ge concentration assay calibration curve at 525 nm (3/2/2006) .....83
B.2	Soluble Ge concentration assay calibration curve at 525 nm (5/4/2006) .....84
B.3	Soluble Ge concentration assay calibration curve at 525 nm (8/10/2006) .....85
B.4	Soluble Ge concentration assay calibration curve at 525 nm (11/22/2006) .....86
B.5	Soluble Si concentration assay calibration curve at 410 nm (3/2/2006) .....87
B.6	Soluble Si concentration assay calibration curve at 410 nm (3/20/2006) .....88
B.7	Soluble Si concentration assay calibration curve at 410 nm (5/1/2006) .....89
B.8	Soluble Si concentration assay calibration curve at 410 nm (6/9/2006) .....90
B.9	Soluble Nitrate concentration assay calibration curve at 530 nm .....91
C.1	Photoluminescence spectra comparison of frustules containing no Ge (40) with that of frustules containing 0.14 wt% Ge (41) along cultivation time .....92
C.2	Photoluminescence spectra comparison of frustules containing no Ge (40) with that of frustules containing 0.14 wt% Ge (41) along cultivation time .....92
C.3	Photoluminescence spectra comparison of frustules containing no Ge (44) with that of frustules containing 0.36 wt% Ge (45) along cultivation time .....93

C.4	Photoluminescence spectra comparison of frustules containing no Ge (44) with that of frustules containing 0.36 wt% Ge (45) along cultivation time .....	93
C.5	Photoluminescence spectra comparison of different Ge-incorporated frustules collected at the end of stage II (120 hours of cultivation) .....	94

## LIST OF APPENDICES TABLES

<u>Table</u>	<u>Page</u>
B.1 Soluble Ge concentration assay calibration data at 525 nm (3/2/2006) .....	79
B.2 Soluble Ge concentration assay calibration data at 525 nm (5/4/2006) .....	80
B.3 Soluble Ge concentration assay calibration data at 525 nm (8/10/2006) .....	81
B.4 Soluble Ge concentration assay calibration data at 525 nm (11/22/2006) .....	82
B.5 Soluble Si concentration assay calibration data at 410 nm (3/2/2006) .....	83
B.6 Soluble Si concentration assay calibration data at 410 nm (3/20/2006) .....	84
B.7 Soluble Si concentration assay calibration data at 410 nm (5/1/2006) .....	85
B.8 Soluble Si concentration assay calibration data at 410 nm (6/9/2006) .....	86
B.9 Soluble Nitrate concentration assay calibration data at 530 nm .....	87

Photoluminescence Properties Investigation of Germanium Inserted Biosilica  
Generated by Bioreactor Culture of Marine Diatom *Nitzschia frustulum*

## **Introduction**

### **Photoluminescence of Ge-doped SiO<sub>2</sub> and its mechanism**

Germanium (Ge) has gained a lot of interest in the past 15 years for making optoelectronic materials. Since Ge has smaller electron and hole effective masses and a larger dielectric constant than Silicon (Si), the effective Bohr radius of the excitons in Ge is larger than that in Si. This implies that the Ge crystals would show a larger blue shift than Si crystals due to the quantum confinement effect (Takagahara and Takeda, 1992).

Quantum confinement describes the increase in energy which occurs when the motion of a particle is restricted in one or more dimensions by a potential well. As the confining dimension decreases, the energy of particles increases. A crystal nanoparticle is treated as a well that is confined in all three dimensions. Therefore, the energy bandgap of the nanocrystal is much higher than the bulk crystal (Brus, 1983). Maeda et al. (1991) reported the first observation of visible photoluminescence (PL) of Ge microcrystals embedded in SiO<sub>2</sub> glassy matrices prepared by an rf-magnetron co-sputtering method. They ascribed the visible luminescence peak at 2.18 eV to quantum confinement of electrons and holes.

After Maeda et al. (1991), many reports showed PL of Ge-doped silica in the visible range. The observed PL was mainly in three visible ranges, red (1.8 eV), green-orange (2.2 - 2.3 eV), and blue-violet (3.0 -3.1 eV). Min et al. (1996) observed a strong red (1.8 eV) PL of Ge nanocrystals in SiO<sub>2</sub> films made by Ge ion implantation. However, the measured PL peak energy and lifetimes showed poor correlations with nanocrystal size, compared to calculations involving radiative recombination of excitons in germanium. This observation suggested that the red PL was not due to the radiative recombination of excitons confined in Ge nanocrystals. Rather, the author suggested that the origin of this red PL was the radiative defect centers in the SiO<sub>2</sub> matrix.

The red PL of germanium-doped SiO<sub>2</sub> films prepared by Ge ion implantation was also reported by Zhang et al. (1998). In contrast to the observation by Min et al. (1996), they observed red shift of the peak position when the mean size of Ge nanocrystals increased. This observation suggested that the red band came from the radiative recombination of excitons confined in Ge nanocrystals. Choi et al. (2000) reported the red PL of Ge-doped silica layer and related the red PL to both the Ge nanocrystals and Ge related defects in the SiO<sub>2</sub> network.

A complete theoretical study on photoabsorption (PA) and photoluminescence (PL) of oxygen related point defects in germanium oxide was done by Zyubin et al. (2005). These surface defects in germanium oxide included  $-\text{O}-\text{Ge}\equiv$  (NBO),  $-\text{OO}-\text{Ge}\equiv$  (peroxy radical),  $\text{O}=\text{Ge}=\text{}$ , and  $\text{O}_2\text{Ge}=\text{}$ . It was found that the PA properties of the four defects were pretty similar and produced PL bands mainly in the visible red and IR energy range. This calculation supports the mechanism of the red PL originated from germanium related defects.

The orange PL (580 nm, 2.1 eV) from Ge-containing SiO<sub>2</sub> films prepared by rf-magnetron sputtering was reported by Ma et al. (2001). They related the observed PL to the luminescence centers (impurities, defects) in SiO<sub>2</sub> because the PL peak was independent of measurement temperature. Ye et al. (2002) also observed orange PL (580nm, 2.1eV) from Ge-SiO<sub>2</sub> thin films and suggested that the photoexcitation (electron-hole pair excitation) happened inside nanocrystal Ge. However, the excitons did not radiate inside the nanocrystals. Instead, the excitons transported out and then emitted light via luminescence centers located at the interface with SiO<sub>2</sub> matrix or in the SiO<sub>2</sub> matrix. Kartopu et al. (2003) reported a PL peak in the 2.2 - 2.3 eV range from chemically etched germanium. The origin was associated with Ge-O defects. Based on previous work, it is clear that the origin of red and orange PL of germanium doped silica is usually ascribed to Ge-related defects or radiative recombination of excitons confined in Ge nanocrystals.

The origin of blue-violet PL, however, is more complicated and is still under debate. Gao et al. (1997) reported an intense UV PL peaked at 286 nm and 396 nm from Ge-ion-implanted SiO<sub>2</sub> film thermally grown on a crystal Si substrate. They proposed that the UV peaks were caused by S1 → S0 and T1 → S0 transitions in GeO color centers formed during implantation and annealing. Shen et al. (2000) fabricated a SiO<sub>2</sub> / Ge: SiO<sub>2</sub> / SiO<sub>2</sub> sandwiched structure and reported enhanced blue-violet emission (395 nm) compared to emission from Ge doped SiO<sub>2</sub> films. They suggested that the PL band originated from T<sub>Σ</sub> → S0 optical transitions in GeO color centers, and ascribed the emission enhancement to improvement of GeO density due to the sandwiched structure. Rebohle et al. (1997) and Zhang et al. (1998) also reported blue-violet emission from Ge implanted SiO<sub>2</sub> films. They both agreed that the observed blue-violet PL emissions were due to ≡Ge-Ge≡ and ≡Ge-Si≡ centers. More blue-violet PL emission of Ge-SiO<sub>2</sub> thin films was reported by Ng et al. (2000), Ye et al. (2002), and Ortiz et al. (2005). They all agreed that the observed blue-violet PL was due to a defect-related mechanism, but varied on where and what the defect was. Ye et al. (2002) suggested that the defect was related to GeO, whereas Ortiz et al. (2005) proposed that the defects existed at the interface between the nanocrystalline Ge and the oxide matrix. Although the proposed mechanism for blue PL of Ge-doped SiO<sub>2</sub> is still controversial, the emission is mainly related to GeO<sub>2</sub>-associated defects.

### **Photoluminescence of other Ge-related materials**

Except for Ge-doped SiO<sub>2</sub>, many other Ge-related materials were fabricated and the PL emission in the visible range was observed. Chen et al. (1996) reported orange PL (569 nm, 2.2 eV) of oxidized amorphous hydrogenated germanium prepared by plasma enhanced chemical vapor deposition (PECVD) and related the PL to GeO<sub>x</sub>. Wu et al. (1999) reported orange PL emission (569 nm, 2.25 eV) of Si coated with Ge films prepared by electrochemical etching. They suggested that the origin was from the Ge-related defects at the interface between porous silicon and the germanium nanocrystals embedded in the pores. Sendova-Vassileva et al.

(1994) observed the green PL located at 525 nm and blue PL at 400 nm of stain-etched and electrochemically-etched germanium. Visible PL from crystal GeO<sub>2</sub> was studied by Fitting et al. (2001). They suggested that tetragonal GeO<sub>2</sub> possessed both slow (200 μs) decay luminescence in the green-yellow range (500 nm) and fast (ns) decay luminescence in the violet range (400nm). They ascribed the different behaviors to triplet-singlet band and singlet-singlet band transition in oxygen deficient centers (ODC), respectively. Zyubin et al. (2007) investigated quartz-like germanium oxide by quantum chemical calculation. They found that there existed single and double oxygen vacancy (OV and DOV) defects in quartz-like germanium oxide that were responsible for PL peak at 3.1 eV (OV) and at 2.6 eV (DOV), respectively. Li et al. (2003) suggested that the Ge neutral oxygen vacancy (NOV) centers were annihilated after the samples were annealed over 700 °C.

### **Methods of Ge-related materials fabrication**

Ge-doped silica layers are generally prepared by Ge ion implantation and rf-magnetron co-sputtering techniques. There are numerous reports on the fabrication of Ge-doped glass by the ion implantation of Ge into SiO<sub>2</sub> (Zhu et al., 1995; Rebohle et al., 1997; Zhang et al., 1998; Dow et al., 2001; Fitting et al., 2001). In this method, Ge is implanted into SiO<sub>2</sub> thermally grown on Si substrates, and then the samples are mostly annealed in nitrogen atmosphere at high temperature. Zhu et al. (1995) found that the Ge dose was the controlling factor for the size distribution. With a decrease in the Ge dose, the fraction of large particles in the size distribution decreased. In contrast to the finding by Zhu et al. (1995), Dow et al. (2001) concluded that the size distribution was independent of the Ge dose.

Another popular method of making germanium-doped silica is rf-magnetron co-sputtering of SiO<sub>2</sub> and Ge. In this method, Ge chips are placed on a Si target and co-sputtered in argon gas (Maeda et al., 1991; Kanemitsu et al., 1992; Ma et al., 1998; Zacharias and Fauchet, 1998; Shen et al., 2000; Choi et al., 2001; Ma et al.,

2001; Ye et al., 2002; Li et al., 2003). In this technique, the size of the Ge nanocrystals can be controlled by changing the volume fraction of Ge in the as-deposited films or by varying the annealing profile. Although these two techniques are widely used, there are many disadvantages. Both methods need very high temperature and high power input. The crystal size is not evenly distributed and is hard to control.

There are many other techniques that are used to fabricate germanium related materials include electrochemical etch (Sendova-Vassileva et al., 1994; Wu et al., 1999; Kartopu et al., 2003), Plasma Enhanced Chemical Vapor Deposition (PECVD) (Chen et al., 1996), evaporation of GeO<sub>2</sub> powder from an electron beam gun (Ardayanian et al., 2006), inert gas condensation (Oku et al., 2000), sol-gel method (Nogami et al., 1994) etc. However, all these methods are top-down strategies, and they either require high temperature or have difficulty in controlling the crystal size distribution.

### **Germanium doped biosilica**

Biogenical doping of Ge into biosilica is a bottom-up and environmentally friendly strategy. The crystal size is controlled by organisms and therefore is predicted to be evenly distributed. Diatoms are a prolific class of single-celled algae that take up soluble silicon to make silica shells or frustules possessing intricate submicron and nanoscale structures. Diatoms have been touted as the paradigm for the biofabrication of nanostructured silica (Sun et al., 2004; Sumper et al., 2006). It is believed that the living diatom itself could be harnessed as a cell factory for massively-parallel fabrication of nanoscale hierarchical metal oxide materials. Controlled metabolic insertion of germanium into the silica frustules was reported by Clayton et al. (2008). They observed morphology change of diatom *Pinnularia sp.* and proposed that it was due to Si-Ge nanocomposite imbedded into the frustule microstructure. Diatoms are known to possess photoluminescence properties due to the nanostructured biosilica (Butcher et al., 2005; Liu et al.,

2005). In our earlier work (Qin et al., 2008), we reported bright blue PL of *N. frustulum* and related the emission to frustule fine structures that were associated with the cell growth cycle.

### **Objectives of our work**

An interesting area of investigation is: what are the optoelectronic properties of the Ge-doped biosilica? To answer this question, our current study focuses on investigating the photoluminescence properties of diatom frustules of *N. frustulum* that contain metabolically inserted germanium oxide. In particular, our research has three objectives: 1) Dope different amount of Ge into the diatom frustules; 2) Study the effect of inserted Ge concentration on PL emission of Ge doped diatom frustules; and 3) Propose a proper origin for observed photoluminescence emission.

## **Materials and Methods**

### **Bioreactor Cultivation**

#### *Culture Maintenance*

Pure cultures of the photosynthetic marine diatom *Nitzschia frustulum* were obtained from the UTEX Culture Collection of Algae (UTEX #2042), and maintained in Nitrate LDM seawater medium under 14:10 light/dark photoperiod of light intensity  $55 \mu\text{Em}^{-2}\text{s}^{-1}$  by artificial light (Feit Electric 9 watt Compact Fluorescent 2700K/PL9). The temperature was kept at 22°C in an incubator (Precision Scientific low temperature incubator 815). Twelve 500 mL flasks with foam stoppers containing 120 mL *N. frustulum* culture were maintained in the incubator, and each flask was swirled for five seconds once per day.

Subculture was performed under sterile conditions inside a laminar flow hood (Baker EdgeGard Hood model #E6-3252) and was performed once per month. Twelve 500 mL flasks with foam stoppers and 1200 mL seawater were autoclaved for 30 minutes at 123 °C and 23 psig. After allowing the glassware to cool, add 7.2 mL sterile PIV Metal solution, 134.4 mL sterile Bristol Nitrate Salt solution, 2.4 mL sterile thawed vitamin stock and 7.2 mL sterile 100 mM Si solution to the autoclaved seawater with aseptic technique. Using a sterile 100mL graduated cylinder, 100 mL Nitrate LDM seawater medium was transferred into each flask. Cultures from three flasks were combined into one parent flask and swirled to mix well. A sterile 10mL volumetric pipette was used to pipette 20 mL of well mixed culture from the parent flask into each of the flasks containing 100 mL fresh medium. The rest of culture in the parent flask was kept under low light at  $10 \mu\text{Em}^{-2}\text{s}^{-1}$  as a backup.

#### *Nitrate LDM Seawater Medium Preparation*

Diatom Nitrate LDM seawater medium was prepared from a natural seawater base (NOAA Lab, Newport, OR, USA) enriched with Bristol's salts, sodium

metasilicate, PIV metal solution and vitamin stock. The seawater was pumped via a peristaltic pump (Cole Parmer Model# 50000-079, Serial # FK 3114, 45W, 10.6 gpm) through a 5  $\mu\text{m}$  nylon fiber Omnifilter whole house water filter cartridge into a clean 55 gallon Poly Drum. Seawater was autoclaved for 30 minutes at 123  $^{\circ}\text{C}$  and 23 psig before medium preparation.

Bristol Nitrate Salt solution was prepared from the super stocks. The super stock solutions were 798.1 mM  $\text{NaNO}_3$ , 5.4 mM  $\text{MgSO}_4\cdot\text{H}_2\text{O}$ , 42.3 mM  $\text{K}_2\text{HPO}_4\cdot 3\text{H}_2\text{O}$ , and 128.6 mM  $\text{KH}_2\text{PO}_4$  dissolved in DI water. After diluting the super stocks with DI water, the stock has a salt composition of 39.9 mM  $\text{NaNO}_3$ , 0.054 mM  $\text{MgSO}_4\cdot\text{H}_2\text{O}$ , 0.423 mM  $\text{K}_2\text{HPO}_4\cdot 3\text{H}_2\text{O}$ , and 1.286 mM  $\text{KH}_2\text{PO}_4$ . Stocks and super stocks were autoclaved for 30 minutes at 123  $^{\circ}\text{C}$  and 23 psig for storage.

The sodium metasilicate, PIV metal and vitamin stocks were prepared by mixing solute with DI water. Sodium metasilicate ( $\text{Na}_2\text{SiO}_3\cdot 5\text{H}_2\text{O}$ ) was prepared to 100 mM and autoclaved before storing in a polyethylene bottle. PIV metal solution was stored in a glass bottle and autoclaved with composition of 2.00 mM  $\text{Na}_2\text{EDTA}$ , 0.36 mM  $\text{Fe}(\text{SO}_4)\cdot 7\text{H}_2\text{O}$ , 0.207 mM  $\text{MnCl}_2\cdot 4\text{H}_2\text{O}$ , 0.037 mM  $\text{ZnCl}_2$ , 0.0084 mM  $\text{CoCl}_2\cdot 6\text{H}_2\text{O}$ , and 0.014 mM  $\text{Na}_2\text{MoO}_4\cdot \text{H}_2\text{O}$ . Vitamin stock was dissolved in DI water with composition of 7.38  $\mu\text{M}$  vitamin  $\text{B}_{12}$ , 40.93  $\mu\text{M}$  biotin ( $\text{C}_{10}\text{H}_{16}\text{N}_2\text{O}_3\text{S}$ ), 2.96  $\mu\text{M}$  thiamine HCl ( $\text{C}_{12}\text{H}_{17}\text{ClN}_4\text{O}_5\text{HCl}$ ), 55.49  $\mu\text{M}$  meso-inositol ( $\text{C}_6\text{H}_{12}\text{O}_6$ ), 7.93  $\mu\text{M}$  thymine ( $\text{C}_5\text{H}_6\text{N}_2\text{O}_2$ ), 3.53  $\mu\text{M}$  Ca pantothenate ( $\text{C}_9\text{H}_{16}\text{NO}_5\text{Ca}_{0.5}$ ), 0.73  $\mu\text{M}$  P-aminobenzoic acid ( $\text{C}_7\text{H}_7\text{NO}_2$ ), and 8.19  $\mu\text{M}$  Nicotinic acid ( $\text{C}_6\text{H}_5\text{NO}_2$ ). The vitamin stock solution was filtered with 3 $\mu\text{m}$  Whatman filter by using Buchner funnels and the side-arm Erlenmeyer flask assembly under vacuum with aseptic technique. The filtered vitamin stock was portioned into 10 mL aliquots and frozen at  $-20^{\circ}\text{C}$  until use.

Nitrate LDM seawater medium was prepared by adding the stock solutions to the filtered and sterilized seawater base. The final concentrations of nutrients in the medium were: 3.98 mM NaNO<sub>3</sub>, 54.1 μM MgSO<sub>4</sub>·H<sub>2</sub>O, 42.2 μM K<sub>2</sub>HPO<sub>4</sub>·3H<sub>2</sub>O, 128.4 μM KH<sub>2</sub>PO<sub>4</sub>, 534.8 μM sodium metasilicate (Na<sub>2</sub>SiO<sub>3</sub>·5H<sub>2</sub>O), 10.8 μM Na<sub>2</sub>EDTA, 1.92 μM Fe(SO<sub>4</sub>)·7H<sub>2</sub>O, 1.11 μM MnCl<sub>2</sub>·4H<sub>2</sub>O, 0.20 μM ZnCl<sub>2</sub>, 0.04 μM CoCl<sub>2</sub>·6H<sub>2</sub>O, 0.08 μM Na<sub>2</sub>MoO<sub>4</sub>·H<sub>2</sub>O, 0.01 μM vitamin B<sub>12</sub>, 0.07 μM biotin (C<sub>10</sub>H<sub>16</sub>N<sub>2</sub>O<sub>3</sub>S), 5.28 μM thiamine HCl (C<sub>12</sub>H<sub>17</sub>ClN<sub>4</sub>O<sub>5</sub>HCl), 98.8 μM meso-inositol (C<sub>6</sub>H<sub>12</sub>O<sub>6</sub>), 14.1 μM thymine (C<sub>5</sub>H<sub>6</sub>N<sub>2</sub>O<sub>2</sub>), 7.47 μM Ca pantothenate (C<sub>9</sub>H<sub>16</sub>NO<sub>5</sub>Ca<sub>0.5</sub>), 1.30 μM p-amino benzoic acid (C<sub>7</sub>H<sub>7</sub>NO<sub>2</sub>), and 14.47 μM nicotinic acid (C<sub>6</sub>H<sub>5</sub>NO<sub>2</sub>).

#### *Bioreactor Operation*

A bubble-column photobioreactor was used to cultivate *N. frustulum* under controlled conditions. The reactor vessel was a glass column with 10.5 cm inner diameter, 4.8 mm wall thickness, and 70.5 cm height to provide a total volume of 6.1 L and working volume of 3.5 L (40.5 cm). The glass column was mounted onto two stainless steel support plates at the base and top. The baseplate assembly contained a stainless steel sparger plate consisting of four 1.0 mm diameter holes on a 3.6 cm square pitch. Pressurized house air was particulate filtered, metered through a flowmeter, sterile filtered at 0.2 μm, and introduced to the baseplate. The headplate assembly contained 8 ports, including a fresh medium delivery port, thermocouple port, a 4.6 mm inner diameter sampling port, 11 mm Dissolved Oxygen (D.O.) electrode port, two air outlet ports, and 9.5 mm outer diameter by 1.09 m length stainless steel internal U-tube heat exchanger. Controlled sampling of the liquid suspension within the vessel was accomplished by pressurizing the vessel headspace and collecting the liquid in a sterile culture bottle. Water from a temperature-controlled chilling circulator was pumped through the internal heat exchanger to provide constant temperature within the bioreactor vessel. The bioreactor was externally illuminated by six 20 W cool white fluorescent lamps of 57 cm length vertically positioned around the glass vessel in a hexagonal array

about 1-2 cm from the vessel surface. The lamps were connected to a photoperiod timer. The incident light flux intensity was measured with a LI-COR SA 190 PAR quantum sensor positioned at the interior surface and pointed towards the light source at 6 radial positions and 3 axial positions (top, middle, and bottom). Detailed process conditions used in this study are provided in Table 1. The schematic of the bioreactor setup and a picture of the setup are shown in Figure 1a and Figure 1b, respectively.

**Table 1.** Summary of process conditions for two-stage photobioreactor cultivation of *Nitzschia frustulum*

Process parameter		Stage I	Stage II
<i>Target initial conditions</i>			
Cell number density	$X_{N,O}$	$3 \times 10^5$ cells/mL	$3\text{--}6 \times 10^6$ cells/mL
Initial silicon concentration	$C_{Si,O}$	0.56 mmolSi/L	0.58~0.62 mmolSi/L
Initial germanium concentration	$C_{Ge,O}$	0.0 $\mu\text{molGe/L}$	0.0 $\mu\text{molGe/L}$ (control)
	$C_{Si,O}/C_{Ge,O}$		1.9~85.1 $\mu\text{molGe/L}$ 304~7 (mole basis) 118~2.8 (mass basis)
<i>Process conditions</i>			
Temperature	T	22°C	22°C
Initial culture volume	$V_O$	3.5 L	2.3 L
Incident light intensity	$I_O$	150 $\mu\text{E/m}^2\text{-s}$	150 $\mu\text{E/m}^2\text{-s}$
Fractional photoperiod	f	0.583 (14 h light /10 h dark)	0.583 (14 h light /10 h dark)
Aeration rate	$v_g$	0.71 L air $\text{L}^{-1}\text{min}^{-1}$	1.1~1.6 L air $\text{L}^{-1}\text{min}^{-1}$
CO <sub>2</sub> partial pressure	$P_{CO_2}$	350 ppm	350 ppm
Cultivation time	t	193~215 h	120 h

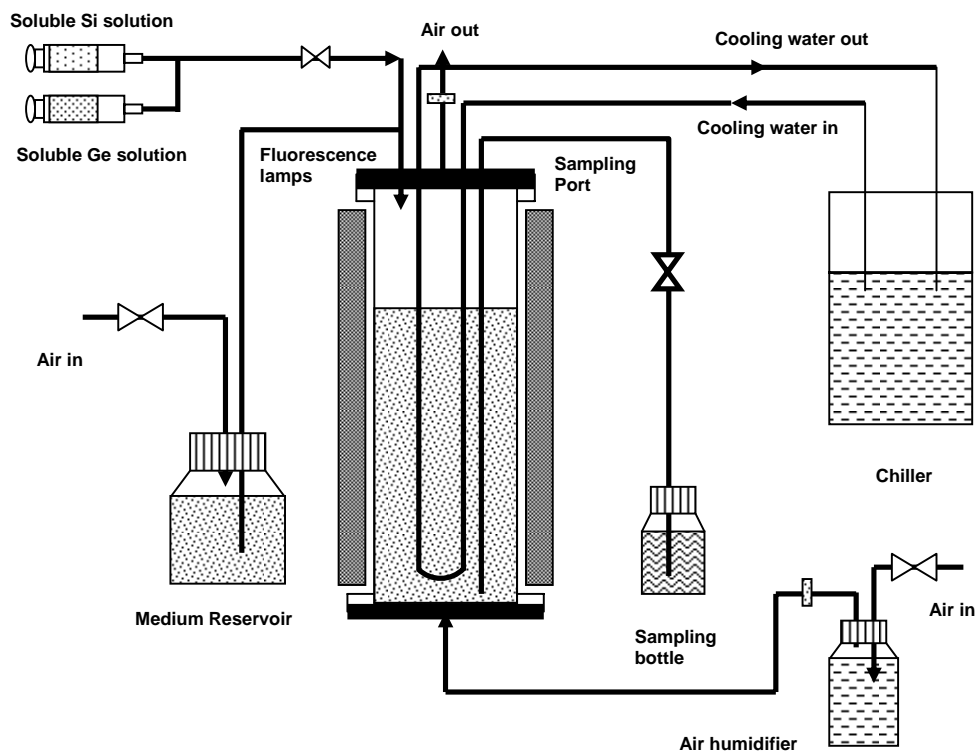


**Figure 1a.** Schematic of bioreactor setup

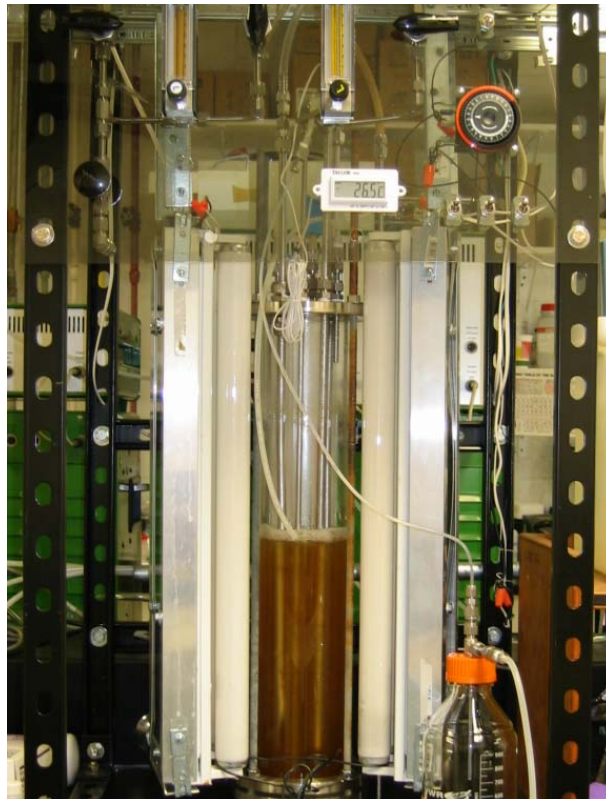


**Figure 1b.** Picture of bioreactor setup

### *Bioreactor Inoculation*

The bioreactor was cleaned and autoclaved for 30 minutes at 123 °C and 23 psig. A timer was set to 14:10 light/dark photoperiod, and the chilling circulator was attached to the reactor heat exchanger port to pump cooling water. The airline was opened and attached to the flowmeter. After the lights, cooling water, and air were checked for proper working order, the reactor was pumped with 3.5 L Nitrate LDM seawater medium ( $V_m$ ) through the medium delivery port by filtered pressurized air. The medium was allowed to reach equilibrium with the inlet reactor over night or over 8 hours. Three inoculum flasks with the same age from the incubator (generally around 15 days) were combined into one flask by using aseptic technique. 1 mL of culture was removed for cell density measurement via a hemocytometer ( $X_N$ ). A volume of inoculum ( $V_{inoculum}$ ) was collected through 60 mL sterile syringe and injected into the reactor through the medium delivery port

to obtain  $3 \cdot 10^5$  cells/mL initial cell number density ( $X_{N,O}$ ). 20 mL sample was immediately taken through the sampling port and the cell number density was measured via hemocytometer. The cell number density should be close to  $3 \cdot 10^5$  cells/mL.

$$V_{inoculum} = \frac{X_{N,O} \times V_m}{X_N - X_{N,O}}$$

### *Sampling*

Controlled sampling of the liquid suspension within the vessel was accomplished by pressurizing the vessel headspace and collecting the liquid in a sterile culture bottle. The first 20 mL culture was used to rinse the sample tube and discarded into a culture waste bottle. Another 20 mL culture was collected for soluble silicon and germanium assay and the cell number density measurement. When a larger volume (e.g. 400 mL) culture was needed for mass density measurement and post-processing (e.g.  $H_2O_2$  treatment to remove organics), a larger volume sterile culture bottle was replaced.

### *Experimental Design for Bioreactor Experiments*

Before inoculation, 20 mL medium was collected to determine the soluble silicon concentration in the medium, which should match with the designed initial silicon concentration. Right after inoculation, a 20 mL culture suspension was collected to determine the cell number density, soluble silicon concentration and pH of the culture suspension. The initial cell mass density ( $X_O$ ) was calculated from the cell mass density of the inoculum ( $X_{inoculum}$ ) and the inoculum volume ( $V_{inoculum}$ ) and the medium volume ( $V_m$ ). The pH, cell number density and soluble silicon concentration were monitored throughout stage I, the initial growth phase. Stage I of reactor experiment was to grow cell culture to a high cell number density and study the growth-related silicon uptake. Specific growth rate ( $\mu$ ) was determined from the least squares slope of the natural log of dry cell number density versus

time data. Liquid phase silicon was depleted in stage I to provide silicon starvation for diatom cells, which prepared the diatom cellular machinery for surge uptake of silicon and germanium.

$$X_o = \frac{X_{inoculum} \times V_{inoculum}}{V_m + V_{inoculum}}$$

The initial silicon concentration in stage I was 0.6 mM, which provided enough substrate to achieve four cell doublings from the inoculum density. The cells were considered to be silicon starved when both the soluble silicon concentration was near zero and the cell number density was constant for at least one photoperiod. After silicon depletion was reached, a large volume of cell culture (800mL) was collected to determine the final cell number density, mass density and soluble silicon concentration in stage I. The reactor was then given a pulse addition of silicon and germanium through the medium delivery port to achieve 0.6 mM initial silicon concentration and 0-85.1  $\mu$ M germanium concentration in stage II. When silicon starved cells are suddenly immersed in an environment with ample silicon and germanium the cells rapidly uptake silicon and germanium. This surge uptake is non-growth associated and is many times faster than growth-related uptake. Germanium and silicon surge uptake kinetics were determined in the first five hours after the pulse addition in stage II. Data for soluble silicon and germanium and cell number density were collected every 1 to 2 hours during surge uptake until a stable germanium concentration was established. Data were then taken every 24 hours for a total of five photoperiods. A large amount of biomass was collected every 24 hours for post treatment and photoluminescence (PL) measurement. The cell culture growth rates were determined by the Monod model and the kinetic substrate (silicon and germanium) uptake rates were determined by the Michaelis-Menten model. Cell number and cell mass yield coefficients were calculated. See appendix for all calculations. The reactor was shut down after five photoperiods.

### *Bioreactor Shutdown*

After shut down the reactor, the airline, water circulation hoses, and thermocouple were detached from the reactor. The headplate, baseplate, sample ports and sample tubes were washed with soap and tap water and then thoroughly rinsed with DI water. The vessel glass was scrubbed with a bottle brush using soap and water and then thoroughly rinsed with tap water followed by DI water. The biomass waste was killed by bleach (diatoms turned white) and then poured down to the lab sink with a high flow of tap water. After the vessel, the headplate and the baseplate were cleaned and dried, they were assembled. All the headplate openings were covered with aluminum foil and the reactor was autoclaved at 123 °C for 1 hour at 23 psig.

### **Analytical Techniques**

#### *Soluble silicon concentration assay*

The concentration of soluble silicon in liquid phase was determined using a spectrophotometric method, in which silicon was complexed with ammonium molybdate ((NH<sub>4</sub>)<sub>6</sub>Mo<sub>7</sub>O<sub>24</sub>·4H<sub>2</sub>O) to form a yellow compound detectable at 410 nm (Fannin and Pilson, 1973). The assay reagents were 6 M HCl and ammonium molybdate color complexing agent. To prepare the ammonium molybdate color complexing reagent, 10 g ammonium molybdate ((NH<sub>4</sub>)<sub>6</sub>Mo<sub>7</sub>O<sub>24</sub>·4H<sub>2</sub>O) was dissolved in 75 mL warm DI water and diluted to 100 mL in a volumetric flask with DI water. The solution was placed on a stir plate with pH meter submerged into the solution. 1 M aqueous NaOH was added drop wise until the pH was 7.5 ± 0.5. The reagent was stored in polyethylene bottle.

A 20 mL sample was taken according to the sampling protocol and was centrifuged in a 50 mL centrifuge tube at 4000 rpm for 10 minutes (International Equipment Company Centra-4B IM219 Bench Top Centrifuge) to separate the liquid medium from the biomass. The clear supernatant was poured into a 25 mL polyethylene bottle and capped. If the supernatant was not clear, a second

centrifugation was needed. The biomass was discarded into the culture waste bottle. 5 mL separated liquid medium was removed from the 20 mL aliquot by pipette and placed in a 6 mL sample vial. 100  $\mu$ L of 6 M HCl and 200  $\mu$ L of ammonium molybdate reagent were added to the sample in the sample vial. After 10 minutes, the sample mixed with reagents was poured into a 4 mL cuvette for absorption measurement. The absorption was recorded at 410 nm by a spectrophotometer (Shimatzu). The spectrophotometer was first warmed up for at least 10 minutes and then zeroed at 410 nm with DI water mixed with the assay reagents. A duplicate silicon assay was performed following the assay protocol. A calibration curve was obtained based on seven standards solutions in the range of 0-0.5 mM. The standards concentrations were 0.01, 0.05, 0.1, 0.2, 0.3, 0.4 and 0.5 mM and were assayed using the assay protocol. The data was fit to the linear relation with the assumption that the absorption was zero at silicon concentration equal to zero.

$$C_{Si} = a_{Si} \times A_{410}$$

where  $A_{410}$  is the sample absorbance at 410 nm measured in arbitrary units, and  $a_{Si}$  is the determined constant from the linear relationship between absorbance and the silicon concentration of standards. The measured sample absorbance was substituted into the above equation to calculate the soluble silicon concentration  $C_{Si}$ .

#### *Soluble germanium concentration assay*

The concentration of soluble silicon in liquid phase was determined using a spectrophotometric method, in which germanium was complexed with phenylfluorone (2,3,7-trihydroxy-9-phenyl-6-fluorone) to form an orange compound detectable at 525 nm (Luke and Campbell, 1956). The assay reagents were 10% (V/V) 12 M HCl solution, 25% (V/V) 98.5% H<sub>2</sub>SO<sub>4</sub> solution, a sodium acetate buffer and phenylfluorone. To prepare the phenylfluorone color

complexing reagent, 0.0500 g phenylfluorone (2,3,7-trihydroxy-9-phenyl-6-fluorone) was dissolved in 50 mL methanol and 1 mL 12 M HCl and diluted to 500 mL in a volumetric flask with methanol. The solution was transferred to a 1 L Pyrex bottle and stored in the dark. The sodium acetate buffer was prepared by adding 900 g sodium acetate trihydrate ( $\text{NaC}_2\text{H}_3\text{O}_2 \cdot 3\text{H}_2\text{O}$ ) to 700 mL DI  $\text{H}_2\text{O}$  in a 2 L beaker and dissolving the solute under heat and agitation. The dissolved contents were transferred to a 2 L volumetric flask containing 480 mL 12 M acetic acid and were diluted to 2 L with DI water. The reagent was allowed to cool before use.

20 mL sample was taken according to the sampling protocol and the liquid sample was separated using the procedure described for the soluble silicon concentration assay. 1 mL separated liquid medium was removed from the 20 mL aliquot by pipette and placed in a 6 mL sample vial. 0.300 mL of  $\text{H}_2\text{SO}_4$  solution, 1.000 mL sodium acetate buffer and 1.000 mL phenylfluorone reagent were added to the sample in the sample vial. After 4 minutes, 1.700 mL 10% HCl solution was added to the sample vial. The mixture was then immediately poured into a 4 mL cuvette for absorption measurement. The absorption was recorded at 525 nm by a spectrophotometer (Shimatzu). The spectrophotometer was first warmed up for at least 10 minutes and then zeroed at 525 nm with DI water mixed with the assay reagents. A duplicate germanium assay was performed following the assay protocol. A calibration curve was obtained based on seven standards solutions in the range of 0-60  $\mu\text{M}$ . The standards concentrations were 5, 10, 20, 30, 40, 50 and 60  $\mu\text{M}$  and were assayed using the assay protocol and the data was fit to the linear relation with the assumption that the absorption was zero at germanium concentration equaled to zero.

$$C_{Ge} = a_{Ge} \times A_{525}$$

where  $A_{525}$  is the sample absorbance at 525 nm measured in arbitrary units, and  $a_{Ge}$  is the determined constant from the linear relationship between absorbance and the germanium concentration of standards. The measured sample absorbance was substituted into the above equation to calculate the soluble germanium concentration  $C_{Ge}$ .

#### *Nitrate Assay*

The nitrate concentration in liquid phase was determined using a spectrophotometric method, in which nitrate was reduced by nitrate reducing reagent to form a purple compound detectable at 530 nm (La-Motte Nitrate Test Kit). The assay reagents were purchased (La-Motte Nitrate Test Kit, Model NCR3110).

20 mL sample was taken according to the sampling protocol and the liquid sample was separated using the procedure described for the soluble silicon concentration assay. 2.5 mL separated liquid medium was removed from the 20 mL aliquot by pipette and placed in a 6 mL sample vial. 2.5 mL of Mixed Acid Reagent (V-6278) was added to the sample in the sample vial and well mixed by repeat inversions. After 2 minutes, 0.1g Nitrate Reducing Reagent (V-6279) was added to the sample vial. The mixture was then immediately inverted for 50-60 times in one minute. After 10 minutes of waiting, the mixture was poured into a 4 mL cuvette for absorption measurement. The absorption was recorded at 530 nm by a spectrophotometer (Shimatzu). The spectrophotometer was first warmed up for at least 10 minutes and then zeroed at 530 nm with deionized water mixed with the assay reagents. A duplicate nitrate assay was performed following the assay protocol. A calibration curve was obtained based on seven standards solutions in the range of 0-300  $\mu\text{M}$ . The standards concentrations are 0, 20, 40, 60, 100, 200 and 300  $\mu\text{M}$  and were assayed using the assay protocol and the data was fit to the linear relation with the assumption that the absorption was zero at nitrate concentration equaled to zero.

$$C_{Nitrate} = a_{Nitrate} \times A_{530}$$

where  $A_{530}$  is the sample absorbance at 530 nm measured in arbitrary units, and  $a_{Nitrate}$  is the determined constant from the linear relationship between absorbance and the nitrate concentration of standards. The measured sample absorbance was substituted into the above equation to calculate the liquid nitrate concentration  $C_{Nitrate}$ .

#### *Cell Counting via Hemocytometer*

A 20 mL sample was taken according to the sampling protocol and was transferred into a 50 mL centrifuge tube. The cell suspension was well mixed by vortexing the centrifuge tube at high speed for 30 seconds. A glass cover slip was placed over the hemocytometer chamber center and cell suspension was filled into the two chambers using a pipette (Fuchs-Rosenthal hemocytometer model 3720, Hauser Scientific, 0.0625 mm between grid lines, 0.02 mm deep). Cell suspension will pass under the cover slip by capillary action. The hemocytometer was placed on the stage of a light microscope and focused at 430X for cell counting. Each small hemocytometer square contained  $1.25 \cdot 10^{-5}$  mL of culture volume. The number of cells in each small square was counted with a tally counter. The counting continued in 10-15 randomly picked squares or at least 150 cells had been counted. In case of dense culture, the suspension was diluted 5 or 10 times with DI water. A duplicate cell counting was performed following the cell counting protocol. The cell number density was calculated by

$$X_N = \frac{D \times N_C}{V_H \times N_S}$$

where  $X_N$  is cell number density,  $D$  is the sample dilution,  $V_H$  is the hemocytometer chamber volume per small square,  $N_C$  is the total cell number counted, and  $N_S$  is the number of small squares counted.

#### *Cell mass density determination*

400 mL sample was collected according to the sampling protocol and divided into two 200 mL aliquots. One aliquot was poured into four 50 mL centrifuge tubes and centrifuged for 10 minutes at 4000 rpm. The biomass was remained and the supernatant was discarded after centrifugation. All biomass was transferred to a single 50 mL centrifuge tube and centrifuged for 10 minutes at 4000 rpm. The supernatant was discarded and biomass was remained. DI water was added into the biomass and then vortexed to clean the biomass. Centrifugation was repeated for 10 minutes at 4000 rpm for three times of DI water cleaning. The clean pellets (around 5 mL) were collected and transferred into an aluminum dish. The biomass was allowed to dry in oven at 80 °C over night or until liquid was gone. The dry cell biomass was scraped off the aluminum dish with a spatula and stored in a 4 mL sealed glass vial in freezer. The cell mass density of another aliquot was determined following the protocol described above. The cell mass density was calculated by

$$X = \frac{m_{cells} - m_{dish}}{V_S}$$

where  $X$  is cell mass density,  $m_{cells}$  is the mass of aluminum dish containing biomass,  $m_{dish}$  is the mass of empty aluminum dish, and  $V_S$  is the sample volume used for cell mass density measurement.

#### *Frustules isolation via H<sub>2</sub>O<sub>2</sub> treatment*

The dry cell biomass was obtained according to the cell mass density determination protocol. 100 mg of dry biomass was weighted and mixed with 30

mL 30 wt% H<sub>2</sub>O<sub>2</sub> in a 250mL Erlenmeyer flask. The flask was covered with aluminum foil and placed in an environmental orbital shaker (Lab-Line® Orbit Environ-Shaker). The flask was shaken at 100 rpm at 80 °C for 24 hours or until all the green biomass turned to white. The suspension was transferred to 50 mL centrifuge tube and added with 20 mL DI water. The solution was centrifuged at 4000 rpm for 10 minutes to collect the white pellets (frustules). After decanting the supernatant 40 mL DI water was added to clean the white pellets. The solution was centrifuged again to collect the inorganic materials. Centrifugation was repeated for 10 minutes at 4000 rpm for three times of DI water cleaning. The clean pellets (around 5 mL) were collected and transferred into an aluminum dish. The frustules were allowed to dry in oven at 80 °C over night or until liquid was gone. The dry frustules were scraped off the aluminum dish with a spatula and stored in a 4 mL sealed glass vial in freezer. The inorganic solid yield was calculated by

$$Y_{gH_2O_2/gDW} = \frac{m_{inorganics} - m_{dish}}{m_{DW}}$$

where  $Y_{gH_2O_2/gDW}$  is the inorganic solid yield,  $m_{inorganics}$  is the mass of aluminum dish containing frustules,  $m_{dish}$  is the mass of empty aluminum dish, and  $m_{DW}$  is the weight of dry cell biomass.

#### *Frustules isolation for imaging*

100 mL cell suspension was collected according to the sampling protocol. The suspension was transferred to 50 mL centrifuge tube and centrifuged at 1000 rpm for 20 minutes to collect the biomass. The supernatant was discarded and 40 mL DI water was added to wash the biomass. Centrifugation was repeated for 3 times of DI water cleaning at 1000 rpm for 20 minutes. After the third cleaning with DI water the supernatant was discarded and the pellets were mixed with 30 mL 30 wt% H<sub>2</sub>O<sub>2</sub> in a 250 mL Erlenmeyer flask. The flask was covered with aluminum foil and placed in an environmental orbital shaker (Lab-Line® Orbit Environ-

Shaker). The flask was shake at 100 rpm at 80 °C for 24 hours or until all the green biomass turned to white. The suspension was transferred to 50 mL centrifuge tube and added with 20 mL DI water. The solution was centrifuged at 1000 rpm for 10 minutes to collect the white pellets (frustules). After decanting the supernatant 40 mL DI water was added to clean the white pellets. The solution was centrifuged again to collect the inorganic materials. Centrifugation was repeated for 10 minutes at 1000 rpm for three times of DI water cleaning. Another centrifugation was repeated for 10 minutes at 1000 rpm for three times of methanol cleaning. The clean pellets (around 5 mL) was then dispersed in methanol and stored in a 25 mL sealed glass vial in refrigerator.

*Germanium and silicon concentration in solid biomass*

The dry cell biomass was obtained according to the cell mass density determination protocol. 30 mg of dry biomass was weighted and mixed with 1 g solid sodium hydroxide pellet in a zirconium crucible. The furnace was preheated to 400 °C first (Barnstead Thermolyne Furnace, Model # FB1315M). The crucible was covered and placed into the furnace using a tong and was heated for 3 hours to allow complete reaction. The crucible was moved out of the furnace for cooling. After 10 minutes of cooling the fusion was added with 10 mL DI water to dissolve the fusions. 5 mL 30% (V/V) 14 M nitric acid was added to react with the sodium hydroxide leftover. The solution was well mixed and was adjusted to neutral pH value with 30% (V/V) 14 M nitric acid and 1 M aqueous sodium hydroxide. Germanium (silicon) concentration in the fusion solution was determined following the soluble germanium (silicon) concentration assay protocol. A duplicate germanium (silicon) concentration in solid biomass assay was performed by using the protocol described above. The germanium (silicon) concentration in the solid biomass was calculated by

$$C_{Ge,DW} (C_{Si,DW}) = \frac{C_{Ge,fusion} (C_{Si,fusion}) \times V_{fusion}}{m_{DW}}$$

where  $C_{Ge,DW}$  ( $C_{Si,DW}$ ) is the germanium (silicon) concentration in dry cell biomass,  $C_{Ge,fusion}$  ( $C_{Si,fusion}$ ) is the germanium (silicon) concentration of the fusion solution,  $V_{fusion}$  is final volume of the fusion solution, and  $m_{DW}$  is the sample mass used for germanium (silicon) concentration in dry cell biomass measurement.

*Germanium and silicon concentration in frustules*

The frustules were obtained according to the frustules isolation via  $H_2O_2$  treatment protocol. 5 mg of frustules were weighted and mixed with 1 g solid sodium hydroxide pellet in a zirconium crucible. The furnace was preheated to 400 °C first (Barnstead Thermolyne Furnace, Model # FB1315M). The crucible was covered and placed into the furnace using a tong, and was heated for 3 hours to allow complete reaction. The crucible was moved out of the furnace for cooling. After 10 minutes of cooling the fusion was added with 10 mL DI water to dissolve the fusions. 5 mL 30% (V/V) 14 M nitric acid was added to react with the sodium hydroxide leftover. The solution was well mixed and was adjusted to neutral pH value with 30% (V/V) 14 M nitric acid and 1 M aqueous sodium hydroxide. Germanium (silicon) concentration in the fusion solution was determined following the soluble germanium (silicon) concentration assay protocol. A duplicate germanium (silicon) concentration in frustules assay was performed by using the protocol described above. The germanium (silicon) concentration in frustules and weight percentage of germanium in frustules were calculated by

$$C_{Ge,frustules} (C_{Si,frustules}) = \frac{C_{Ge,fusion} (C_{Si,fusion}) \times V_{fusion}}{m_{frustules}}$$

$$Wt\%Ge = \frac{C_{Ge,fusion} \times M_{Ge} / 1000}{C_{Si,frustules} \times M_{SiO_2}} \times 100\%$$

where  $C_{Ge,frustules}$  ( $C_{Si,frustules}$ ) is the germanium (silicon) concentration in dry cell biomass,  $C_{Ge,fusion}$  ( $C_{Si,fusion}$ ) is the germanium (silicon) concentration of the fusion solution,  $V_{fusion}$  is final volume of the fusion solution,  $m_{frustules}$  is the sample mass

used for germanium (silicon) concentration in frustules measurement,  $Wt\%Ge$  is the weight percentage of germanium in frustules,  $M_{Ge}$  is the molecular weight of germanium, and  $M_{SiO_2}$  is the molecular weight of  $SiO_2$ .

#### *Thermal Annealing*

The frustules were obtained according to the frustules isolation via  $H_2O_2$  treatment protocol. 5 mg of frustules were weighed and placed into a ceramic crucible. The furnace was preheated to 800 °C first (Barnstead Thermolyne Furnace, Model # FB1315M). The crucible was covered and placed into the furnace using a tong, and was heated for 1 hour. The crucible was moved out of the furnace for cooling after 1 hour annealing. The annealed sample was transferred and stored in a 4 mL sealed glass vial in freezer.

#### *TEM sample preparation*

Intact frustules were isolated via the frustules isolation for imaging protocol. One drop of the intact frustules was pipetted onto the sample side of the TEM grid that was placed on a glass slide (300 mesh copper grid with Holey carbon film). The TEM grid was immediately moved around by a tweezer to avoid the carbon network sticking onto the glass slide surface. After the sample was dried, the status of frustules mounted on the TEM grid was checked. If the number of frustules dispersed on the grid was too small, add another drop following the above protocol. If the frustules were too dense to disperse on the grid, dilute the frustule suspension and add another drop following the above protocol. The TEM grid was placed into a tabbed grid storage box and sent to Portland State University (PSU) for Transmission Electron Microscopy (TEM) analysis (FEI Tecnai F20 high resolution TEM (200 keV) equipped with embedded Scanning Transmission Electron Microscopy (STEM) and an X-ray energy dispersive analysis (EDS) probe).

#### *Photoluminescence (PL) measurement*

The frustules were obtained according to the frustules isolation via  $\text{H}_2\text{O}_2$  treatment protocol. 1 mg of frustules were weight and poured into a self-made Delrin sample mount (a 20mm diameter and 4mm thick disc with a 3mm long and 1mm deep square notch at the center). Frustules were pressed by a spatula to allow tight packing inside the notch. The sample mount was covered by a glass cover slip. The sample mount was placed on the PL system sample holder and excited with a VSL-337-NDS nitrogen laser source (Laser Science, Inc. Peak power is 30 kW and the average power is 2.4 mW at 20 Hz. 4 nsec pulses at 337 nm in the UV with pulse energy of up to 120  $\mu\text{J}$ ). The PL emission was detected by using Acton InSpectrum-300 spectrometer equipped with CCD detector (Acton InSpectrum™-300 0.150m Fully Integrated Imaging CCD Spectrometer, Acton Research Corporation, Model # INS-150-122B). The emission spectrum was recorded in the range of 300-800 nm by the software SpectraSense™ version 4.0 with 200  $\mu\text{m}$  slit width and 2000 msec integration time. The UV cut filter was used to remove interference from the excitation source. Schematic of PL system setup was shown in Figure 2.

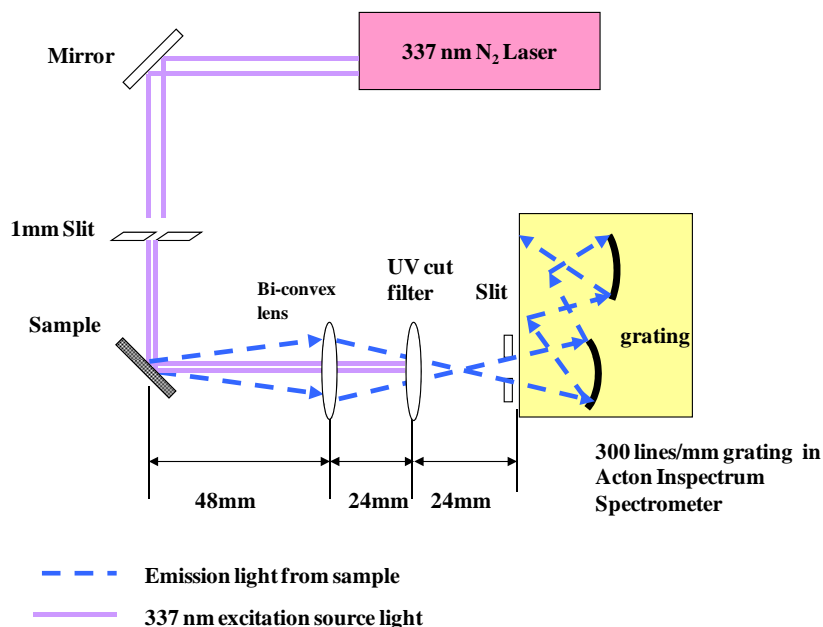


**Figure 2.** Schematic of PL system setup

## **Results**

### **Bioreactor Cultivation**

#### *Effect of initial germanium concentration in stage II on growth of *N. frustulum**

The cell number density and soluble silicon concentration vs. time for bioreactor cultivation of *N. frustulum* with different initial germanium concentration in stage II are presented in Figure 3. During Stage I of the cultivation process, soluble silicon uptake was growth associated. The dissolved silicon concentration went to zero after around 120 hours in stage I. The cells continued growing until they reached the stationary phase, where cell number density did not change with time any more. The initial silicon concentration in stage I was 0.6 mM, which provided enough substrate to achieve four cell doublings from the inoculum density. The cells were considered to be silicon starved, when both the soluble silicon concentration was near zero and the cell number density was constant for at least one photoperiod.

The initial silicon concentration in stage II was 0.6 mM, which provided enough substrate to achieve one cell doubling from the final density in stage I. The initial germanium concentration in stage II was set to 0.0, 12.1, and 85.1  $\mu\text{M}$ . By fixing the initial silicon concentration to 0.6 mM, germanium to silicon molar ratio 0.00, 0.02, and 0.14 were achieved. As shown in Figure 3a, silicon concentration decreased to zero and cell number density doubled after 12 hours of cultivation in stage II, when no germanium was added into the culture. Figure 3b illustrates that silicon went to a certain level after 36 hours, and then decreased to zero in the next 84 hours, when initial germanium concentration was 12.1  $\mu\text{M}$ . Figure 3c shows that silicon was not completely uptaken after 120 hours of cultivation in stage II, and the cell number density was not doubled, when initial germanium concentration was 85.1  $\mu\text{M}$ .

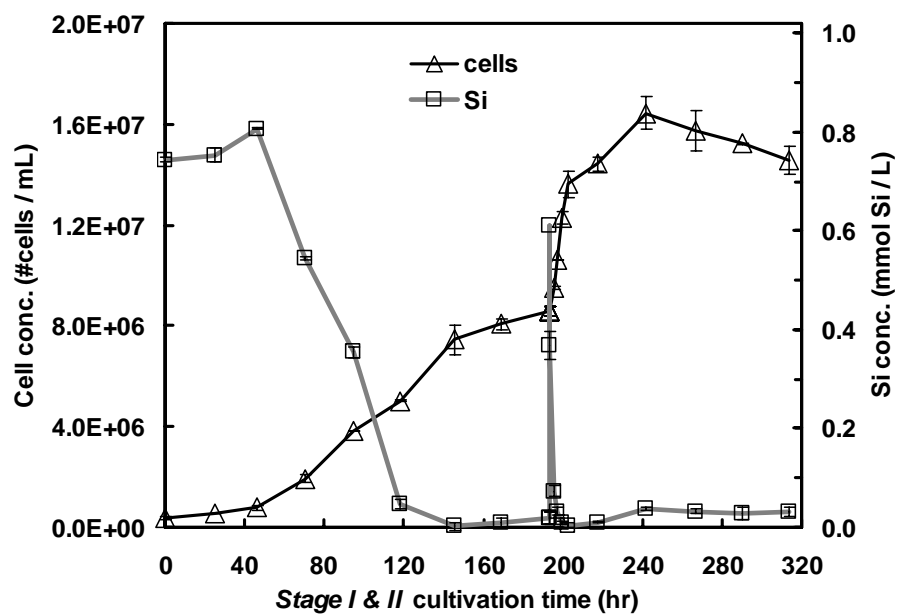


**Figure 3a.** The cell number density and Si concentration in liquid phase versus time  $C_{Si,O} = 0.6$  mM (Ge / Si = 0 mol Ge / mol Si)

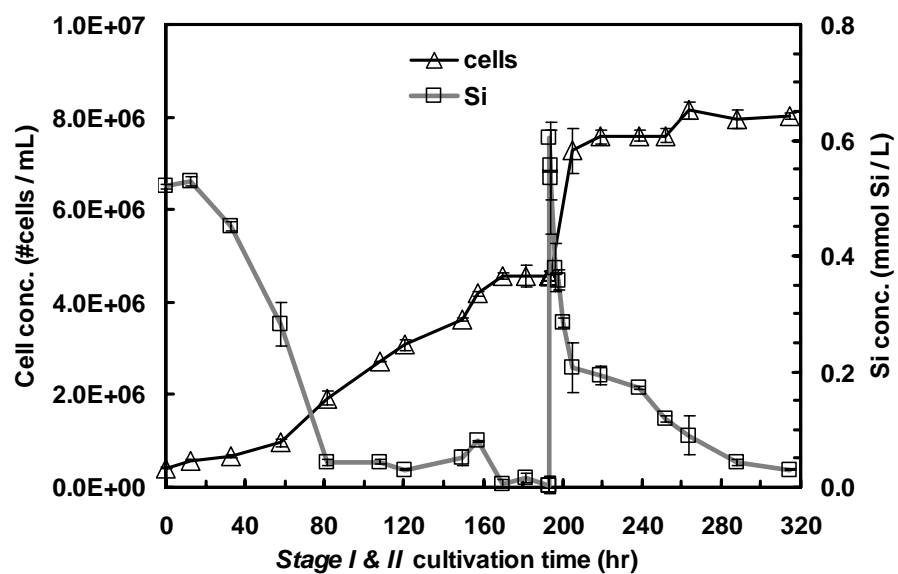


**Figure 3b.** The cell number density and Si concentration in liquid phase versus time  $C_{Si,O} = 0.6$  mM (Ge / Si = 0.02 mol Ge / mol Si)

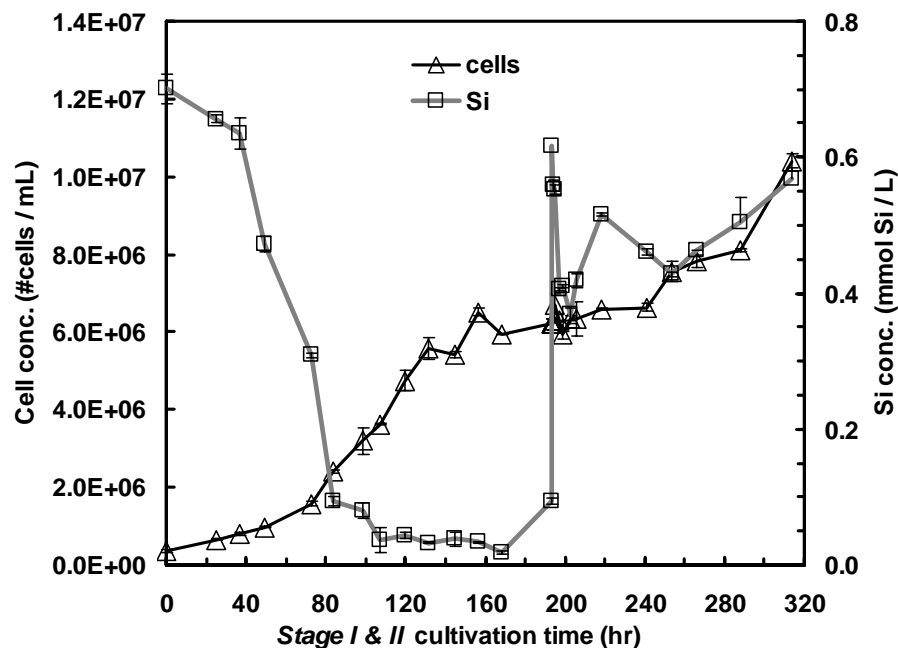


**Figure 3c.** The cell number density and Si concentration in liquid phase versus time  $C_{Si,O} = 0.6$  mM (Ge / Si = 0.14 mol Ge / mol Si)

Germanium and silicon concentration in liquid phase vs. time during stage II for bioreactor cultivation of *N. frustulum* with different initial germanium concentration in stage II are compared in Figure 4. The initial silicon concentration was fixed to 0.6 mM. Germanium to silicon molar ratio 0.02, 0.04 and 0.14 were achieved by setting the initial germanium concentration to 12.1, 23.4 and 85.1  $\mu$ M. During stage II of the cultivation process, surge uptake of silicon and germanium was observed in the first 12 hours. Soluble germanium uptake profile was similar to soluble silicon uptake profile in all three cases (Figure 4). In Figure 4a, both germanium and silicon went to zero after 120 hours of cultivation, when initial germanium concentration was 12.1  $\mu$ M. Germanium was completely consumed and silicon was 90% consumed after 120 hours of cultivation, when initial germanium concentration was 23.4  $\mu$ M (Figure 4b). Only 56% of germanium and 20% of silicon were uptaken, when initial germanium concentration was 85.1  $\mu$ M (Figure 4c).

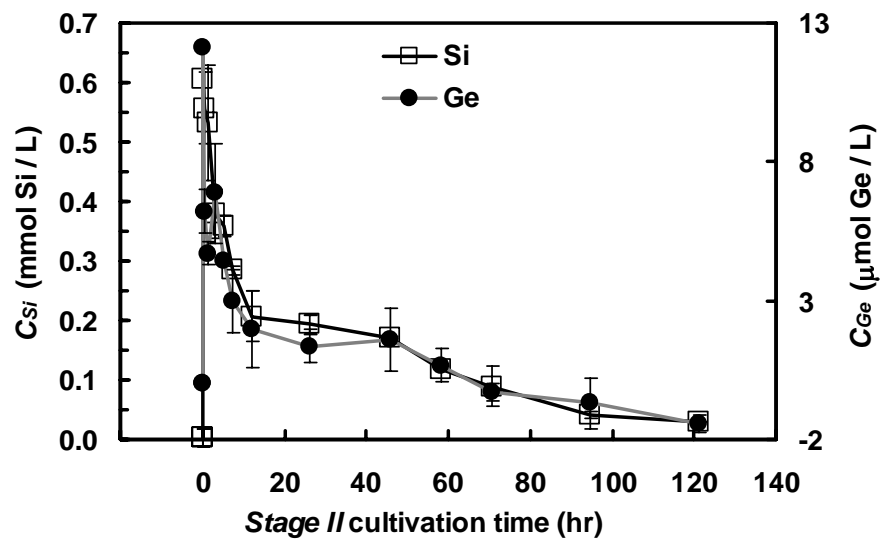


**Figure 4a.** The Ge and Si concentration in liquid phase versus time  $C_{Si,0} = 0.6$  mM (Ge / Si = 0.02 molGe / mol Si)

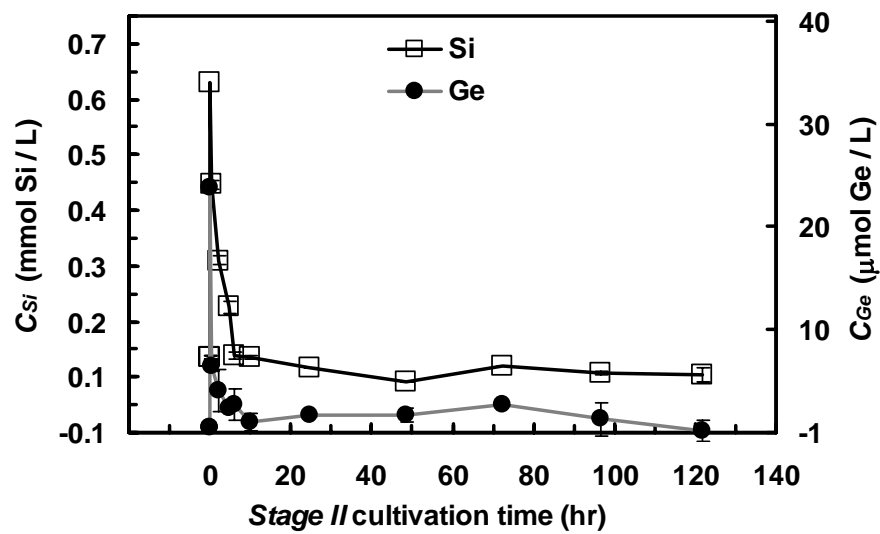


**Figure 4b.** The Ge and Si concentration in liquid phase versus time  $C_{Si,0} = 0.6$  mM (Ge / Si = 0.04 molGe / mol Si)

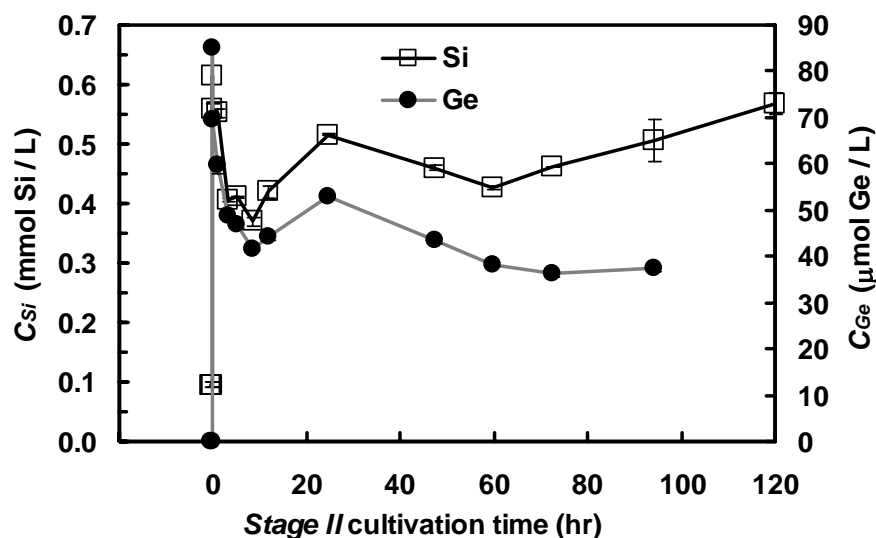


**Figure 4c.** The Ge and Si concentration in liquid phase versus time  $C_{Si,0} = 0.6$  mM (Ge / Si = 0.14 molGe / mol Si)

The growth parameters of *N. frustulum* with different initial germanium concentration in stage II are compared in Figure 5. The initial germanium concentration in stage II was set in the range of 0 to 85.1  $\mu$ M. The specific growth rate over the first 120 hours in stage I was  $0.0349 \pm 0.0053$   $\text{h}^{-1}$ , averaged from five independent cultivation experiments. The specific growth rate over the first 12 hours in stage II was not significantly different from that in stage I, when the initial germanium concentration was in the range of 0 to 30.4  $\mu$ M. However, when the initial germanium concentration was increased above 43.3  $\mu$ M, specific growth rate was much lower in stage II compared to that in stage I (Figure 5a).

The cell number yield and cell mass yield coefficients are presented in Figure 5b and 5c. No significant changes were observed for both cell number yield and cell mass yield coefficients, when the initial germanium concentration was increased from 0 to 43.3  $\mu$ M. However, regardless of the initial germanium concentration, cell mass yield coefficient was consistently much lower in stage II than in stage I. The cell number yield coefficient ( $Y_{Xn/Si}$ ) in stage I and stage II were  $8.39 \pm$

$1.00 \cdot 10^9$  and  $8.43 \pm 0.28 \cdot 10^9$  cells formed / mmol Si consumed, respectively, averaged from four independent cultivation runs. The cell mass yield coefficient ( $Y_{X/Si}$ ) in stage I and stage II were  $0.266 \pm 0.051$  and  $0.102 \pm 0.035$  g dry cell mass/ mmol Si consumed, respectively, averaged from four independent cultivation runs.

Uptake rate of silicon and germanium in the first 5 hours in stage II are shown in Figure 5d and 5e. When initial germanium concentration was increased from 12.1 to 85.1  $\mu\text{M}$ , both silicon and germanium uptake rates decreased. As shown in Figure 3d, silicon uptake rate decreased from  $0.339 \pm 0.052$  mL /  $10^7$  cells-hr to  $0.177 \pm 0.057$  mL /  $10^7$  cells-hr. Similarly, Figure 3e shows that germanium uptake rate decreased from  $0.458 \pm 0.018$  mL /  $10^7$  cells-hr to  $0.183 \pm 0.017$  mL /  $10^7$  cells-hr. All growth parameters of *N. frustulum* with different initial germanium concentration are summarized in Table 2.

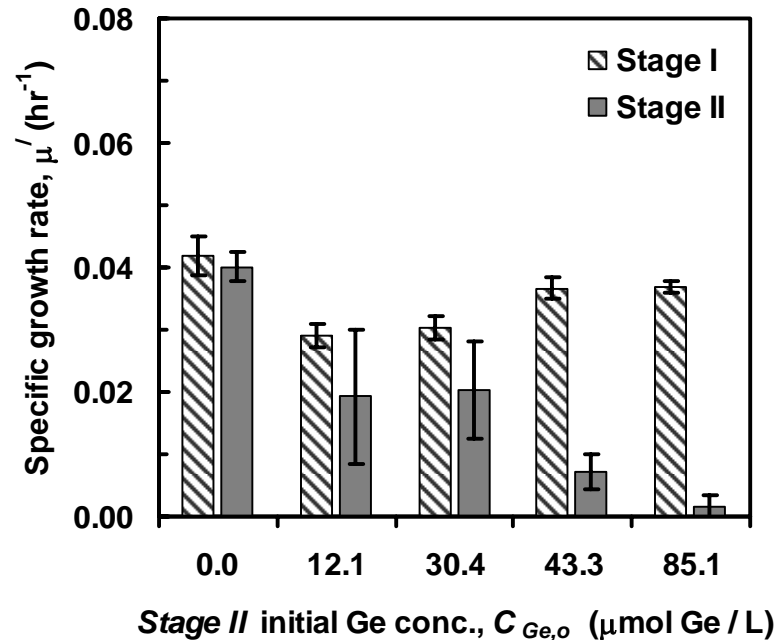


**Figure 5a.** Effect of initial Ge concentration on growth parameter, specific growth rate  $\mu'$  in stage I and II

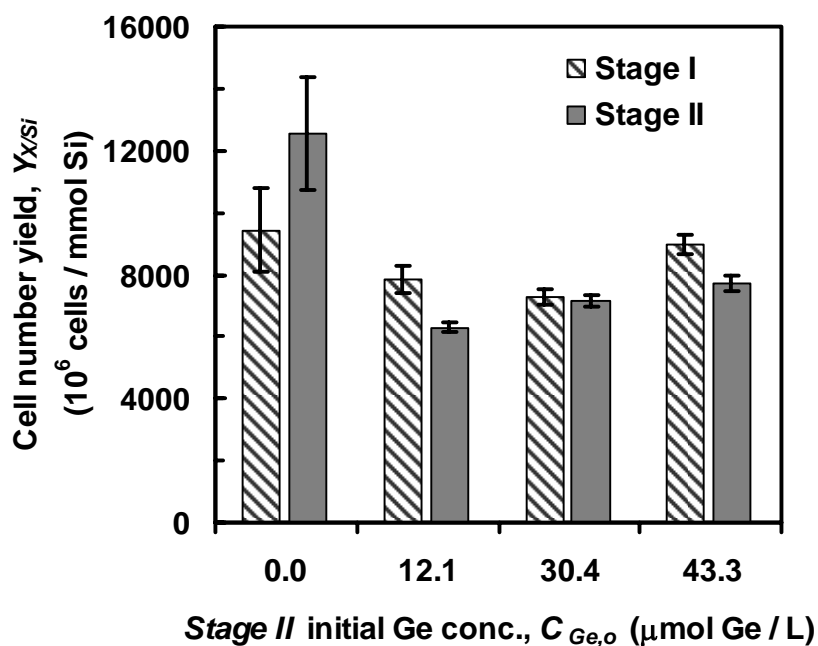


**Figure 5b.** Effect of initial Ge concentration on growth parameter, cell number yield  $Y_{X/Si}$  in stage I and II

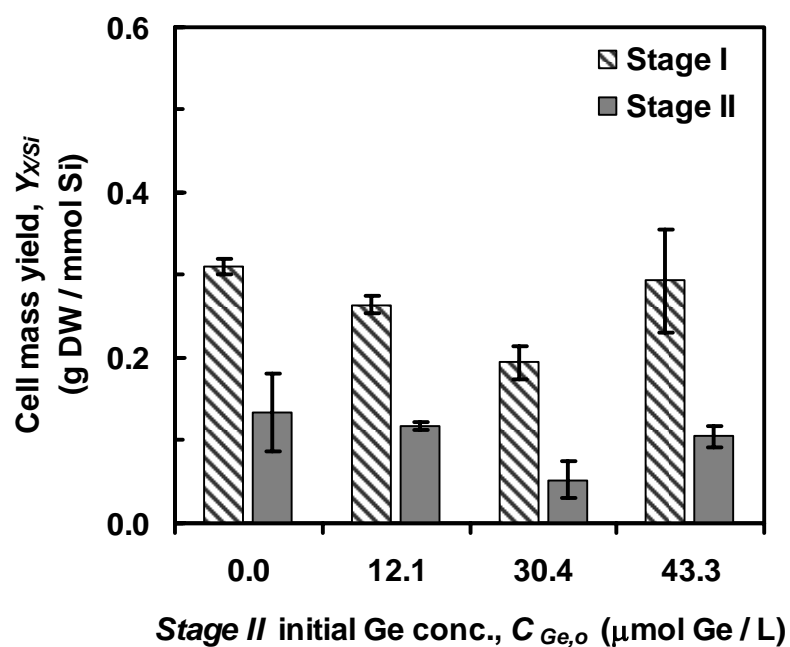


**Figure 5c.** Effect of initial Ge concentration on growth parameter, cell mass yield  $Y_{X/Si}$  in stage I and II

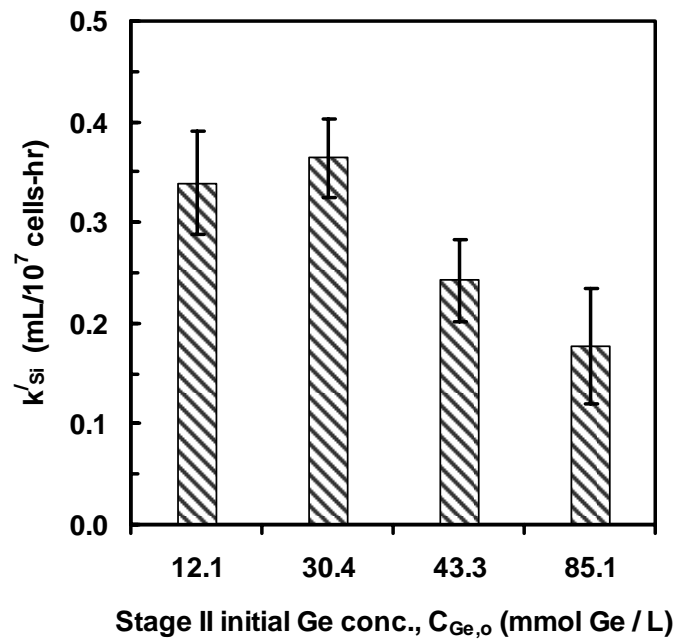


**Figure 5d.** Effect of initial Ge concentration on growth parameter, uptake rate of Si  $k'_{Si}$  in stage II

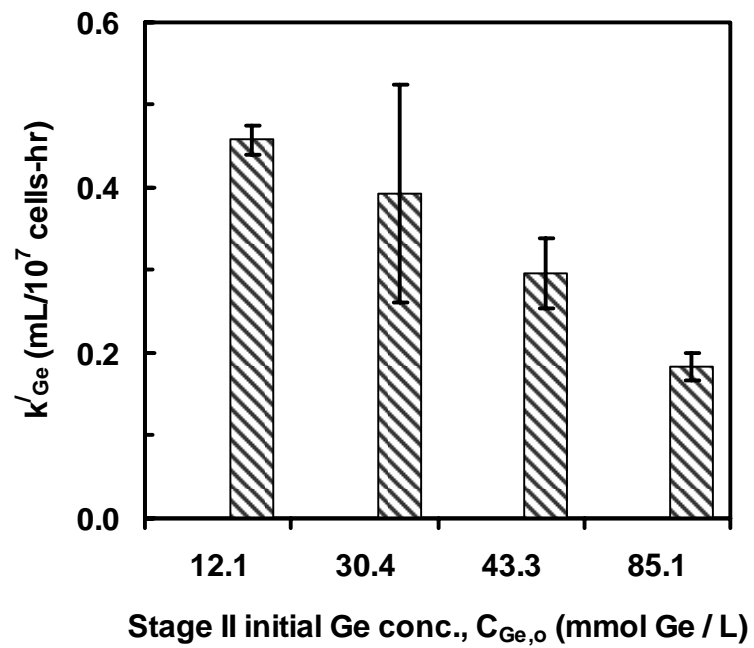


**Figure 5e.** Effect of initial Ge concentration on growth parameter, uptake rate of Ge  $k'_{Ge}$  in stage II

**Table 2.** Comparison of growth parameters of *Nitzschia frustulum* with Ge addition

Growth Parameter	Stage	Initial Germanium Concentration in Stage II					
		0.0 $\mu\text{mol/L}$			12.1 $\mu\text{mol/L}$		
Specific growth rate $\mu'$ ( $\text{hr}^{-1}$ )	I	0.0419	$\pm$	0.0032	0.0291	$\pm$	0.0018
	II	0.0401	$\pm$	0.0024	0.0192	$\pm$	0.0109
Cell number yield $Y_{Xn/Si}$ (#cells/mmol Si)	I	9.44E+09	$\pm$	1.33E+09	7.85E+09	$\pm$	4.25E+08
	II	1.26E+10	$\pm$	1.83E+09	6.30E+09	$\pm$	1.70E+08
Dry cell mass yield $Y_{X/Si}$ (g DW/mmol Si)	I	0.310	$\pm$	0.0103	0.265	$\pm$	0.0105
	II	0.135	$\pm$	0.047	0.117	$\pm$	0.023
Final cell mass density $X_f$ (g DW/L)	I	0.227	$\pm$	0.0000	0.150	$\pm$	0.0047
	II	0.301	$\pm$	0.104	0.215	$\pm$	0.041
Final cell number density $X_{N,f}$ (#cells/mL)	I	6.70E+06	$\pm$	5.97E+05	4.56E+06	$\pm$	1.06E+05
	II	1.30E+07	$\pm$	1.89E+06	8.04E+06	$\pm$	1.57E+05
Initial Si uptake rate $k'_{Si}$ (mL/10 <sup>7</sup> cells-hr)	II	0.285	$\pm$	0.036	0.339	$\pm$	0.052
Initial Ge uptake rate $k'_{Ge}$ (mL/10 <sup>7</sup> cells-hr)	II				0.458	$\pm$	0.018

**Table 2.** Comparison of growth parameters of *Nitzschia frustulum* with Ge addition (continued)

Growth Parameter	Stage	Initial Germanium Concentration in Stage II					
		30.4 $\mu\text{mol/L}$			43.3 $\mu\text{mol/L}$		
Specific growth rate	I	0.0302	$\pm$	0.0019	0.0366	$\pm$	0.0017
$\mu'(\text{hr}^{-1})$	II	0.0204	$\pm$	0.0078	0.0072	$\pm$	0.0028
Cell number yield	I	7.27E+09	$\pm$	2.35E+08	8.97E+09	$\pm$	3.39E+08
$Y_{Xn/Si}$ (#cells/mmol Si)	II	7.16E+09	$\pm$	2.30E+08	7.71E+09	$\pm$	7.60E+08
Dry cell mass yield	I	0.195	$\pm$	0.0194	0.293	$\pm$	0.0621
$Y_{X/Si}$ (g DW/mmol Si)	II	0.053	$\pm$	0.012	0.105	$\pm$	0.025
Final cell mass density	I	0.120	$\pm$	0.0114	0.212	$\pm$	0.0448
$X_f$ (g DW/L)	II	0.144	$\pm$	0.030	0.265	$\pm$	0.030
Final cell number density	I	4.51E+06	$\pm$	5.23E+04	6.56E+06	$\pm$	2.40E+05
$X_{N,f}$ (#cells/mL)	II	7.86E+06	$\pm$	2.53E+05	1.04E+07	$\pm$	1.02E+06
Initial Si uptake rate	II						
$k'_{Si}$ (mL/10 <sup>7</sup> cells-hr)		0.364	$\pm$	0.039	0.242	$\pm$	0.041
Initial Ge uptake rate	II						
$k'_{Ge}$ (mL/10 <sup>7</sup> cells-hr)		0.392	$\pm$	0.132	0.296	$\pm$	0.042

**Table 2.** Comparison of growth parameters of *Nitzschia frustulum* with Ge addition (continued)

Growth Parameter	Stage	Initial Germanium Concentration in Stage II				
		0.0	$\mu\text{mol/L}$		85.1	$\mu\text{mol/L}$
Specific growth rate	I	0.0419	$\pm$	0.0032	0.0369	$\pm$ 0.0010
$\mu'$ ( $\text{hr}^{-1}$ )	II	0.0401	$\pm$	0.0024	0.0015	$\pm$ 0.0020
Cell number yield	I	9.44E+09	$\pm$	1.33E+09	8.50E+09	$\pm$ 1.34E+09
$Y_{Xn/Si}$ (#cells/mmol Si)	II	1.26E+10	$\pm$	1.83E+09		
Dry cell mass yield	I	0.310	$\pm$	0.0103	0.323	$\pm$ 0.0383
$Y_{X/Si}$ (g DW/mmol Si)	II	0.135	$\pm$	0.047		
Final cell mass density	I	0.227	$\pm$	0.0000	0.234	$\pm$ 0.0278
$X_f$ (g DW/L)	II	0.301	$\pm$	0.104	0.282	$\pm$ 0.087
Final cell number density	I	6.70E+06	$\pm$	5.97E+05	6.28E+06	$\pm$ 2.54E+05
$X_{Nf}$ (#cells/mL)	II	1.30E+07	$\pm$	1.89E+06		
Initial Si uptake rate	II					
$k'_{Si}$ ( $\text{mL}/10^7\text{cells-hr}$ )		0.285	$\pm$	0.036	0.177	$\pm$ 0.057
Initial Ge uptake rate	II					
$k'_{Ge}$ ( $\text{mL}/10^7\text{cells-hr}$ )					0.183	$\pm$ 0.017

*Effect of initial germanium concentration in stage II on incorporation of germanium into biomass of N. frustulum*

The silicon content in dry cell biomass at the end of stage II with different initial germanium concentration in stage II are presented in Figure 6a. Silicon content in dry cell biomass was slightly increased as the initial germanium concentration was increased from 0 to 57.6  $\mu\text{M}$ . The germanium content in dry cell biomass was increased with initial germanium concentration, for both 24 and 120 hours of cultivation times in stage II. The results are compared in Figure 6b. The germanium content after 24 hours of cultivation time was consistently the same as germanium content after 120 hours. This probably indicated that the germanium uptake was completed in 24 hours, without being influenced by initial germanium concentration.

The germanium content in silica frustules isolated by hydrogen peroxide treatment of *N. frustulum* obtained at stage II cultivation times of 24 and 120 hours are compared in Figure 6c. The initial germanium concentration in stage II was in the range of 1.9 to 85.1  $\mu\text{M}$ . The hydrogen peroxide treatment was designed to gently oxidize the organic materials away from the insoluble silica frustules. Only 5-9 wt% of the dry cell biomass remained insoluble after hydrogen peroxide treatment, and this inorganic solid yield was not affected by the initial germanium concentration in stage II (Table 3). The germanium content in silica frustules after 120 hours of cultivation was much higher than germanium content after 24 hours, which probably indicated that the germanium incorporation was not completed by 24 hours of cultivation. The germanium content after 120 hours of cultivation was increased from  $0.154 \pm 0.012$  wt% to  $1.196 \pm 0.222$  wt%, when the initial germanium concentration increased from 1.9  $\mu\text{M}$  to 30.4  $\mu\text{M}$ . However, the germanium concentration then dropped back to  $0.509 \pm 0.124$  wt%, when initial germanium concentration was increased to 85.1  $\mu\text{M}$ .

**Table 3.** Spectroscopy analysis of Ge content in silica frustules isolated by hydrogen peroxide treatment of *Nitzschia frustulum* cell mass containing metabolically inserted germanium

Stage II Time (hr)		Initial Germanium Concentration in Stage II					
		1.9	$\mu\text{mol/L}$	23.4	$\mu\text{mol/L}$	30.4	$\mu\text{mol/L}$
24 [a]	Ge (wt%)	0.185	$\pm$ 0.023	0.202	$\pm$ 0.147	0.553	$\pm$ 0.087
120 [a]	Ge (wt%)	0.154	$\pm$ 0.012	0.344	$\pm$ 0.148	1.196	$\pm$ 0.222
0-120 [b]	g H <sub>2</sub> O <sub>2</sub> solid/ g DW	0.068	$\pm$ 0.048	0.177	$\pm$ 0.049	0.046	$\pm$ 0.049

**Table 3.** (continued)

Stage II Time (hr)		Initial Germanium Concentration in Stage II					
		43.3	$\mu\text{mol/L}$	57.6	$\mu\text{mol/L}$	85.1	$\mu\text{mol/L}$
24 [a]	Ge (wt%)	0.215	$\pm$ 0.157	0.045	$\pm$ 0.006	0.076	$\pm$ 0.028
120 [a]	Ge (wt%)	0.857	$\pm$ 0.391	1.070	$\pm$ 0.061	0.509	$\pm$ 0.124
0-120 [b]	g H <sub>2</sub> O <sub>2</sub> solid/ g DW	0.088	$\pm$ 0.000	0.085	$\pm$ 0.000	0.091	$\pm$ 0.000

[a] Average from 2 samples with 2 replicates per sample

[b] Average from stage II cultivation times of 0, 24, 72, and 120 hrs

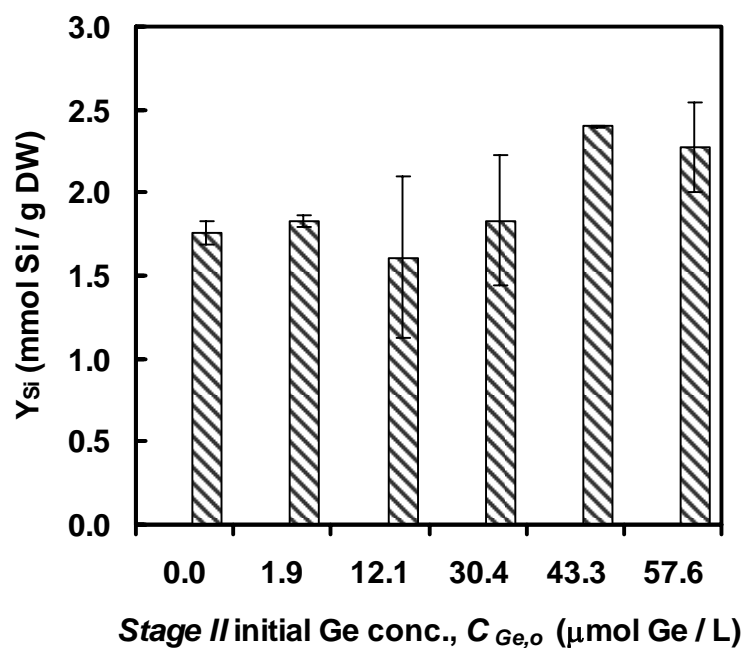


**Figure 6a.** Effect of initial Ge concentration on Si concentration in biomass  $Y_{Si}$  in stage II

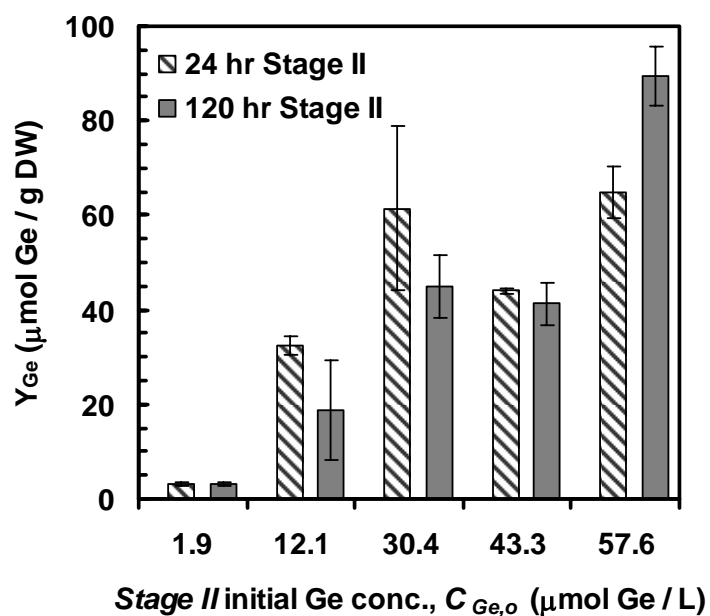


**Figure 6b.** Effect of initial Ge concentration on Ge concentration in biomass  $Y_{Ge}$  in stage II

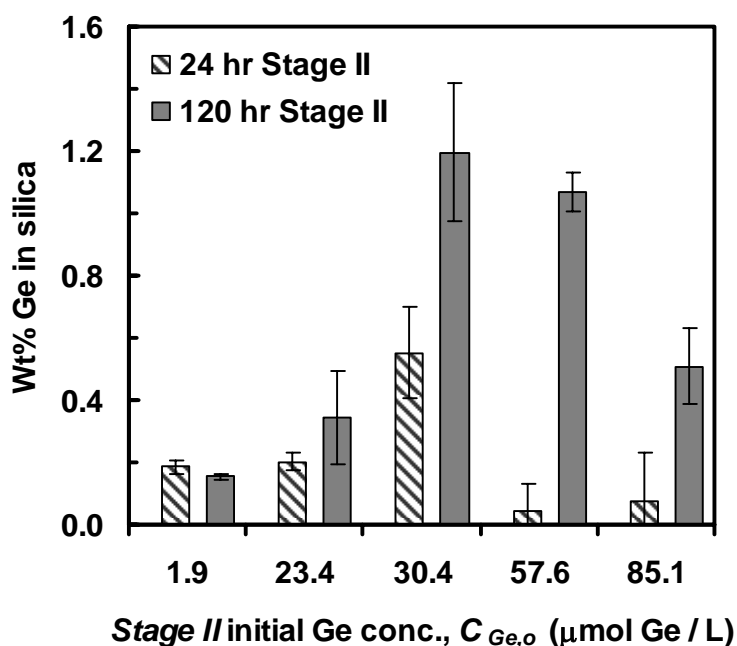


**Figure 6c.** Effect of initial Ge concentration on Ge concentration in silica frustules wt % Ge in stage II

*Effect of nitrate limitation in stage II on growth of *N. frustulum**

The cell number density and soluble silicon concentration vs. time for bioreactor cultivation of *N. frustulum* with different initial nitrogen concentration in stage I are presented in Figure 7. During Stage I of the cultivation process, soluble silicon uptake was growth associated. The dissolved silicon concentration went to zero after around 120 hours in stage I. The cells continued growing until they reached the stationary phase, where cell number density did not change with time any more. The initial silicon concentration in stage I was 0.6 mM, which provided enough substrate to achieve four cell doublings from the inoculum density. The cells were considered to be silicon starved, when both the soluble silicon concentration was near zero and the cell number density was constant for at least one photoperiod.

The initial nitrate concentration in stage I was 4.00 mM for the experiment shown in Figure 7a. This nitrate concentration was designed to be enough to achieve four

cell doublings from the inoculum density, but not enough to achieve another one cell doubling in stage II from the stage I final density. As shown, with nitrate limitation, silicon was not completely uptaken, although the cell number density was actually doubled after 120 hours of cultivation in stage II. The initial nitrate concentration in stage I was 8.00 mM for the experiment shown in Figure 7b. This nitrate concentration was designed to be enough to achieve four cell doublings from the inoculum density, and also enough to achieve another one cell doubling in stage II from the stage I final density. In this case, silicon was completely uptaken and the cell number density doubled after 120 hours of cultivation in stage II. As shown in Figure 7c, nitrate nutrient was limited when initial nitrate concentration was 4.00 mM. Nitrate concentration went to nearly zero after around 200 hours in the nitrate limitation experiment. Conversely, in the experiment with 8.00 mM initial nitrate concentration, nitrate concentration remained around 5.00 mM after approximately 330 hours, the end of the experiment.

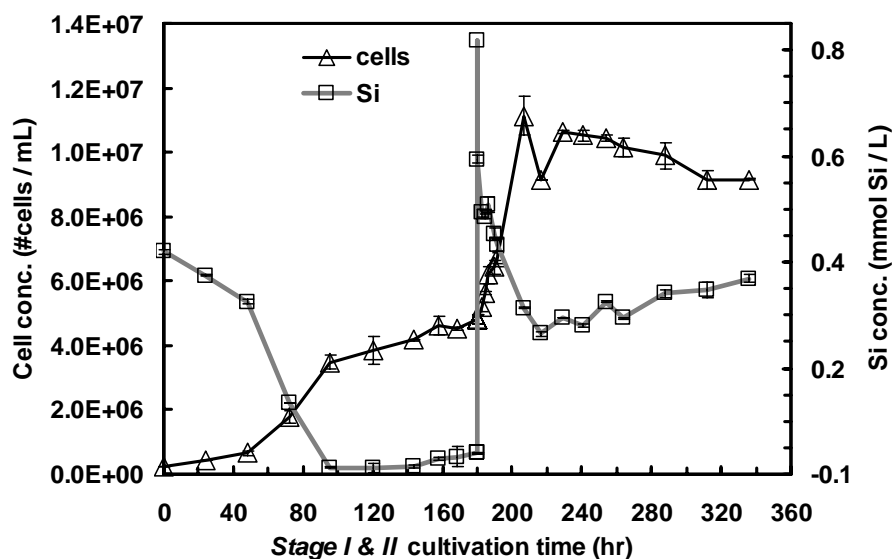


**Figure 7a.** Effect of initial nitrate concentration on Si uptake,  $C_{N,O} = 4.00$  mmol/L

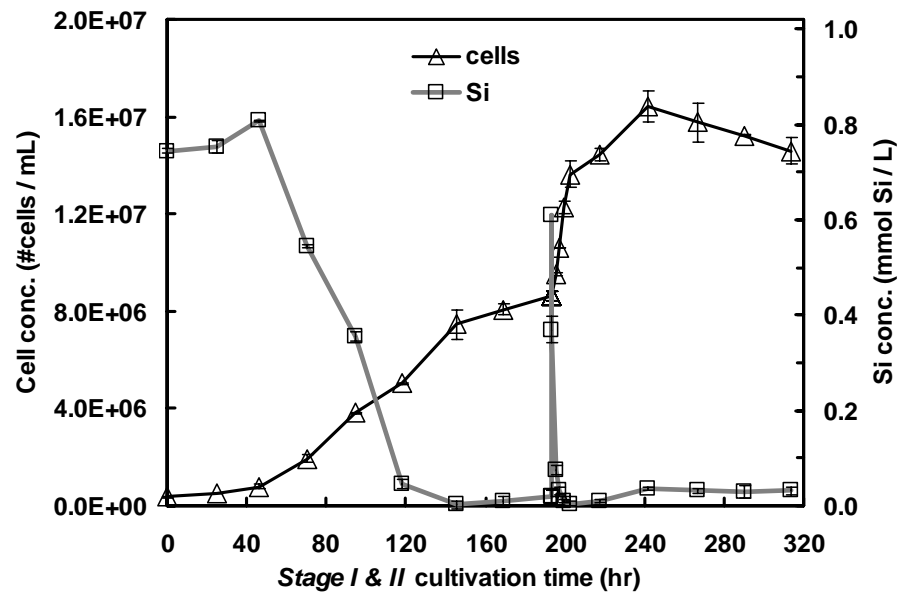


**Figure 7b.** Effect of initial nitrate concentration on Si uptake,  $C_{N,0} = 8.00$  mmol/L

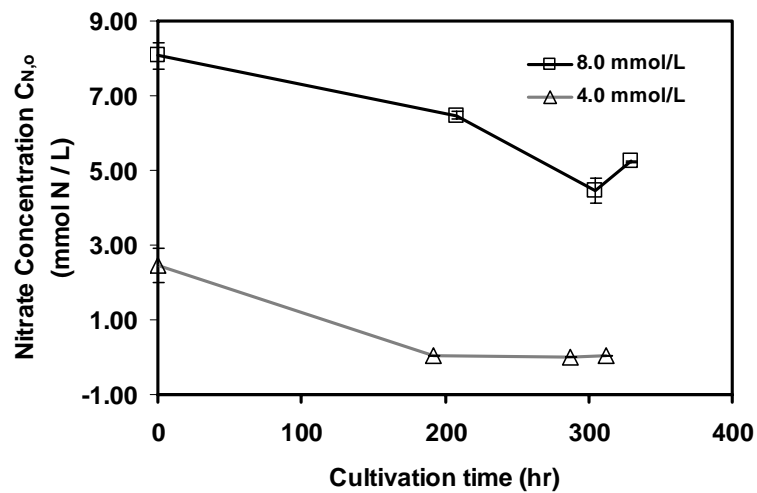


**Figure 7c.** Nitrate concentration in liquid phase versus time during stage I and stage II

The growth parameters of *N. frustulum* with different initial nitrate concentration in stage I are compared in Figure 8. The experiment results are based on different initial nitrate concentration in stage I. The 4.00 mM concentration was designed to

be enough for cell growth in stage I but not enough for cell growth in stage II (Nitrate limitation experiment). However, the 8.00 mM concentration in stage I was designed to be enough for cell growth in both stages (control experiment). The specific growth rate over the first 120 hours in stage I was the same for the two experiments (Figure 8a). With nitrate limitation, the specific growth rate over the first 12 hours of cultivation in stage II was much lower than specific growth rate of control experiment (Figure 8b). However, the cell number yield coefficient ( $Y_{Xn/Si}$ ) in stage II was not affected by nitrate limitation (Figure 8c). Figure 6d compares the uptake rate of silicon in the first 5 hours in stage II of the nitrate limitation experiment, with the control experiment. The silicon uptake rate of the nitrate limitation experiment was much lower than the silicon uptake rate of the control experiment. All growth parameters of *N. frustulum* with different initial nitrate concentration are summarized in Table 4.

**Table 4.** Comparison of growth parameters of *Nitzschia frustulum* with nitrate limitation

Growth Parameter	Stage	Initial Nitrate Concentration in Stage I			
		4.0	mmol/L	8.0	mmol/L
Specific growth rate	I	0.0431	± 0.0040	0.0419	± 0.0032
$\mu'$ (hr <sup>-1</sup> )	II	0.0282	± 0.0032	0.0401	± 0.0024
Cell number yield	I	9.31E+09	± 1.34E+09	9.44E+09	± 1.33E+09
$Y_{Xn/Si}$ (#cells/mmol Si)	II	9.84E+09	± 5.73E+08	1.26E+10	± 1.83E+09
Dry cell mass yield	I	0.486	± 0.0739	0.310	± 0.0103
$Y_{X/Si}$ (g DW/mmol Si)	II			0.135	± 0.047
Final cell mass density	I	0.243	± 0.0157	0.227	± 0.0000
$X_f$ (g DW/L)	II			0.301	± 0.104
Final Nitrate concentration	I	0.02	± 0.00		
$X_{Nitrate}$ (mmolNitrates/L)	II	0.03	± 0.00	5.23	± 0.03
Final cell number density	I	4.65E+06	± 1.96E+05	6.70E+06	± 5.97E+05
$X_{N,f}$ (#cells/mL)	II	9.40E+06	± 4.43E+05	1.30E+07	± 1.89E+06
$k'_{Si}$ (mL/10 <sup>7</sup> cells-hr)					
Initial Si uptake rate	II	0.109	± 0.050	0.285	± 0.036

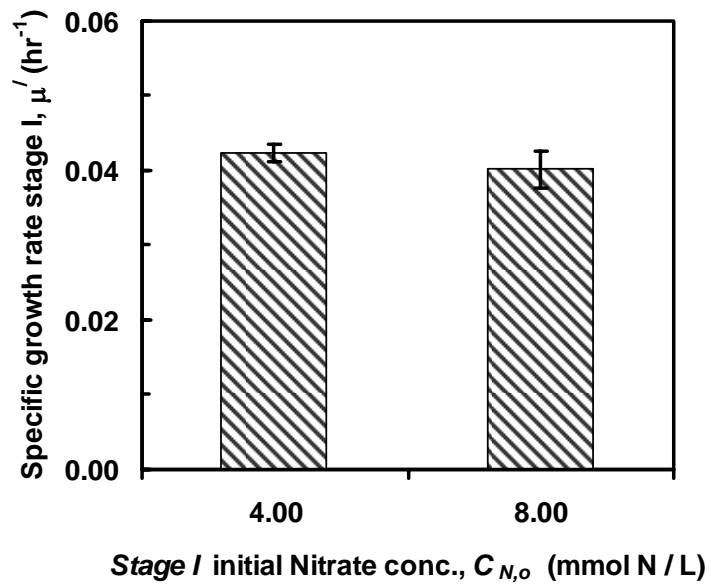


**Figure 8a.** Effect of nitrate limitation on growth parameters, specific growth rate  $\mu'$  in stage I

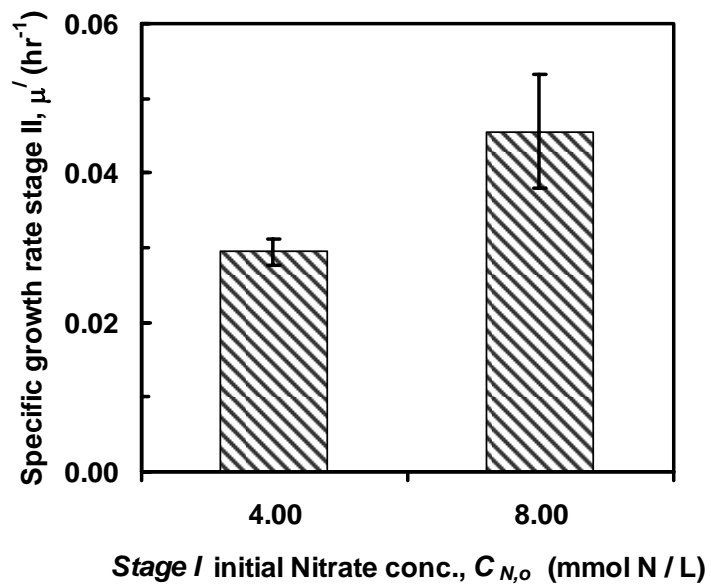


**Figure 8b.** Effect of nitrate limitation on growth parameters, specific growth rate  $\mu'$  in stage II

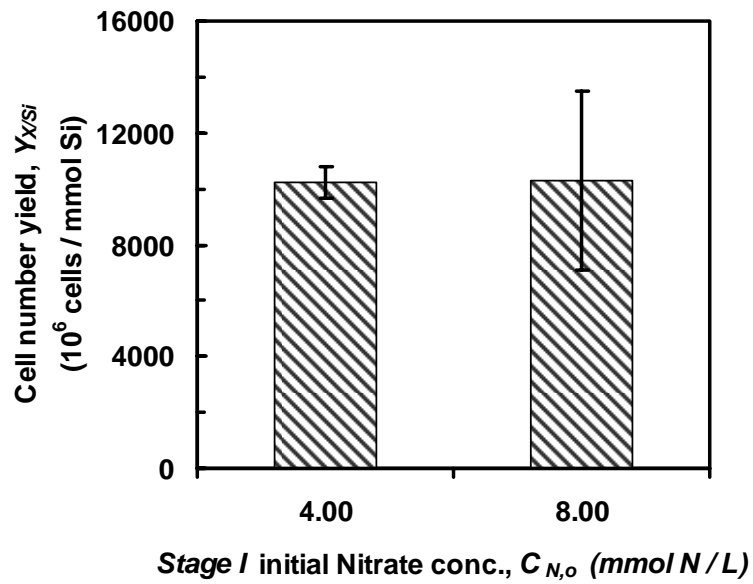


**Figure 8c.** Effect of nitrate limitation on growth parameters, cell number yield  $Y_{X/Si}$  in stage II

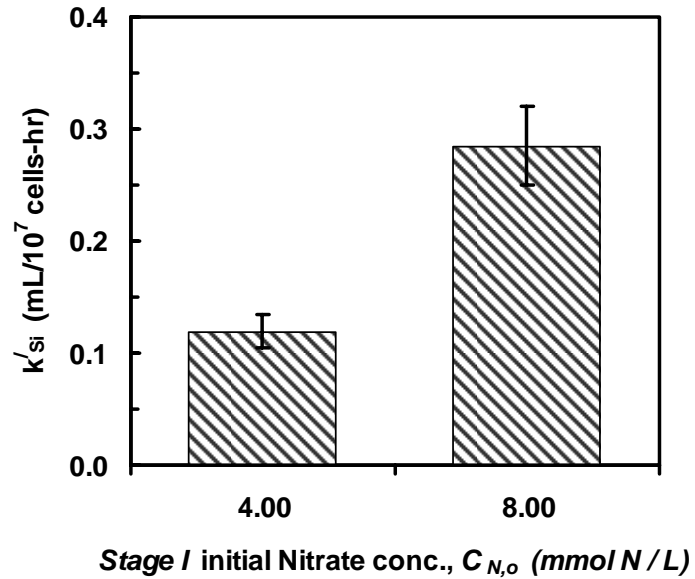


**Figure 8d.** Effect of nitrate limitation on growth parameters uptake rate of Si  $k'_{Si}$  in the first 5 hours in stage II

## Photoluminescence of diatoms

### *Effect of germanium insertion in silica frustules on photoluminescence (PL) properties*

The photoluminescence (PL) spectra of germanium inserted frustules and plain frustules (controls) of diatom *N. frustulum* are compared in Figure 9. PL intensity of germanium inserted frustules was consistently weaker than the controls at the cultivation time of 120 hours in stage II (Figure 9a and b). The PL spectra of germanium inserted frustules at the cultivation time of 97 hours before and after annealing are compared in Figure 9c. The PL intensity was completely quenched due to the heat treatment process (800 °C in air). The PL peak intensity of the controls and frustules containing metabolically inserted germanium along cultivation times are compared in Figure 10a and 10b. Each PL peak intensity was first averaged by duplicate measurements of intensities, and then normalized by the PL peak intensity at  $t = 0$  in stage II ( $I_{\text{ref}}$ ).  $I_{\text{ref}}$  was also averaged by duplicate measurements of intensities.

The PL peak wavelength of frustules containing no germanium (controls) and containing metabolically inserted germanium along cultivation times are compared in Figure 10c and 10d. Each PL peak wavelength was averaged by duplicate measurements of emission wavelengths. During the first 48 hours of cultivation (the exponential phase of stage II), the PL peak intensity of germanium inserted frustules was not very stable. In one set of experiments, the PL peak intensity of germanium inserted frustules was not different from the intensity of controls (Figure 10a), but the intensity was 2 to 5 times less intense in another set of experiments (Figure 10b). However, after 48 hours of cultivation (the stationary phase in stage II), the PL peak intensity of germanium inserted frustules was consistently weaker than the intensity of controls in both experiments (Figure 10a and b). Interestingly, the PL peak wavelength was not dependent upon the cell cultivation cycle, as shown in Figure 10c and d. Compared to PL peak wavelength of controls at 122 hours of cultivation in stage II, the 0.36 wt% germanium

inserted frustules had a blue shift around 34nm, whereas the 0.14 wt% germanium inserted frustules did not show an obvious wavelength shift. This might be explained by that the germanium content in the latter sample was too low to cause wavelength shift.

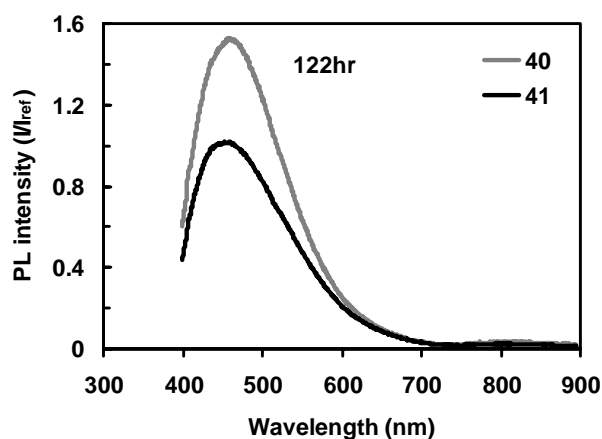


**Figure 9a.** Comparison of PL spectrum of frustules that contains no Ge (40) with that of 0.14 wt% Ge contained frustules (41)

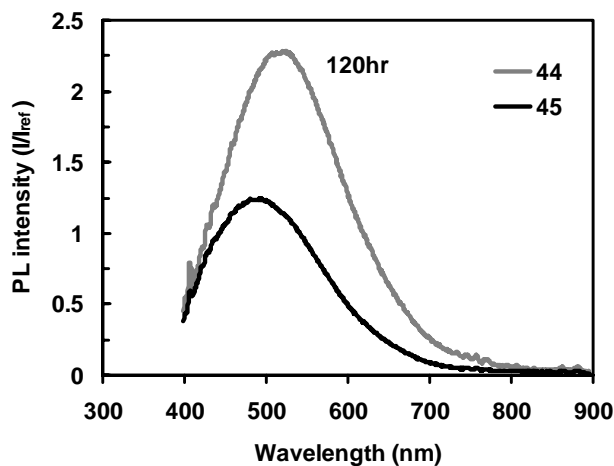


**Figure 9b.** Comparison of PL spectrum of frustules that contains no Ge (44) with that of 0.36 wt% Ge contained frustules (45)

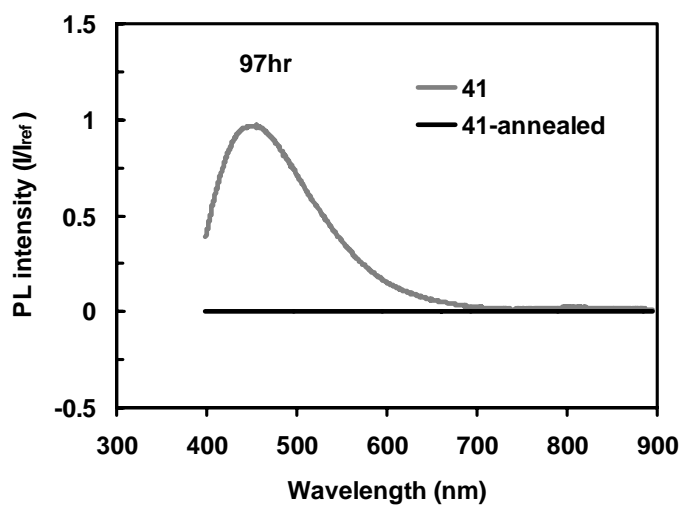


**Figure 9c.** Comparison of PL spectrum of Ge inserted frustules (0.14wt%) before and after annealing (800 °C in air)

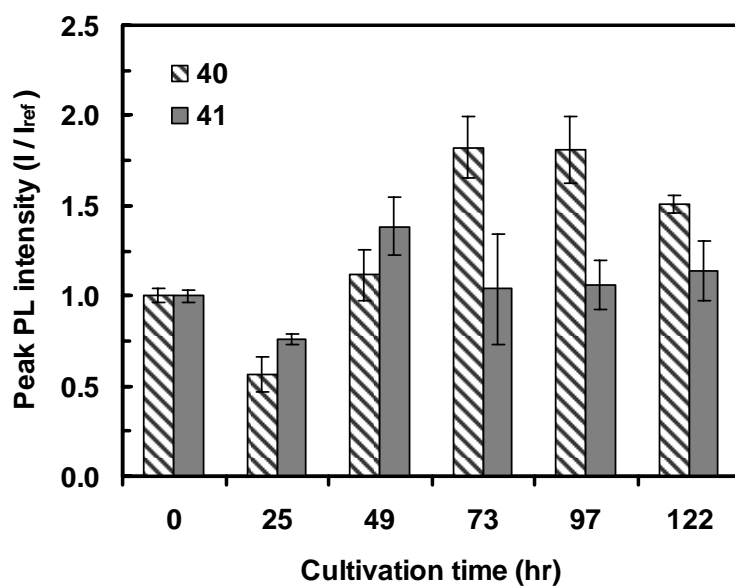


**Figure 10a.** PL peak intensity comparison of frustules containing no Ge (40) with that of frustules containing 0.14 wt% Ge (41)

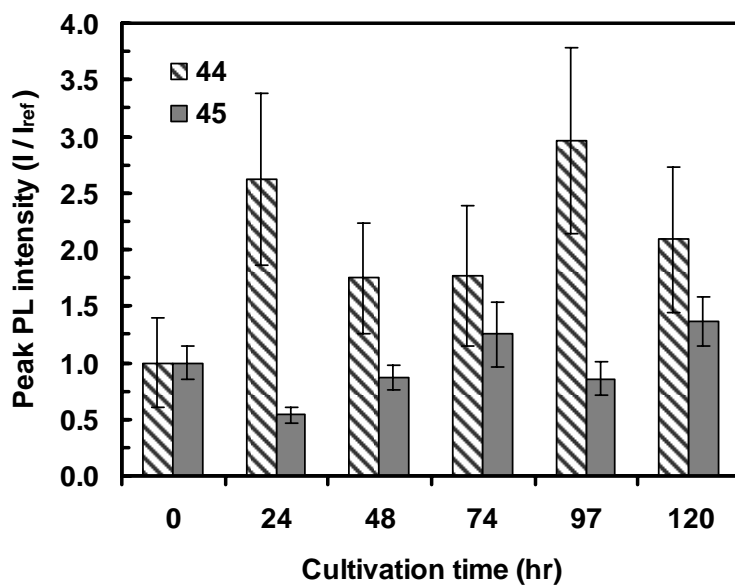


**Figure 10b.** PL peak intensity comparison of frustules containing no Ge (44) with that of frustules containing 0.36 wt% Ge (45)

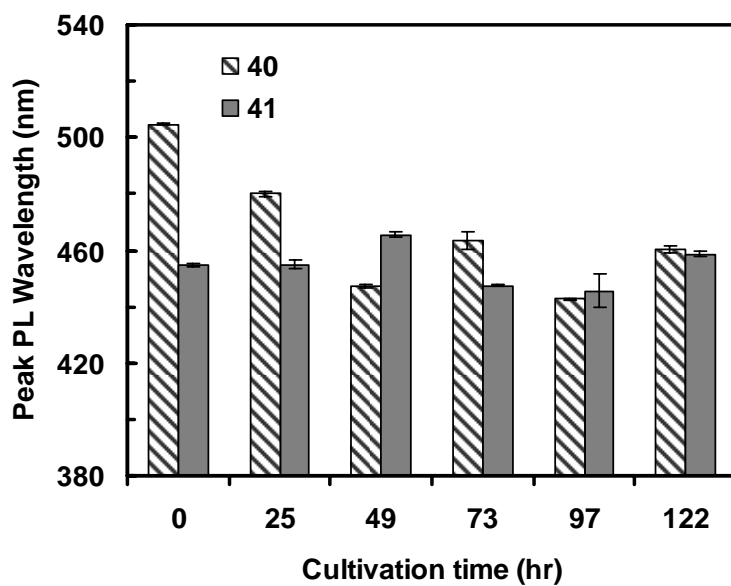


**Figure 10c.** PL peak wavelength comparison along cultivation time in stage II 0 wt% Ge (40) and 0.14 wt% Ge (41)

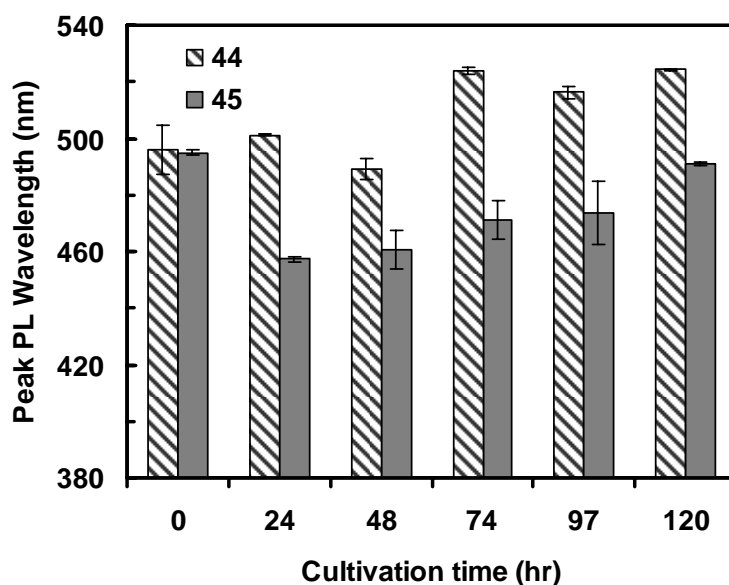


**Figure 10d.** PL peak wavelength comparison along cultivation time in stage II 0 wt% Ge (44) and 0.36 wt% Ge (45)

*Effect of germanium concentration incorporated in silica frustules on photoluminescence (PL) properties*

The photoluminescence (PL) spectra of frustules containing 0 wt% Ge (controls) and 1.20 wt% Ge at the cultivation time of 120 hours in stage II are compared in Figure 11a. Compared to the controls, the PL peak intensity was diminished by 7 times when 1.20 wt% Ge was inserted into *N. frustulum* diatom frustules. The PL peak intensity and peak wavelength of frustules containing five different amounts of metabolically inserted germanium at 120 hours of cultivation in stage II are presented in Figure 11b and c. The amounts of germanium, ranging from 0 – 1.20 wt% Ge, were obtained in five different cultivation experiments. “Control” refers to a sample that had no germanium addition at the beginning of stage II, and ended up with 0 wt% Ge incorporation. Each PL peak intensity was first averaged by duplicate measurements of intensities, and then normalized by the PL peak intensity at  $t = 0$  in stage II ( $I_{ref}$ ).  $I_{ref}$  was also averaged by duplicate measurements of intensities. Each PL peak wavelength was averaged by duplicate measurements of peak emission. The results show that the PL peak intensity was decreased with

germanium content incorporated in frustules. The PL peak wavelength of 1.20 wt% germanium incorporated frustules had a blue shift around 67 nm compared to the control; however, the PL peak wavelength was not very sensitive to the germanium concentration incorporated in silica frustules.

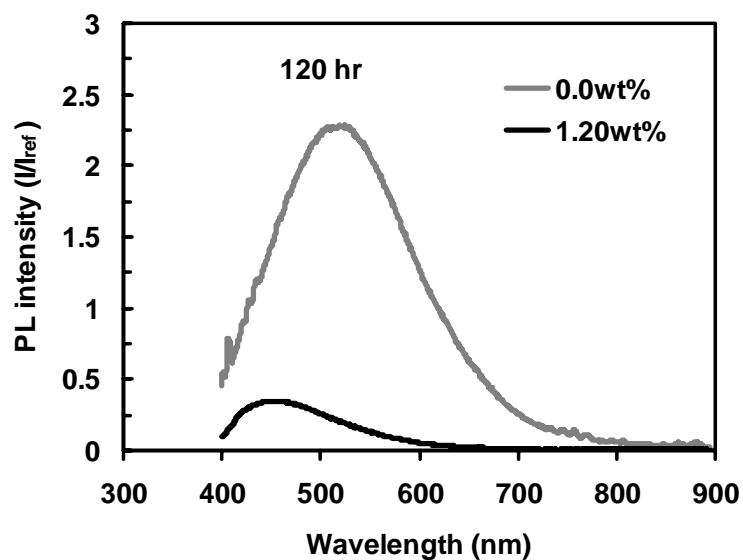


**Figure 11a.** Comparison of PL spectrum of 0 wt% Ge inserted frustules with 1.20 wt% Ge inserted frustules in stage II

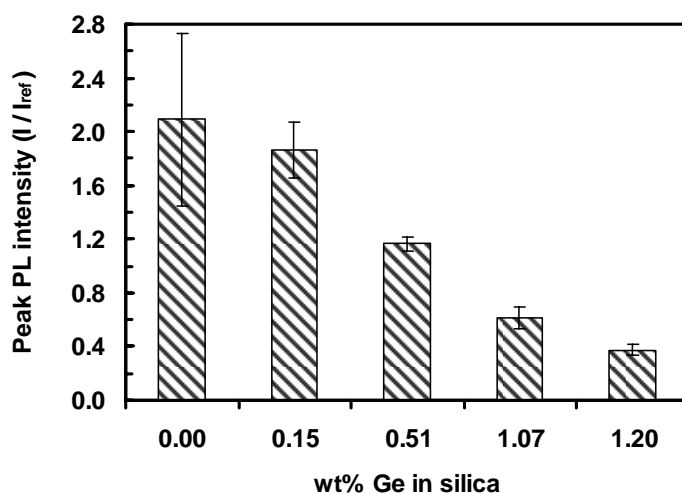


**Figure 11b.** Effect of Ge concentration in biosilica in stage II on PL peak intensity of the frustules in stage II

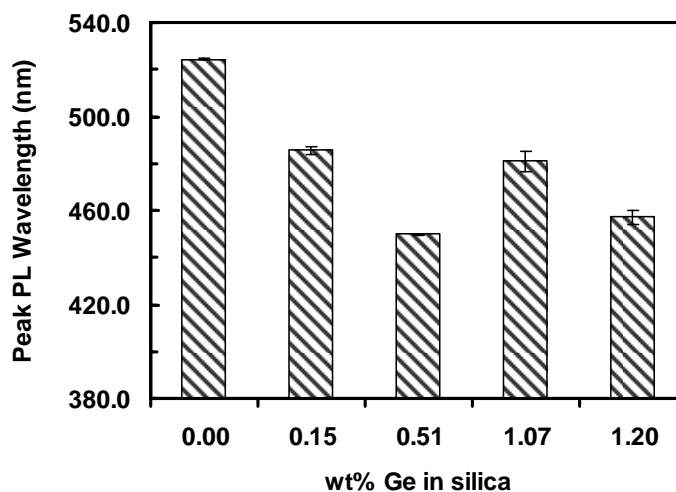


**Figure 11c.** Effect of Ge concentration in biosilica in stage II on PL peak wavelength of the frustules in stage II

*Effect of nitrate limitation on photoluminescence (PL) of frustules*

The photoluminescence (PL) peak intensity and peak wavelength of *N. frustulum* diatom frustules along cultivation times in stage II are presented in Figure 12a and b. Each PL peak intensity was determined from an average of intensities of samples, from two independent cultivation experiments. For each sample, duplicate PL intensity measurements were taken. Each averaged intensity was then normalized by the PL peak intensity at  $t = 0$  in stage II ( $I_{\text{ref}}$ ).  $I_{\text{ref}}$  was determined using the same process described above, with samples taken at  $t = 0$  in stage II. Each PL peak wavelength was determined from an average of wavelengths of samples, from two independent cultivation experiments. For each sample, duplicate emission wavelength measurements were taken. As shown in Figure 12, the PL peak intensity and wavelength did not change much along the cultivation times.

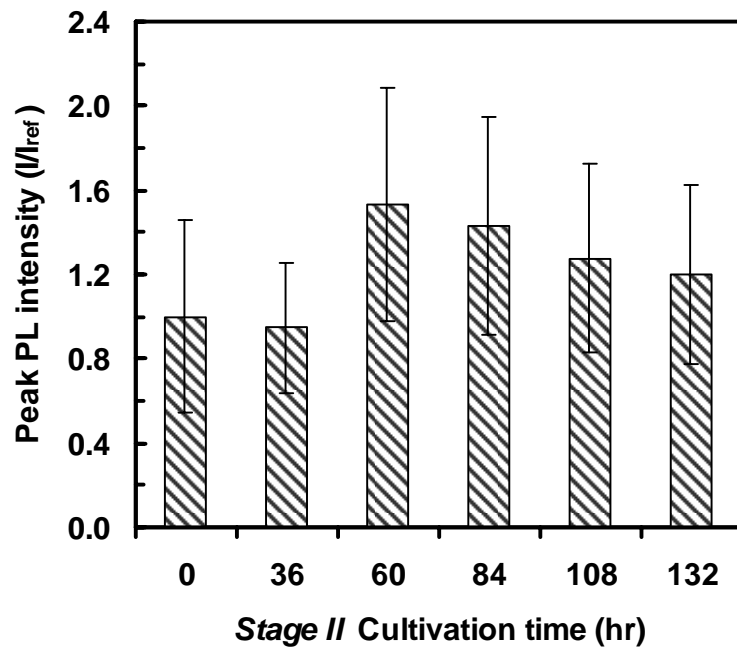


**Figure 12a.** PL peak intensity of frustules along cultivation time in stage II with nitrate limitation in stage II

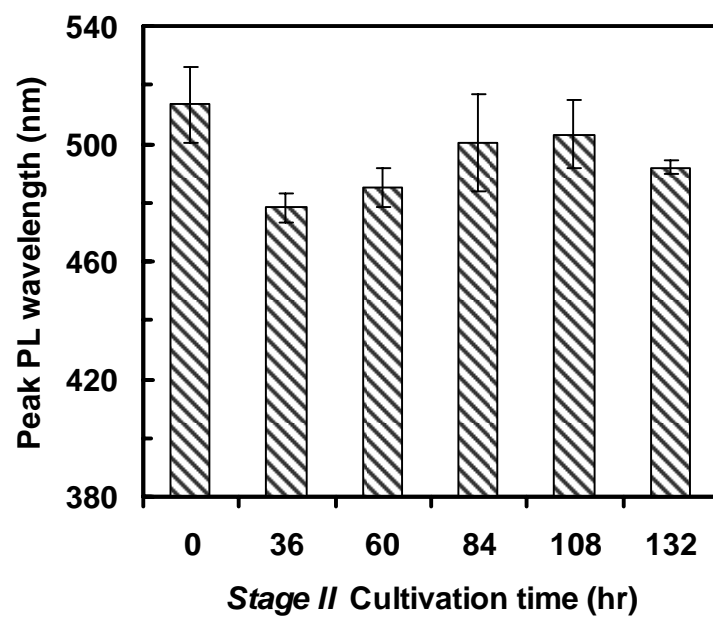


**Figure 12b.** PL peak wavelength of frustules along cultivation time in stage II with nitrate limitation in stage II

### TEM analysis of submicron morphology

TEM images of intact silica frustules of *N. frustulum* obtained after 120 hours of cultivation in stage II are presented in Figure 13. The images of frustules with no germanium addition in stage II (control) are shown in Figure 13a, b, and c at micron (1  $\mu\text{m}$ ), submicron (0.2  $\mu\text{m}$ ), and nanoscale (100 nm), respectively. As shown, the pennate diatom *N. frustulum* has an ellipsoidal shape of nominally 3  $\mu\text{m}$  width by 10  $\mu\text{m}$  length. The frustule possesses upper and lower shells called theca that fit together like a Petri dish. Each theca consists of a top lid called a valve, which has an array of pores running parallel to the transverse axis, and a girdle band, which consists of a ring of pores that are wrapped around the valve. The diameter of the frustule valve pores nominally ranged from 175 to 200 nm. The images of frustules with 50.4  $\mu\text{M}$  initial germanium addition in stage II are shown in Figure 13d, e, and f at micron, submicron, and nanoscale, respectively. Compared to the microstructure of the control, the overall shape and the length of the Ge-doped frustule remained the same (Figure 13 d). However, the two valves were opened up without wrapping by the girdle band, and the pore structure disappeared. The close-up images show that the array of pores were fused together to form a “slit-like” structure (Figure 13e and f).

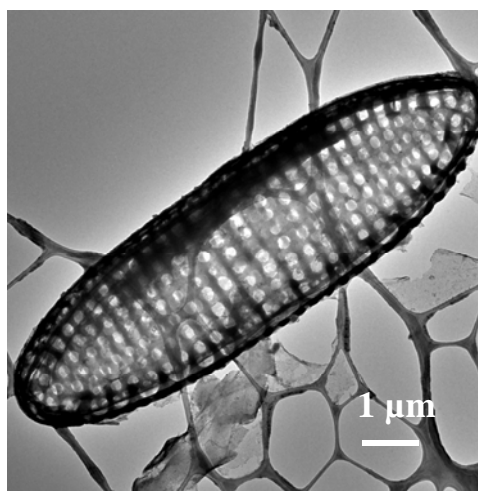


**Figure 13a.** TEM images of intact silica frustules at micron scale with 0  $\mu\text{mol}$  Ge/L (control) being added in stage II

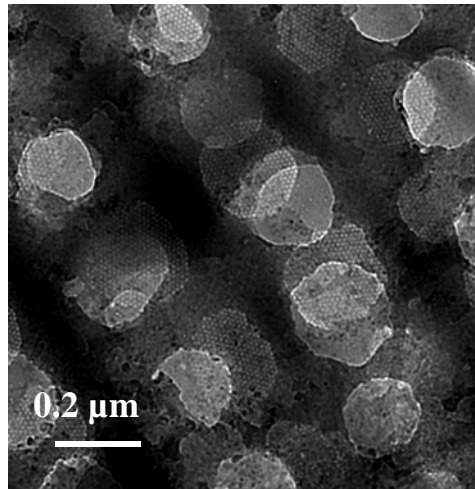


**Figure 13b.** TEM images of intact silica frustules at submicron scale with 0 μmol Ge/L (control) being added in stage II

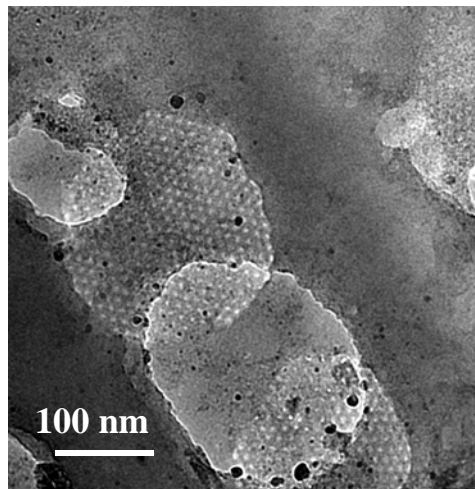


**Figure 13c.** TEM images of intact silica frustules at nano scale with 0 μmol Ge/L (control) being added in stage II

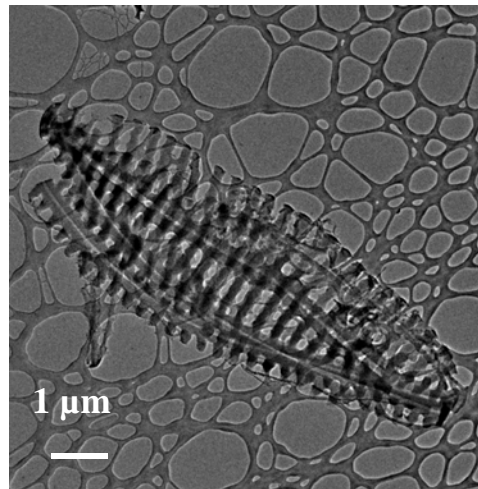


**Figure 13d.** TEM images of intact silica frustules at micron scale with 50.4  $\mu\text{mol Ge/L}$  being added in stage II

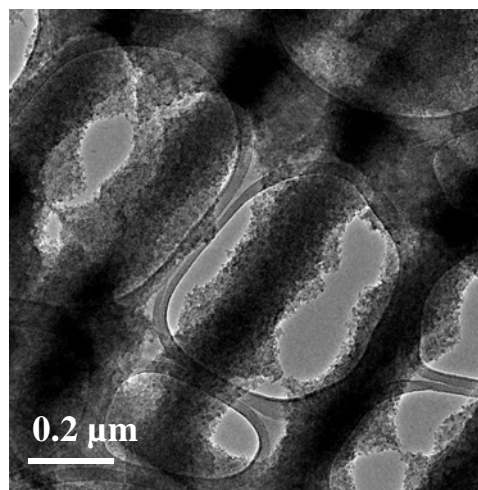


**Figure 13e.** TEM images of intact silica frustules at submicron scale with 50.4  $\mu\text{mol Ge/L}$  being added in stage II

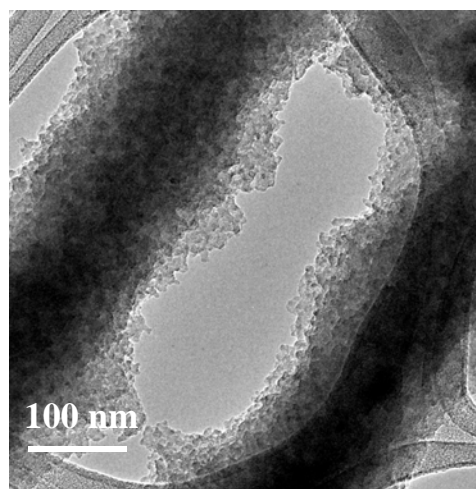


**Figure 13f.** TEM images of intact silica frustules at nano scale with 50.4  $\mu\text{mol Ge/L}$  being added in stage II

#### **FT-IR Analysis**

FT-IR spectra of *N. frustulum* frustule powder isolated by aqueous hydrogen peroxide treatment of diatom cells obtained at the end of stage II (120 hours) is presented in Figure 14. FT-IR spectra clearly showed characteristic peaks for diatom biosilica, including for Si-O-Si bending at 470 and 800  $\text{cm}^{-1}$  (Schmidt et al., 2001 and Gendron-Badou et al., 2003), Si-O stretching of Si-OH groups at 950  $\text{cm}^{-1}$  (Schmidt, et al., 2001 and Gendron-Badou et al., 2003), Si-O-Si stretching at 1095  $\text{cm}^{-1}$  (Schmidt et al., 2001 and Gelabert et al., 2004), and O-H stretching of bound water surface hydroxyl groups at 3435  $\text{cm}^{-1}$  (Khraisheh et al., 2005), which could also include an H-O-Si stretching mode. There were no discernable peaks corresponding to H-SiO<sub>3</sub>, H-Si(O<sub>2</sub>Si) and H-Si(OSi<sub>2</sub>) stretching at 2250, 2180, 2080  $\text{cm}^{-1}$  respectively (Zhu et al., 1998). Consequently, the frustule biosilica possessed silanol ( $\equiv\text{Si-OH}$ ) groups but not silicon hydride ( $\equiv\text{Si-H}$ ) groups.

*N. frustulum* frustules isolated by hydrogen peroxide treatment of diatom cells were thermally annealed in air at 800°C for 1.0 hr. The FT-IR spectra of thermally-annealed frustule powder from diatom cells obtained at the end of stage II (120 hours) is also presented in Figure 14. After thermal annealing in air, the

950  $\text{cm}^{-1}$  peak characteristic of silanol (Si-OH) disappeared, a result consistent with an early IR spectroscopy study of cultured diatom biosilica (Kamatani, et al., 1971)

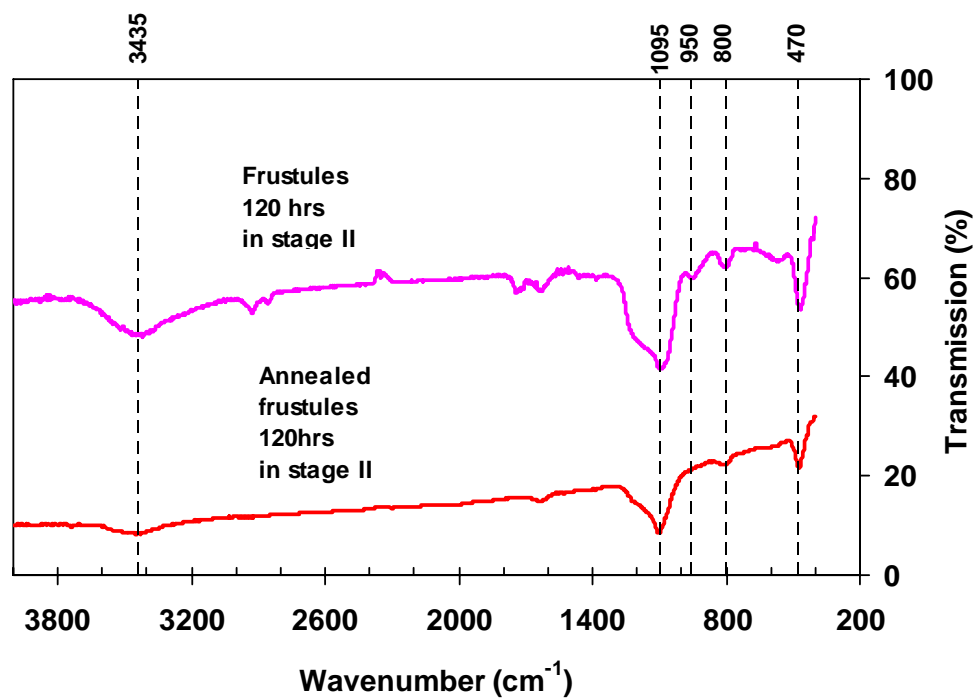


**Figure 14.** FT-IR spectra of *N. frustulum* frustules before and after annealing

## **Discussion**

### **Effect of germanium insertion on growth of *N. frustulum***

In this study we developed a two-stage photobioreactor process to metabolically insert germanium into the marine diatom *N. frustulum*. Cells were grown to silicon starvation in stage I, and germanium and silicon were co-added into the culture in stage II (Figure 3). Surge uptake happened after silicon starvation, which largely increased the germanium and silicon uptake rate (Sullivan, 1977). Early studies reported germanium as an inhibitor of diatom growth even at a very low concentration (Lewin, 1966). However, no inhibition of growth or silicon uptake was observed when germanium and silicon was co-added at a low molar ratio (Azam et al., 1973; Azam and Volcani, 1974; Mehard et al., 1974). Our current study also showed that the germanium did not inhibit diatom *N. frustulum* growth or the silicon uptake when germanium to silicon molar ratio was less than 0.05 (Figure 3-5). Inhibition of diatom growth and silicon uptake was observed when germanium to silicon molar ratio was increased to 0.14 (Figure 3-5); our result was in agreement with the finding by Azam et al. (1973), who found the inhibition molar ratio was 0.1 for *N. alba*. The specific growth rate was largely decreased due to high germanium addition (Figure 5a), which will, as a result, affect the silicon and germanium content in the biomass (Figure 6a and b).

It was believed that the silicon metabolism in diatom was linked to the cell cycle and not directly to photosynthesis (Martin-Jezequel et al., 2000). The cell cycle is classically divided into four phases: G1, S, G2, and M. The DNA are replicated during the S phase, mitosis and cell division happen in the M phase, and G1 and G2 are “gaps” in the cycle, during which most of the cell growth takes place (Mitchison 1971). It was found that the lower cell growth rate tended to elongate G2 + M phase, during which the greatest portion of silicon uptake took place (Claquin et al., 2002). Therefore, the amount of biogenic silica per cell can be speculated to increase at a lower growth rate due to higher germanium addition

(Figure 6a and b). The germanium incorporation into the frustules had been verified by spectroscopy measurements (Figure 6c). We also verified germanium incorporation by TEM-EDX (Figure 15b). Since the germanium uptake profile was similar to silicon uptake (Figure 4) and the TEM-EDX line scan also showed a similar profile of germanium and silicon incorporation in biosilica (Figure 15a), it could be predicted that biogenic germanium per cell should also be increased due to higher initial germanium addition. However, the biogenic germanium incorporation might not keep on increasing, as the cell growth would be completely inhibited when initial germanium concentration was too high, e.g., Ge / Si = 0.14 mol Ge / mol Si (Figure 6c).

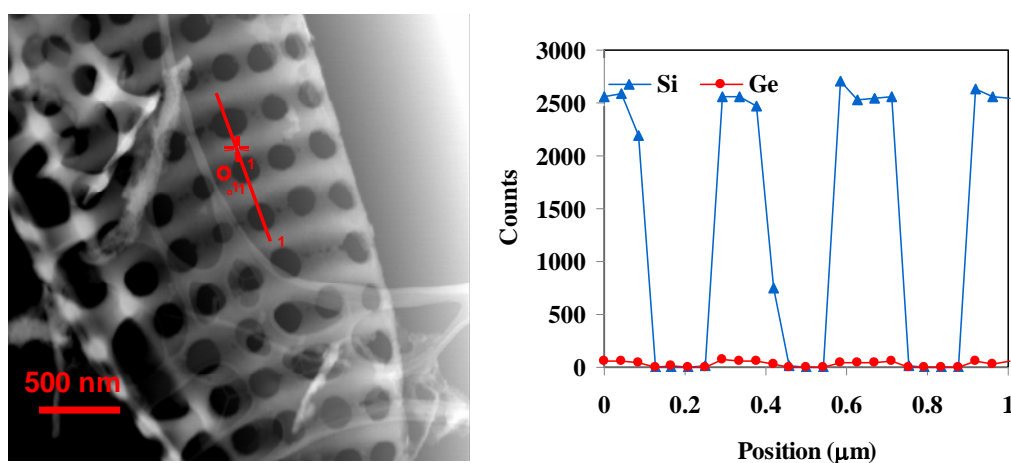


**Figure 15a.** A representative spectrum of STEM line scans of frustule with Ge incorporation (sample Ni-BC-45)

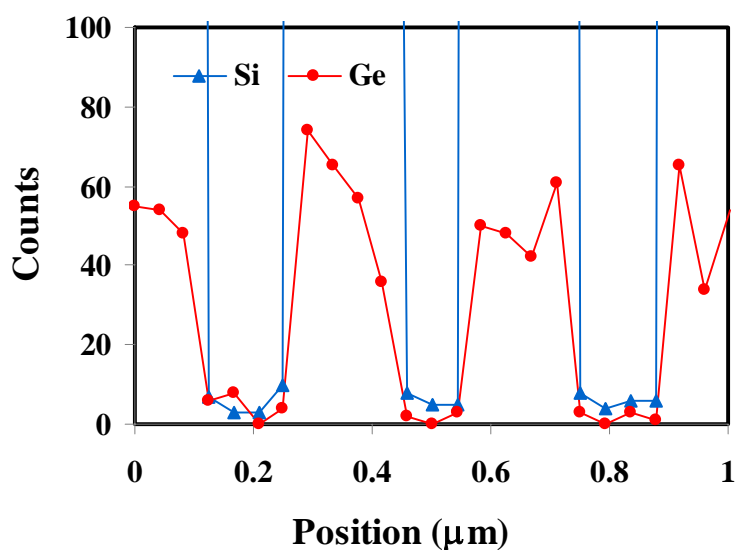


**Figure 15b.** The blowup of spectrum of STEM line scans from figure 15a.

Our experiments showed that cell growth rate and silicon uptake rate were largely reduced during cultivation with nitrate limitation (Figure 8). Nitrogen metabolism is regulated during the course of the cell cycle (Hildebrand and Dahlin, 2000). Studies have shown that nitrogen-starved cells were arrested in the G1 phase for species *H. carterae* and *T. weissflogii*, which implied that the G1 phase was nitrogen dependent (Olson et al. 1986). The elongation of the G1 phase due to nitrogen deficiency will cause lower cell growth rate and smaller mean cell volume. Another study on species *T. pseudonana* showed the nitrogen-dependent phase was G2 + M (Claquin et al., 2002). Although the nitrogen-dependent phase was different, both authors drew the conclusion that cell growth rate was decreased due to nitrogen limitation, which agreed with our results.

High concentration germanium addition ( $\text{Ge} / \text{Si} = 0.1 \text{ mol Ge} / \text{mol Si}$ ) interrupted the development of cell walls of diatoms and ended up with abnormal valves (Chiappino et al., 1977). This morphology aberration on diatom *Synedra acus* was also observed in the presence of germanic acid by Safonova et al. (2007). They thought that the dehydration of silica inside SDV was crucial for forming a

normal morphology of diatoms. Therefore, the observed accelerated coagulation of silica in the presence of germanic acid could cause the aberrant morphology. We observed that the fine pore structures disappeared and a new slit structure was formed with germanium insertion (Figure 13). Since the amount of germanium incorporated into the diatom *N. frustulum* was different (Table 4), a different level of distortion of the valve morphologies could be expected.

#### **Effect of germanium insertion on PL properties of frustules of diatom *N. frustulum*.**

Germanium has gained a lot of interest in the past 15 years for making optoelectronic materials. Among them, Ge-doped silica is the most popular one, which is generally prepared by Ge ion implantation and rf-magnetron co-sputtering techniques. Three different visible room temperature PL in red (1.8 eV), orange (2.2 - 2.3 eV), and violet-blue (3.1 eV) have been reported. In particular, the origin of red and orange PL of germanium doped silica was usually ascribed to Ge-related defects (e.g. non-bridging oxygen hole centers NBOHC) (Chen et al., 1996; Min et al., 1996; Ma et al., 1998; Wu et al., 1999; Choi et al., 2000; Fitting et al., 2001; Ma et al., 2001; Ye et al., 2002) or radiative recombination of excitons confined in Ge nanocrystals (Maeda et al., 1991; Takagahara and Takeda, 1992; Nogami and Abe, 1994; Zhang et al., 1998).

The violet-blue PL was said to be associated with radiative defects of Ge and GeO<sub>2</sub> nanocrystals such as ≡Ge-Si≡ defect centers and GeO color centers (Gao et al., 1997; Rebohle et al., 1997; Zhang et al., 1998; Shen et al., 2000). Violet-blue PL (3.1eV) of crystal GeO<sub>2</sub> was reported and related to oxygen deficient centers (ODC) (Zacharias and Fauchet, 1997; Zacharias and Fauchet, 1998; Fitting et al., 2001). Recently Zyubin et al. (2007) did theoretical calculations on germanium oxide. They found that the single and double oxygen vacancy (OV and DOV) defects in quartz-like germanium oxide were responsible for PL peak at 3.1 eV (OV) and at 2.6 eV (DOV), respectively. Other germanium related materials, e.g.,

chemically etched germanium, also showed PL associated with GeO defects in visible range (Sendova-Vassileva et al., 1994; Wu et al., 1999; Kartopu et al., 2003).

To the best of our knowledge, PL of germanium oxide doped biogenic silica has not been explored. Based on previous studies with Ge-doped silica, one could speculate that germanium oxide doped biogenic silica would have visible PL associated with germanium related defects. If GeO<sub>2</sub> contributed to the blue PL (460 nm), then the intensity would be expected to increase. This is because the GeO<sub>2</sub> induced PL would superimpose with the PL emission from the surface silanol (Si-OH) groups associated with frustules nanostructure (Qin et al, 2008). However, our results showed that PL intensity decreased and emission wavelength was blue shifted with germanium oxide incorporation. Also, the PL was fully quenched when the germanium inserted biosilica was annealed at 800 °C for one hour in air, at which temperature silanol group was known to disappear (He et al., 2004). The silanol group existence and disappearance were verified by using FTIR (Figure 14). This PL quench further indicated that germanium oxide was unlikely to be responsible for the observed PL change.

The question now arises: what is the reason for PL change? As mentioned before, silicon content per cell was increased due to germanium insertion. The heavier silicification might lead to decreased surface area, which, in turn, decreases the number of attached silanol groups, and therefore decreases the PL intensity. Butcher et al. (2005) observed a weaker PL from field-collected diatoms compared with fresh diatom samples. They suggested that it could be the reason that the diatoms collected from field were more heavily silicified. Although the silicon content change might explain the PL intensity change, it failed to explain the PL wavelength blue shift, which might indicate that there existed a different reason for the PL change. It is worth mentioning that germanium insertion altered the morphology of diatom frustules. Our previous study showed that the PL intensity

was closely related to the pore structure, which could be distorted due to germanium insertion (Figure 13). This might explain why PL intensity was decreased with more germanium incorporation. Furthermore, the closer spacing between nanoparticles due to pore alternation would increase hydrogen bonding interactions between neighboring surface silanol groups, which, in turn, shifts the peak PL towards a higher energy (Anedda et al., 2003; Carbonaro et al., 2005). This could be the underlying mechanism for the observed PL blue shift (Figure 11).

## **Conclusions and Recommendations**

### **Conclusions**

In conclusion, we successfully doped different amount of germanium into diatom frustules. As Ge to Si molar ratio was increased to 0.14, both cell growth and Ge uptake was inhibited due to biogenic Ge addition. As initial Ge concentration in stage II increased, the Ge incorporation into the frustule biosilica reached a maximum amount of  $1.20 \pm 0.22$  wt% in biosilica. TEM analysis showed that the Ge incorporation altered the pore structure of the diatom frustules into a slit-like structure. It was also found that increasing Ge in diatom biosilica decreased photoluminescence (PL) emission peak intensity. Finally, the possible origins of photoluminescence emission in diatom biosilica were proposed.

### **Recommendations**

Since the doped Ge in biosilica could be a mix of Ge in forms of  $\text{GeO}_2$  separated from  $\text{SiO}_2$  phase, or Ge and Si composite like  $\text{Ge}_x\text{Si}_y\text{O}_2$ , or  $\text{SiO}_2\text{-GeO}_2$  alloy metal oxides. It will be better to add some proteins into the culture medium to control the Ge doping in a defined form. The Ge incorporated in diatom biosilica seemed not play a significant role in the PL emission of Ge-doped biosilica. It is probably because either the amount of Ge doped into biosilica was too small to change the intrinsic electronic properties of the biosilica, or the Ge existed in biosilica was amorphous. Since cell growth will be inhibited as more Ge was added using our current method, the Ge incorporation was limited. To increase the amount of Ge incorporated in diatom biosilica, some other proteins need to be add into the medium to specifically transport soluble Ge into the cell and built into silica shell. The Ge-doped biosilica could also be annealed under different conditions to crystallize the Ge or  $\text{GeO}_2$  particles. In that way, Ge incorporation should contribute to the visible PL emission.

## References

1. Anedda, A.; Carbonaro, C. M.; Clemente, F.; Corpino, R.; Grandi, S.; Mustarelli, P.; and Magistris, A. (2003) OH-dependence of ultraviolet emission in porous silica. *Journal of Non-Crystalline Solids*, 322:68–72.
2. Anedda, A.; Carbonaro, C. M.; Clemente, F.; Corpino, R.; and Ricci, P. C. (2003) Mesoporous silica photoluminescence properties in samples with different pore size. *Materials Science and Engineering*, 23:1073–1076.
3. Ardyanian, M.; Rinnert, H.; Devaux, X.; Vergnat, M. (2006) Structure and photoluminescence properties of evaporated GeO<sub>x</sub> thin films. *Applied Physics Letters*, 89(1), 011902/1-011902/3.
4. Azam, F.; Hemmingsen, B.B.; and Volcani, B.E. (1973) Germanium incorporation into the silica of diatom cell walls. *Arch. Mikrobiol.*, 92, 11-20.
5. Azam, F. and Volcani, B.E. (1974) Role of silicon in diatom metabolism. VI. Active transport of Germanic acid in the heterotrophic diatom *Nitzschia alba*. *Arch. Microbiol.*, 101, 1-8.
6. Brus, L.E. (1983). A simple model for the ionization potential, electron affinity, and aqueous redox potentials of small semiconductor crystallites. *J. Chem. Phys.*, 79 (11), 5566-5571.
7. Butcher, K. S. A.; Fefrries, J. M.; Philips, M. R.; Wintrebert-Fouquet, M.; Jong Wah, J. W.; Jovanovic, N.; Vyverman, W.; and Chepurinov, V. A. (2005) A luminescence study of porous diatoms. *Materials Science and Engineering, C* 25:658–663.
8. Carbonaro, M. C.; Clemente, F.; Corpino, R.; Ricci, C. P.; and Anedda, A. (2005) Ultraviolet photoluminescence of silanol species in mesoporous silica. *Journal of Physical Chemistry B*, 109:14441–14444.
9. Chen, J.H.; Pang, D.; Wickboldt, P.; Cheong, H.M.; and Paul, W. (1996) Visible room-temperature photoluminescence from oxidized germanium. *Journal of Non-Crystalline Solids*, 198-200, 128-131.
10. Chippino, M.L.; Azam, F.; and Volcani, B.E. (1977) Effect of Germanic acid on developing cell walls of diatoms. *Protoplasma*, 93, 191-204.

11. Choi, W.K.; Ho, Y.W.; Ng, S.P.; and Ng, V. (2001) Microstructural and photoluminescence studies of germanium nanocrystals in amorphous silicon oxide films. *Journal of Applied Physics*, 89 (4), 2168-2172.
12. Choi, W.K.; Thio, H.H.; Ng, S.P.; and Ng, V. (2000) Synthesizing germanium nanocrystals in amorphous silicon oxide by Rapid Thermal Annealing. *Philosophical Magazine B*, 80 (4), 729-739.
13. Clauquin, P.; Martin-Jezequel, V.; Kromkamp, J.C.; Veldhuis, M.J.W.; and Kraay, G.W. (2002) Uncoupling of silicon compared with carbon and nitrogen metabolisms and the role of the cell cycle in continuous cultures of *Thalassiosira Pseudonana* (Bacillariophyceae) under light, nitrogen, and phosphorus control. *J. Phycol.*, 38, 922-930.
14. Dowd, A. R.; Liewllyn, D.; Gerald, J.D.F.; and Elliman, T.G. (2001) The size distribution of Ge nanocrystals in implanted and annealed silica. *Mater. Res. Soc. Symp. Proc.* 650, R3.39/1-R3.39/6.
15. Fanning, K.A. and Pilson, M.E.Q. (1973) On the spectrophotometric determination of dissolved silica in natural waters. *Anal. Chem.*, 45: 136.
16. Fitting, H.J.; Barfels, T.; Trukhin, A.N.; and Schmidt, B. (2001) Cathodoluminescence of crystalline and amorphous SiO<sub>2</sub> and GeO<sub>2</sub>. *Journal of Non-Crystalline Solids*, 279, 51-59.
17. Gao, T.; Bao, X.M.; Yan, F.; and Tong, S. (1997) Photoluminescence from Ge<sup>+</sup>-implanted SiO<sub>2</sub> films on Si substrate and its mechanism. *Physics Letters A*, 232, 321-325.
18. Gelabert, A.; Pokrovsky, O. S.; Schott, J.; Boudou, A.; Feurtet-Mazel, A.; Mielczarski, J.; Mielczarski, E.; Mesmer-Dudons, N.; Spalla, O. (2004) Study of diatoms/aqueous solution interface. I. Acid-base equilibria and spectroscopic observation of freshwater and marine species. *Geochimica et Cosmochimica Acta*, 68(20), 4039-4058.
19. Gendron-Badou, A.; Coradin, T.; Maquet, J.; Frohlich, F.; Livage, J. (2003) Spectroscopic characterization of biogenic silica. *Journal of Non-Crystalline Solids*, 316(2, 3), 331-337.
20. He, N.; Ge, S. X.; Yang, C.; Cao, J. M.; and Gu, M. (2004) Effect of calcinations and synthetic conditions on the photoluminescence of hexagonal mesoporous materials. *Materials Letters*, 58:3304–3307.

21. Hildebrand, M. and Dahlin, K. (2000) Nitrate transporter genes from the diatom *Cylindrotheca Fusiformis* (Bacillariophyceae): mRNA levels controlled by nitrogen source and by the cell cycle. *J. Phycol.*, 36, 702-713.
22. Jeffryes, C.; Gutu, T.; Jun, J.; Rorrer, G. L. (2008) Two-stage photobioreactor process for the metabolic insertion of nanostructured germanium into the silica microstructure of the diatom *Pinnularia sp.* *Materials Science & Engineering, C: Biomimetic and Supramolecular Systems*, 28(1), 107-118.
23. Kanemitsu, Y.; Uto, H.; and Masumoto, Y. (1992) On the origin of visible photoluminescence in nanometer-size Ge crystallites. *Appl. Phys. Lett.*, 61 (18), 2187-2189.
24. Kartopu, G.; Bayliss, S.C.; Karavanskii, V.A.; Curry, R.J.; Turan, R.; and Sapelkin, A.V. (2003) On the origin of the 2.2-2.3 eV photoluminescence from chemically etched germanium. *Journal of Luminescence*, 101, 275-283.
25. Khraisheh, M. A. M.; Al-Ghouti, M. A.; Allen, S. J.; Ahmad, M. N. (2005) Effect of OH and silanol groups in the removal of dyes from aqueous solution using diatomite. *Water Research*, 39(5), 922-932.
26. Lewin, J. (1966) Silicon metabolism in diatoms. V. Germanium dioxide, a specific inhibitor of diatom growth. *Phycologia*, 6 (1), 1-12.
27. Li, J.; Wu, X.L.; Yang, Y.M.; Yang, X.; and Bao, X.M. (2003) Strong violet-blue photoluminescence from Ge oxide films by magnetron sputtering. *Physics Letters A*, 314, 299-303.
28. Liu, S.; Jeffryes, C.; Rorrer, G. L.; Chang, C.; Jiao, J.; Gutu, T. (2005) Blue luminescent biogenic silicon-germanium oxide nanocomposites. *Materials Research Society Symposium Proceedings*, 873E, K1.4.
29. Liu, X.; Calata, N. J.; Liang, H.; Shi, W.; Lin, X.; Lin, K.; and Qin, G. G. (2000) Photoluminescence and photoluminescence excitation mechanisms for porous silicon and silicon oxynitride. In *Materials society symposium proceedings*, volume 588, pages 141-146.
30. Luke, C.L. and Campbell, M.E. (1956) Photometric determination of germanium with phenylfluorone. In *Standard Methods for the*

Examination of Water and Wastewater 18<sup>th</sup> Ed (1992) pp. 1273-1276. American Public Health Association. Washington, D.C.

31. Ma, S.Y.; Ma, Z.C.; Zong, W.H.; Han, H.X.; Wang, Z.P.; Li, G.H.; Qin, G.; and Qin, G.G. (1998) Photoluminescence from nanometer Ge particle embedded Si oxide films. *Journal of Applied Physics*, 84 (1), 559-563.
32. Ma, S.Y.; Qin, G.G.; and Wang, Y.Y. (2001) A study on photoluminescence from Si-rich silicon oxide films and Ge-containing silicon oxide films. *Materials Letters*, 49, 63-68.
33. Maeda, Y.; Tsukamoto, N.; and Yazawa, Y. (1991) Visible photoluminescence of Ge microcrystals embedded in SiO<sub>2</sub> glassy matrices. *Applied Physics Letters*, 59 (24), 3168-3170.
34. Martin-Jezequel, V.; Hildebrand, M.; and Brezinski, M.A. (2000) Silicon metabolism in diatoms: implications for growth. *J. Phycol.*, 36, 821-840.
35. Mehard, C.W.; Sullivan, C.W.; Azam, F.; and Volcani, B.E. (1974) Role of silicon in diatom metabolism. IV. Subcellular localization of silicon and germanium in *Nitzschia alba* and *Cylindrotheca fusiformis*. *Physiol. Plant.*, 30: 265-272.
36. Min, K.S.; Shcheglov, K.V.; Yang, C.M.; Atawter, H.A.; Brongersma, M.L.; and Polman, A. (1996) The role of quantum-confined excitons vs. defects in the visible luminescence of SiO<sub>2</sub> films containing Ge nanocrystals. *Applied Physics Letters*, 68, 2511.
37. Mitchison, J.M. (1971). *The biology of the cell*. Cambridge University Press, Cambridge, pp313.
38. Ng, V.; Ng, S.P.; Thio, H.H.; Choi, W.K.; Wee, A.T.S.; and Jie, Y.X. (2000) Luminescence and X-ray diffraction studies of Ge nanocrystals in amorphous silicon oxide. *Materials Science and Engineering A*, 286, 161-164.
39. Nogami, M. and Abe, Y. (1994) Sol-gel method for synthesizing visible photoluminescent nanosized Ge-crystal-doped silica glasses. *Applied Physics Letters*, 65 (20), 2545-2547.

40. Oku, T.; Nakayama, T.; Kuno, M.; Nozue, Y.; Wallenberg, L. R.; Niihara, K.; and Suganuma, K. (2000) Formation and photoluminescence of Ge and Si nanoparticles encapsulated in oxide layers. *Materials Science and Engineering B*, 74, 242-247.
41. Olson, R.J.; Vaultot, D.; and Chisholm, S.W. (1986) Effects of environmental stresses on the cell cycle of two marine phytoplankton species. *Plant Physiol.*, 80, 918-925.
42. Ortiz, M.I.; Rodríguez, A.; Sangrador, J.; Rodríguez, T.; Avella, M.; Jiménez, J.; and Ballesteros, C. (2005) Luminescent nanostructures based on Ge nanoparticles embedded in an oxide matrix. *Nanotechnology*, 16, S197-S201.
43. Qin, T.; Gutu, T.; Jiao, J.; Chang, C. H.; and Rorrer, L. G. (2008) Photoluminescence of Silica Nanostructures from Bioreactor Culture of Marine Diatom *Nitzschia frustulum*. *Journal of Nanoscience and Nanotechnology*, 8, 2392-2398.
44. Rebohle, L.; Borany, J.V.; Yankov, R.A.; Skorupa, W.; Tyschenko, I.E.; Fröb, H.; and Leo, K. (1997) Strong blue and violet photoluminescence and electroluminescence from germanium-implanted and silicon-implanted silicon-dioxide layers. *Appl. Phys. Lett.*, 71 (19), 2809-2811.
45. Safonova, T.A.; Annenkov, V.V.; Chebykin, E.P.; Danilovtseva, E.N.; Likhoshway, Y.V.; and Grachev, M.A. (2007) Aberration of morphogenesis of siliceous frustule elements of the diatom *Synedra acus* in the presence of Germanic acid. *Biochemistry (Moscow)*, 72 (11), 1261-1269.
46. Schmidt, M.; Botz, R.; Rickert, D.; Bohrmann, G.; Hall, S. R.; and Mann, S. (2001) Oxygen isotopes of marine diatoms and relations to opal-A maturation. *Geochimica et Cosmochimica Acta*. 65(2), 201-211.
47. Sendova-Vassileva, M.; Tzenov, N.; Dimoav-Malinovska, D.; Rosenbauer, M.; Stutzmann, M.; and Josepovits, K.V. (1994) Structural and luminescence studies of stain-etched and electrochemically etched germanium. *Thin Solid Films*, 225, 282-285.
48. Shen, J.K.; Wu, X.L.; Yuan, R.K.; Tang, N.; Zou, j.p.; Mei, Y.F.; Tan, C.; Bao, X.M.; and Siu, G.G. (2000) Enhanced ultraviolet photoluminescence

from SiO<sub>2</sub>/Ge:SiO<sub>2</sub>/SiO<sub>2</sub> sandwiched structure. *Applied Physics Letters*, 77 (20), 3134-3136.

49. Sullivan, C.W. (1977) Diatom mineralization of silicic acid. II. Regulation of Si(OH)<sub>4</sub> transport rates during the cell cycle of *Navicula Pelliculosa*. *J. Phycol.*, 13, 86-91.
50. Sumper, M. and Brunner, E. (2006) Learning from Diatoms: Nature's Tools for the Production of Nanostructured Silica. *Advanced Functional Materials*, 16 (1), 17-26.
51. Sun, Q.; Vrieling, E. G.; Santen, van R. A.; Sommerdijk, N.A.J.M. (2004) Bioinspired synthesis of mesoporous silicas. *Current Opinion in Solid State and Materials Science*, 8, 111-120.
52. Takagahara, T. and Takeda, K. (1992) Theory of the quantum confinement effect on excitons in quantum dots of indirect-gap materials. *Phys. Rev. B*, 46, 15578.
53. Wu, X.L.; Gu, Y.; Siu, G.G.; Fu, E.; Tang, N.; Gao, T.; and Bao, X.M. (1999) Orange-green emission from porous Si coated with Ge films: The role of Ge-related defects. *Journal of Applied Physics*, 86 (1), 707-709.
54. Yang, D. Q.; Ethier, V.; Sacher, E.; and Meunier, M. (2005). Photoluminescence of highly porous nanostructured Si-based thin films deposited by pulsed laser ablation. *Journal of Applied Physics*, 98:024310/1-024310/8.
55. Ye, C.N.; Wu, X.M.; Tang, N.Y.; Zhuge, L.J.; Yao, W.G.; Chen, J.; Dong, Y.M.; and Yu, Y.H. (2002) Origin of photoluminescence peaks in Ge-SiO<sub>2</sub> thin films. *Science and Technology of Advanced Materials*, 3, 257-260.
56. Zacharias, M. and Fauchet, P.M. (1997) Blue luminescence in films containing Ge and GeO<sub>2</sub> nanocrystals: The role of defects. *Applied Physics Letters* 71 (3), 380-382.
57. Zacharias, M. and Fauchet, P.M. (1998) Light emission from Ge and GeO<sub>2</sub> nanocrystals. *Journal of Non-Crystalline Solids*, 227-230, 1058-1962.
58. Zhang, J.Y.; Bao, X.M.; Ye, Y.H.; and Tan, X.L. (1998) Blue and red photoluminescence from Ge<sup>+</sup> implanted SiO<sub>2</sub> films and its multiple mechanism. *Applied Physics Letters*, 73 (13), 1790-1792.

59. Zhao, Y.; Li, D.; and Yang, D. (2005) Effect of post-treatment processes on the photoluminescence of porous silicon. *Physica B*, 364:180–185.
60. Zhu, M.; Han, Y.; Wehrspohn, R. B.; Godet, C.; Etemadi, R.; and Ballutaud, D. (1998) The origin of visible photoluminescence from silicon oxide thin films prepared by dual-plasma chemical vapor deposition. *Journal of Applied Physics*, 83 (10), 5386-5393.
61. Zhu, J.G.; White, C.W.; Budai, J.D.; Withrow, S.P.; and Chen, Y. (1995) Growth of Ge, Si, and SiGe nanocrystals in SiO<sub>2</sub> matrixes. *J. Appl. Phys.*, 78 (7), 4386-9.
62. Zyubin, A.S.; Mebel, A.M.; and Lin, S.H. (2007) Optical properties of oxygen vacancies in germanium oxides: quantum chemical modeling of photoexcitation and photoluminescence. *J. Phys. Chem. A*, 111, 9479-9485.
63. Zyubin, A.S.; Mebel, A.M.; and Lin, S.H. (2005) Photoluminescence of oxygen-containing surface defects in germanium oxides: A theoretical study. *The Journal of Chemical Physics*, 123, 044701/1-044701/14.

## **Appendices**

## Appendix A Calculations

### *Specific growth rate calculation*

Materials balance on cell number and silicon substrate in the cell culture is

$$V \times \mu \times X_N \times \Delta t = V \times X_{N,(t+\Delta t)} - V \times X_{N,t} \quad (1)$$

Where  $V$  is the culture volume (L),  $X_N$  is the average cell number density (cells/mL) at the time interval  $\Delta t$  (hr),  $\mu$  is the specific growth rate ( $\text{h}^{-1}$ ). The resulting differential equation is

$$\frac{dX_N}{dt} = \mu \times X_N, t = 0, X_N = X_{N,0} \quad (2)$$

The specific growth rate ( $\mu$ ) was calculated by using Monod model

$$\mu = \frac{\mu_{\max} \times C_{Si}}{K_{\mu} + C_{Si}} \quad (3)$$

Where  $K_{\mu}$  is the half saturation constant for silicon (mmol Si/L) that corresponds to the silicon concentration when the specific growth rate is half the maximum  $\mu_{\max}$  ( $\text{h}^{-1}$ )

Literature values for  $K_{\mu}$  for diatoms are in the range of 0.02  $\mu\text{M}$  to 8.6  $\mu\text{M}$  (Martin-Jezequel et al, 2000), which is much less than  $C_{Si}$ , equation (3) is approximated by

$$\mu = \mu_{\max}, \text{ when } K_{\mu} \ll C_{Si} \quad (4)$$

And equation (2) is approximated by

$$\frac{dX_N}{dt} = \mu_{\max} \times X_N, t = 0, X_N = X_{N,0} \quad (5)$$

And the  $X_N$  can be solved as

$$X_N = X_{N,0} e^{\mu_{\max} t} \quad (6)$$

And the specific growth rate can be determined from the least squares slope of the natural log of cell number density versus time data.

The cell doubling time can be estimated from

$$\mu_{\max} = \ln\left(\frac{X_N}{X_{N,0}}\right) / t = \frac{\ln 2}{t}$$

$$t = \frac{\ln 2}{\mu_{\max}} \quad (7)$$

An example using least squares slope to find specific growth rate  $\mu$  was shown in Figure 1. The specific growth rate  $\mu$  was found to be  $0.0213 \text{ hr}^{-1}$  in this example.

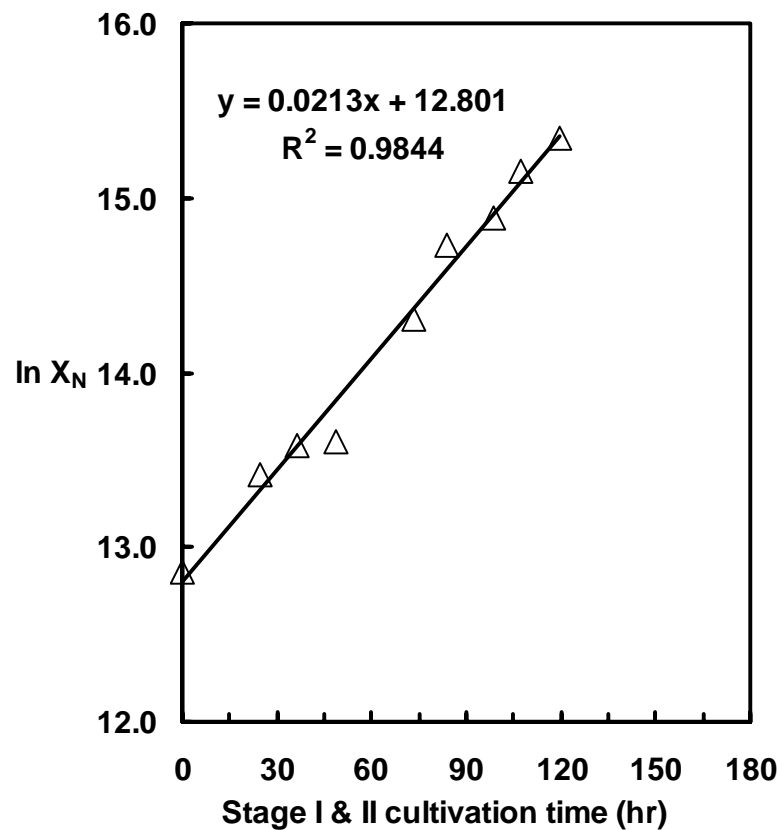


**Figure A.1** The natural log of cell number density versus time for experiment Ni-BC-32, and the specific growth rate was found to be  $0.0213 \text{ h}^{-1}$

*Germanium and silicon uptake rate calculation*

Materials balance on cell number and silicon substrate in the cell culture is

$$V \times R_{Si} \times \Delta t = V \times C_{Si,t} - V \times C_{Si,(t+\Delta t)} \quad (8a)$$

$$V \times R_{Ge} \times \Delta t = V \times C_{Ge,t} - V \times C_{Ge,(t+\Delta t)} \quad (8b)$$

Where  $V$  is the culture volume (L),  $C_{Si,t}$  is the silicon concentration in liquid phase (mM) at the time  $t$  (hr),  $C_{Ge,t}$  is the germanium concentration in liquid phase ( $\mu\text{M}$ ) at the time  $t$  (hr),  $R_{Si}$  is the silicon uptake rate ( $\text{mM Si h}^{-1}$ ),  $R_{Ge}$  is the germanium uptake rate ( $\mu\text{M Ge h}^{-1}$ ), and  $\Delta t$  is the time interval. The resulting differential equations are

$$\frac{dC_{Si}}{dt} = R_{Si}, t = 0, C_{Si} = C_{Si,0} \quad (9a)$$

$$\frac{dC_{Ge}}{dt} = R_{Ge}, t = 0, C_{Ge} = C_{Ge,0} \quad (9b)$$

The germanium and silicon uptake rates are defined by Michaelis-Menten kinetics as

$$R_{Si} = -X_N \frac{R_{Si,\max} \times C_{Si}}{K_{Si} + C_{Si}} \quad (10a)$$

$$R_{Ge} = -X_N \frac{R_{Ge,\max} \times C_{Ge}}{K_{Ge} + C_{Ge}} \quad (10b)$$

Where  $K_{Si}$  and  $K_{Ge}$  are the Michaelis-Menten half saturation constants for silicon (mmol Si/L) and germanium ( $\mu\text{M}$ ) that corresponds to the silicon and germanium concentration when the uptake rate is half the maximum  $R_{Si,\max}$  and  $R_{Ge,\max}$

At short time uptake, equation 10a and 10b can be approximated as

$$R_{Si} = -X_N \frac{R_{Si,\max} \times C_{Si}}{K_{Si}} \quad (11a)$$

$$R_{Ge} = -X_N \times \frac{R_{Ge,max} \times C_{Ge}}{K_{Ge}} \quad (11b)$$

And equation 9a and 9b are approximated by

$$\frac{dC_{Si}}{dt} = -X_N \frac{R_{Si,max} \times C_{Si}}{K_{Si}}, t = 0, C_{Si} = C_{Si,0} \quad (12a)$$

$$\frac{dC_{Ge}}{dt} = -X_N \frac{R_{Ge,max} \times C_{Ge}}{K_{Ge}}, t = 0, C_{Ge} = C_{Ge,0} \quad (12b)$$

The solutions of equation 12a and 12b are

$$\ln\left(\frac{C_{Si}}{C_{Si,0}}\right) = -X_N k'_{Si} t, k'_{Si} = \frac{R_{Si,max}}{K_{Si}} \quad (13a)$$

$$\ln\left(\frac{C_{Ge}}{C_{Ge,0}}\right) = -X_N k'_{Ge} t, k'_{Ge} = \frac{R_{Ge,max}}{K_{Ge}} \quad (13b)$$

Where  $k'_{Si}$  and  $k'_{Ge}$  are defined as the maximum specific uptake rate constant (mL/cells-hr)

And the silicon and germanium maximum specific uptake rate constant  $k'_{Si}$  and  $k'_{Ge}$  can be determined from the least squares slope of the natural log of silicon and germanium versus time data.

An example using least squares slope to find specific uptake rate constant  $k'_{Si}$  and  $k'_{Ge}$  was shown in Figure

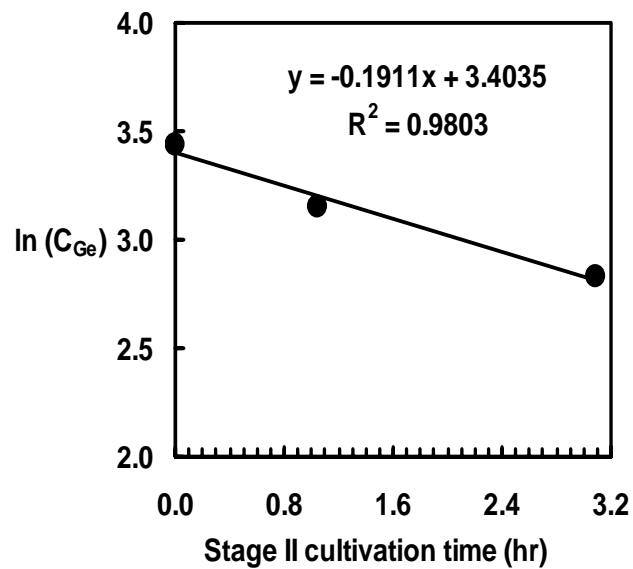
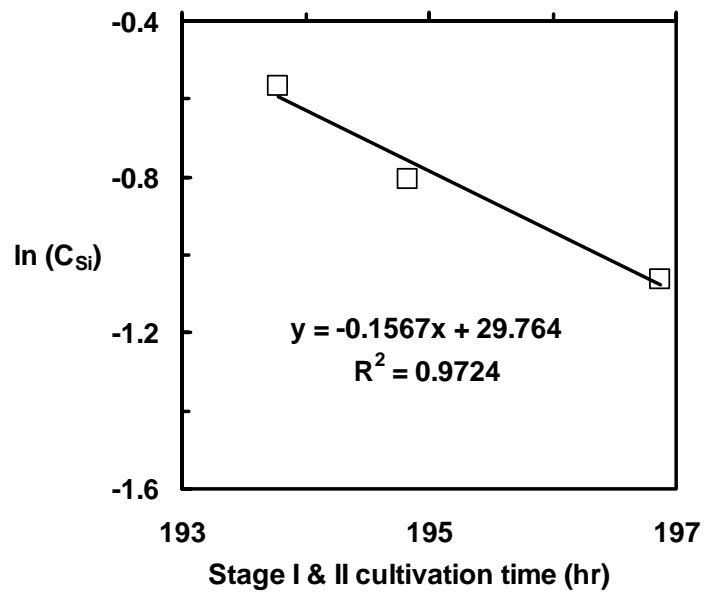


**Figure A.2** The natural log of silicon concentration and germanium concentration versus time for experiment Ni-BC-32, and the maximum specific uptake rate constants were found to be  $0.242 \text{ mL}/10^7 \text{ cells-hr}$  for silicon uptake and  $0.296 \text{ mL}/10^7 \text{ cells-hr}$  for germanium uptake.

*Cell number and cell mass yield coefficient calculation*

The cell number yield coefficient ( $Y_{Xn/Si}$ ) and cell mass yield coefficient ( $Y_{X/Si}$ ) are defined as

$$Y_{Xn/Si} = \frac{X_{N,f} - X_{N,o}}{C_{Si,o} - C_{Si,f}} = \frac{\Delta X_N}{\Delta C_{Si}} \quad (14a)$$

$$Y_{X/Si} = \frac{X_f - X_o}{C_{Si,o} - C_{Si,f}} = \frac{\Delta X}{\Delta C_{Si}} \quad (14b)$$

Where  $X_{N,f}$  and  $X_{N,o}$  are the final and initial cell number density,  $X_f$  and  $X_o$  are the final and initial cell mass density,  $C_{Si,o}$  and  $C_{Si,f}$  are the initial and final silicon concentration in liquid phase.

Example Calculation for Ni-BC-32:

Final cell number density in stage I,  $X_{N,f} = 6.56e6$  cells/mL

Initial cell number density in stage I,  $X_{N,o} = 3.83e5$  cells/mL

Final cell mass density in stage I,  $X_f = 0.212$  gDW/L

Initial cell mass density in stage I,  $X_o = 0.0098$  gDW/L

Final Si concentration in liquid phase in stage I,  $C_{Si,f} = 0.056$  mmolSi/L

Initial Si concentration in liquid phase in stage I,  $C_{Si,o} = 0.744$  mmolSi/L

$$Y_{Xn/Si} = \frac{X_{N,f} - X_{N,o}}{C_{Si,o} - C_{Si,f}} = \frac{(6.56e6 - 3.83e5) \text{ cells / mL}}{(0.774 - 0.056) \text{ mmolSi / L}} \times \frac{1000 \text{ mL}}{1 \text{ L}} = 8.97e9 \text{ cells / mmolSi}$$

$$Y_{X/Si} = \frac{X_f - X_o}{C_{Si,o} - C_{Si,f}} = \frac{(0.212 - 0.0098) \text{ gDW / L}}{(0.774 - 0.056) \text{ mmolSi / L}} = 0.293 \text{ gDW / mmolSi}$$

*Materials balance in stage I and stage II*

Materials balance based on silicon and germanium concentration are

$$Y_{Si/X,I} = \frac{C_{Si,O,I} - C_{Si,f,I}}{X_{f,I} - X_{O,I}} = \frac{\Delta C_{Si,I}}{\Delta X_I} \quad \text{in stage I} \quad (15)$$

$$Y_{Si/X,II} = \frac{C_{Si,O,II} - C_{Si,f,II}}{X_{f,II}} + \frac{X_{O,II}}{X_{f,II}} Y_{Si/X,I} \quad \text{in stage II} \quad (16)$$

$$Y_{Ge/X,II} = \frac{C_{Ge,O,II} - C_{Ge,f,II}}{X_{f,II}} \quad \text{in stage II} \quad (17)$$

Where  $Y_{Si/X,I}$  and  $Y_{Si/X,II}$  are silicon yield coefficients in stage I and stage II,  $Y_{Ge/X,II}$  is germanium yield coefficient in stage II.  $X_{f,I}$  and  $X_{O,I}$  are the final and initial cell mass density in stage I,  $X_{f,II}$  and  $X_{O,II}$  are the final and initial cell mass density in stage II,  $C_{Si,O,I}$  and  $C_{Si,f,I}$  are the initial and final silicon concentration in liquid phase in stage I, and  $C_{Si,O,II}$  and  $C_{Si,f,II}$  are the initial and final silicon concentration in liquid phase in stage II

Example Calculation for Ni-BC-32:

Final cell mass density in stage I,  $X_{f,I} = 0.212$  gDW/L

Initial cell mass density in stage I,  $X_{o,I} = 0.0098$  gDW/L

Final cell mass density in stage II,  $X_{f,II} = 0.265$  gDW/L

Initial cell mass density in stage II,  $X_{oII} = 0.212$  gDW/L

Final Si concentration in liquid phase in stage I,  $C_{Si,f,I} = 0.056$  mmolSi/L

Initial Si concentration in liquid phase in stage I,  $C_{Si,o,I} = 0.744$  mmolSi/L

Final Si concentration in liquid phase in stage II,  $C_{Si,f,II} = 0.111$  mmolSi/L

Initial Si concentration in liquid phase in stage II,  $C_{Si,o,II} = 0.621$  mmolSi/L

Final Ge concentration in liquid phase in stage II,  $C_{Ge,f,II} = -0.54$   $\mu$ molGe/L

Initial Ge concentration in liquid phase in stage II,  $C_{Ge,o,II} = 31.04$   $\mu$ molSi/L

$$Y_{Si/X,I} = \frac{C_{Si,O,I} - C_{Si,f,I}}{X_{f,I} - X_{O,I}} = \frac{(0.744 - 0.056) \text{ mmolSi} / \text{L}}{(0.212 - 0.0098) \text{ gDW} / \text{L}} = 3.403 \text{ mmolSi} / \text{gDW}$$

$$\begin{aligned} Y_{Si/X,II} &= \frac{C_{Si,O,II} - C_{Si,f,II}}{X_{f,II}} + \frac{X_{O,II}}{X_{f,II}} Y_{Si/X,I} \\ &= \frac{(0.621 - 0.111) \text{ mmolSi} / \text{L}}{0.265 \text{ gDW} / \text{L}} + \frac{0.212 \text{ gDW} / \text{L}}{0.265 \text{ gDW} / \text{L}} \times 3.403 \text{ mmolSi} / \text{gDW} = 4.647 \text{ mmolSi} / \text{gDW} \end{aligned}$$

$$Y_{Ge/X,II} = \frac{C_{Ge,O,II} - C_{Ge,f,II}}{X_{f,II}} = \frac{(31.04 - (-0.54)) \mu\text{molGe} / \text{L}}{0.265 \text{ gDW} / \text{L}} = 119.17 \mu\text{molGe} / \text{gDW}$$

Compared to measured  $Y_{Si/X,II} = 2.398 \text{ mmolSi} / \text{gDW}$  and  $Y_{Ge/X,II} = 41.241 \mu\text{molGe} / \text{gDW}$

$$\begin{aligned} \% \text{iloss}(Si) &= \frac{Y_{Si/X,II, \text{calculated}} - Y_{Si/X,II, \text{measured}}}{Y_{Si/X,II, \text{calculated}}} \times 100\% \\ &= \frac{(4.647 - 2.398) \text{ mmolSi} / \text{gDW}}{4.647 \text{ mmolSi} / \text{gDW}} \times 100\% = 48.4\% \end{aligned}$$

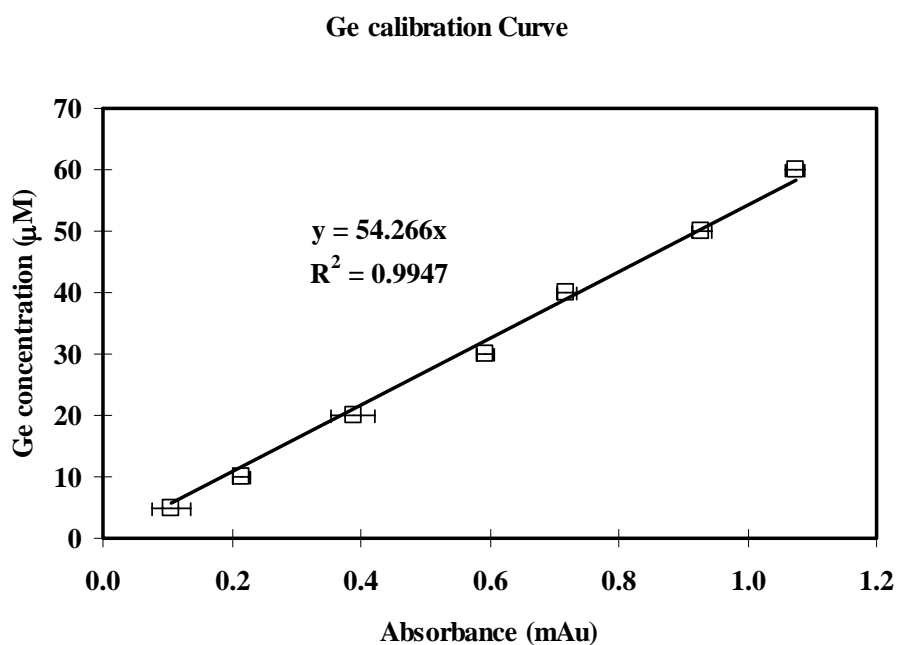
$$\begin{aligned} \% \text{iloss}(Ge) &= \frac{Y_{Ge/X,II, \text{calculated}} - Y_{Ge/X,II, \text{measured}}}{Y_{Ge/X,II, \text{calculated}}} \times 100\% \\ &= \frac{(119.17 - 41.241) \mu\text{molGe} / \text{gDW}}{119.17 \mu\text{molGe} / \text{gDW}} \times 100\% = 65.4\% \end{aligned}$$

## Appendix B Calibrations

*Soluble Ge concentration assay calibration at 525nm*

**Table B.1** Soluble Ge concentration assay calibration data at 525nm (3/2/2006)

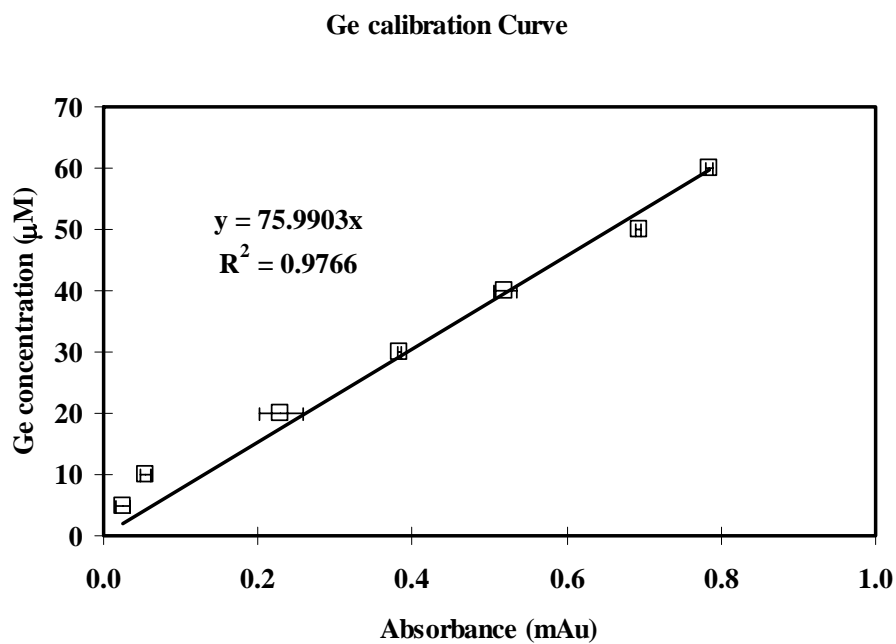
Concentration ( $\mu\text{M}$ )	Abs (mAu)	Average	STDEV
5	0.126	0.105	0.030
5	0.084		
10	0.204	0.215	0.015
10	0.225		
20	0.364	0.388	0.034
20	0.412		
30	0.584	0.594	0.013
30	0.603		
40	0.708	0.719	0.016
40	0.73		
50	0.918	0.929	0.016
50	0.94		
60	1.063	1.074	0.015
60	1.084		



**Figure B.1** Soluble Ge concentration assay calibration curve at 525nm (3/2/2006)

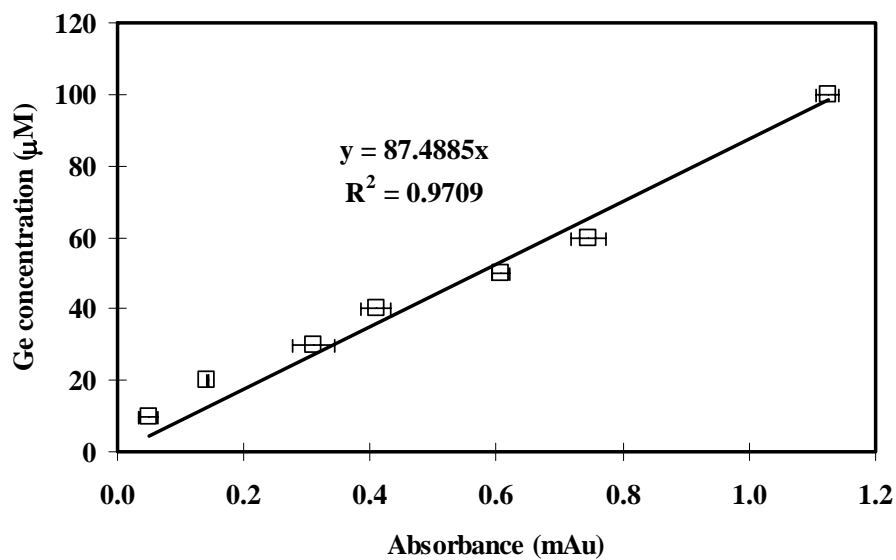
**Table B.2** Soluble Ge concentration assay calibration data at 525nm (5/4/2006)

Concentration ( $\mu\text{M}$ )	Abs (mAu)	Average	STDEV
5	0.018	0.025	0.009
5	0.031		
10	0.049	0.054	0.006
10	0.058		
20	0.25	0.230	0.028
20	0.21		
30	0.384	0.383	0.002
30	0.381		
40	0.53	0.520	0.014
40	0.51		
50	0.691	0.693	0.003
50	0.695		
60	0.782	0.785	0.004
60	0.788		

**Figure B.2** Soluble Ge concentration assay calibration curve at 525nm (5/4/2006)

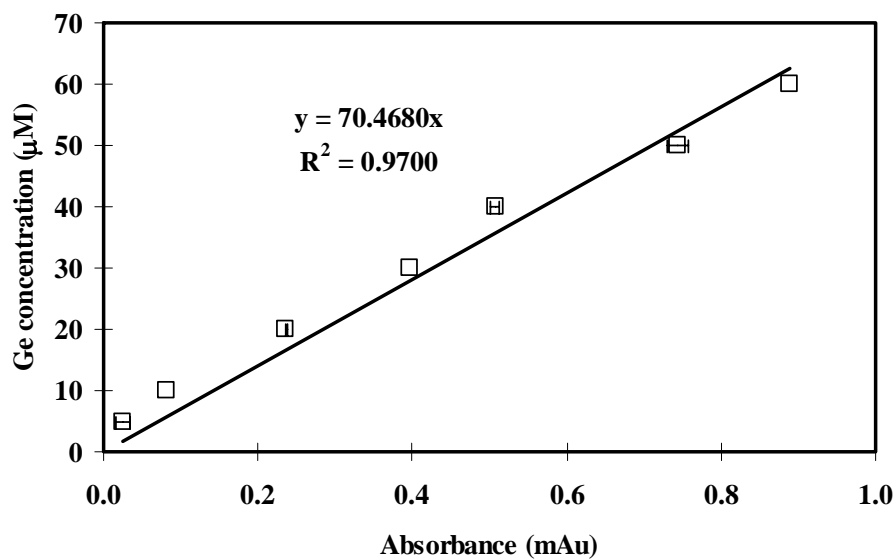
**Table B.3** Soluble Ge concentration assay calibration data at 525nm (8/10/2006)

Concentration ( $\mu\text{M}$ )	Abs (mAu)	Average	STDEV
10	0.059	0.049	0.015
10	0.038		
20	0.141	0.142	0.001
20	0.143		
30	0.334	0.310	0.034
30	0.286		
40	0.393	0.409	0.023
40	0.425		
50	0.616	0.606	0.014
50	0.596		
60	0.727	0.747	0.028
60	0.766		
100	1.112	1.125	0.018
100	1.137		

**Ge calibration Curve****Figure B.3** Soluble Ge concentration assay calibration curve at 525nm (8/10/2006)

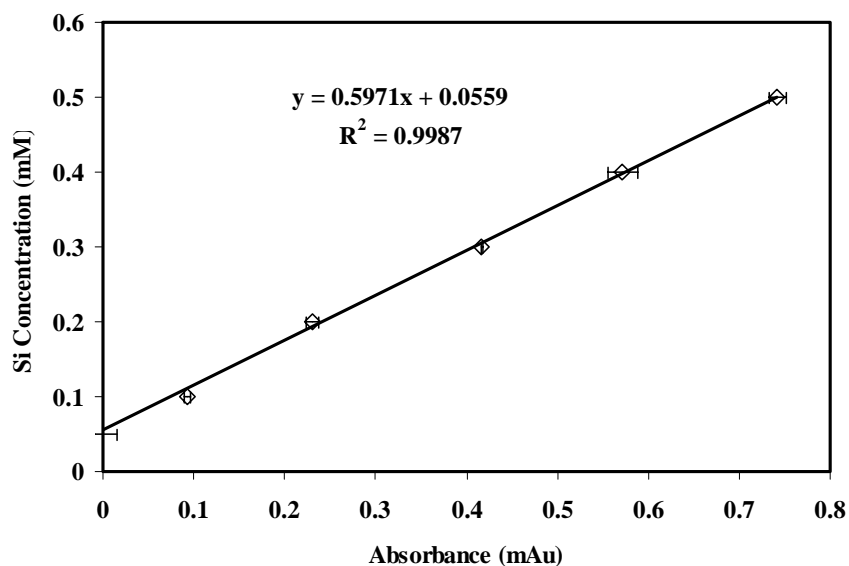
**Table B.4** Soluble Ge concentration assay calibration data at 525nm (11/22/2006)

Concentration ( $\mu\text{M}$ )	Abs (mAu)	Average	STDEV
5	0.031	0.025	0.009
5	0.018		
10	0.081	0.081	
10			
20	0.237	0.237	0.001
20	0.236		
30	0.397	0.397	
30			
40	0.503	0.507	0.006
40	0.511		
50	0.735	0.745	0.013
50	0.754		
60	0.889	0.889	
60			

**Ge calibration Curve****Figure B.4** Soluble Ge concentration assay calibration curve at 525nm (11/22/2006)

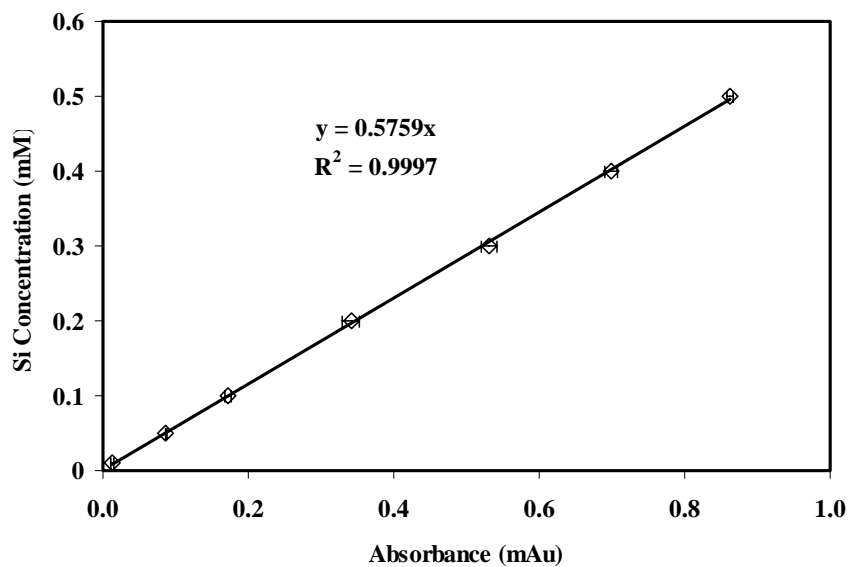
*Soluble Si concentration assay calibration at 410nm***Table B.5** Soluble Si concentration assay calibration data at 410nm (3/2/2006)

Concentration (mM)	Abs (mAu)	Average	STDEV
0.01	-0.095	-0.089	0.009
0.01	-0.082		
0.05	-0.024	-0.008	0.023
0.05	0.008		
0.1	0.091	0.093	0.003
0.1	0.095		
0.2	0.235	0.230	0.007
0.2	0.225		
0.3	0.416	0.417	0.001
0.3	0.417		
0.4	0.561	0.572	0.016
0.4	0.583		
0.5	0.748	0.742	0.009
0.5	0.735		

**Si Assay Calibration Curve****Figure B.5** Soluble Si concentration assay calibration curve at 410nm (3/2/2006)

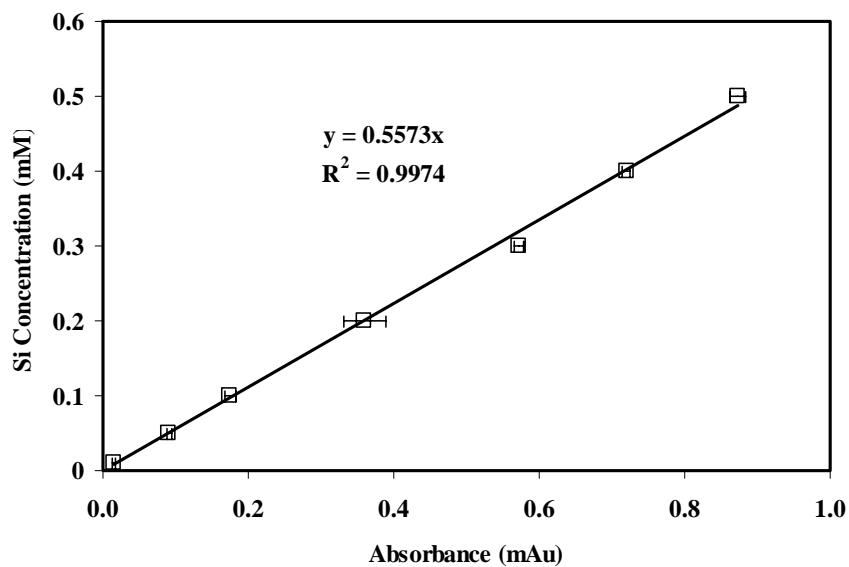
**Table B.6** Soluble Si concentration assay calibration data at 410nm (3/20/2006)

Concentration (mM)	Abs (mAu)	Average	STDEV
0.01	0.015	0.013	0.003
0.01	0.011		
0.05	0.088	0.087	0.001
0.05	0.086		
0.1	0.169	0.172	0.004
0.1	0.175		
0.2	0.332	0.341	0.013
0.2	0.350		
0.3	0.523	0.531	0.011
0.3	0.538		
0.4	0.692	0.698	0.008
0.4	0.704		
0.5	0.865	0.863	0.004
0.5	0.860		

**Si Assay Calibration Curve****Figure B.6** Soluble Si concentration assay calibration curve at 410nm (3/20/2006)

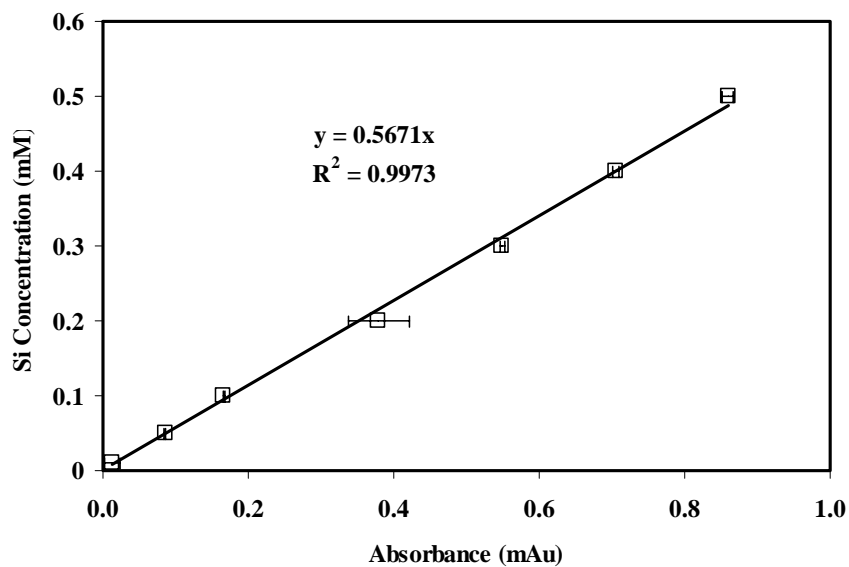
**Table B.7** Soluble Si concentration assay calibration data at 410nm (5/1/2006)

Concentration (mM)	Abs (mAu)	Average	STDEV
0.01	0.014	0.016	0.002
0.01	0.017		
0.05	0.093	0.091	0.003
0.05	0.089		
0.1	0.170	0.175	0.007
0.1	0.180		
0.2	0.339	0.360	0.030
0.2	0.381		
0.3	0.567	0.572	0.007
0.3	0.577		
0.4	0.716	0.720	0.006
0.4	0.724		
0.5	0.866	0.874	0.011
0.5	0.881		

**Si Assay Calibration Curve****Figure B.7** Soluble Si concentration assay calibration curve at 410nm (5/1/2006)

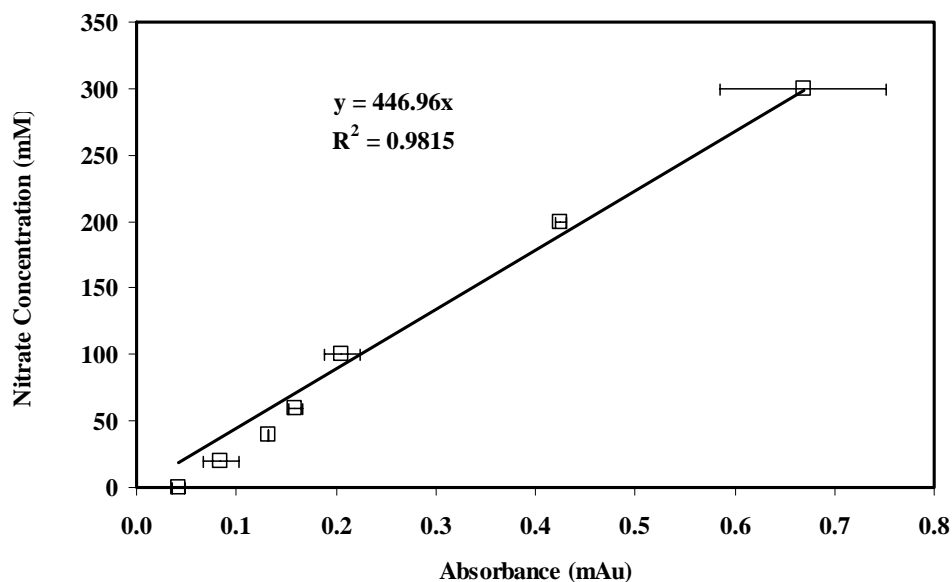
**Table B.8** Soluble Si concentration assay calibration data at 410nm (6/9/2006)

Concentration (mM)	Abs (mAu)	Average	STDEV
0.01	0.006	0.014	0.011
0.01	0.021		
0.05	0.085	0.086	0.001
0.05	0.086		
0.1	0.166	0.167	0.001
0.1	0.167		
0.2	0.349	0.379	0.042
0.2	0.409		
0.3	0.551	0.549	0.003
0.3	0.547		
0.4	0.702	0.706	0.005
0.4	0.709		
0.5	0.854	0.860	0.008
0.5	0.865		

**Si Assay Calibration Curve****Figure B.8** Soluble Si concentration assay calibration curve at 410nm (6/9/2006)

*Soluble Nitrate concentration assay calibration at 530nm***Table B.9** Soluble Nitrate concentration assay calibration data at 530nm

Concentration ( $\mu\text{M}$ )	Abs (mAu)	Average	STDEV
0	0.046	0.042	0.006
0	0.037		
20	0.072	0.085	0.018
20	0.097		
40	0.133	0.133	0.000
40	0.133		
60	0.154	0.159	0.007
60	0.164		
100	0.193	0.206	0.018
100	0.219		
200	0.429	0.426	0.005
200	0.422		
300	0.727	0.669	0.083
300	0.610		

**Nitrate Assay Calibration Curve****Figure B.9** Soluble Nitrate concentration assay calibration curve at 530nm

## Appendix C Photoluminescence Spectra

*PL Spectra of frustules with and without Ge doping along cultivation time*

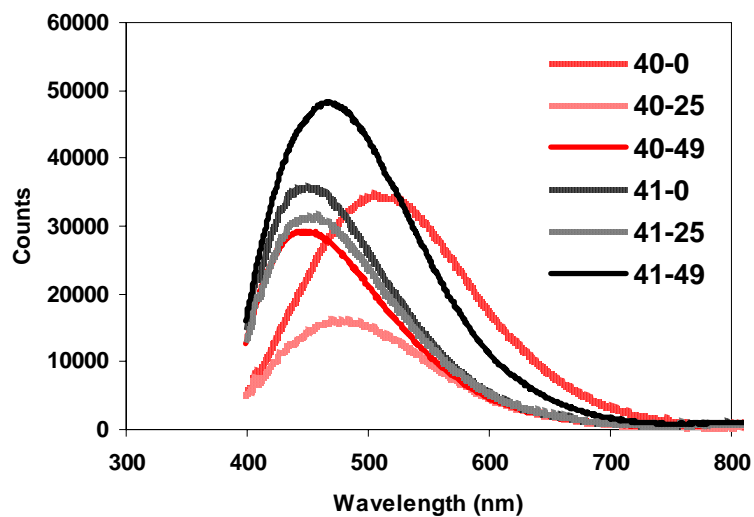


**Figure C.1** Photoluminescence spectra comparison of frustules containing no Ge (40) with that of frustules containing 0.14 wt% Ge (41) along cultivation time

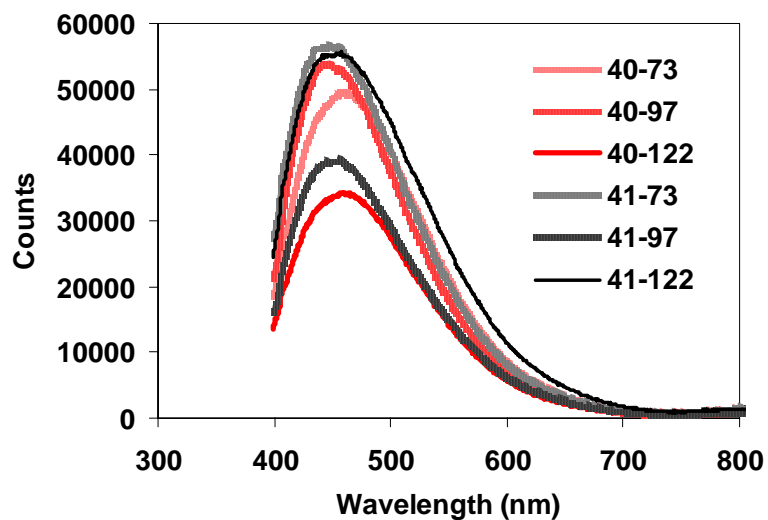


**Figure C.2** Photoluminescence spectra comparison of frustules containing no Ge (40) with that of frustules containing 0.14 wt% Ge (41) along cultivation time

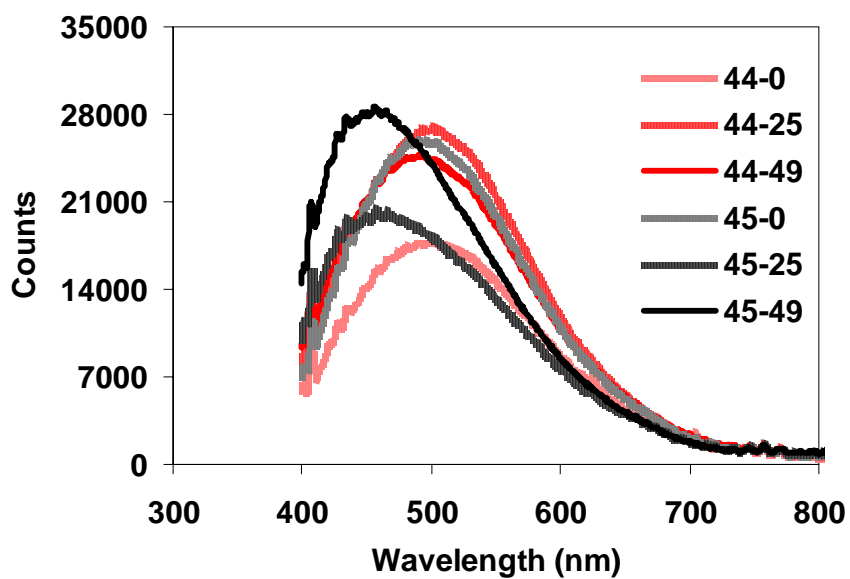


**Figure C.3** Photoluminescence spectra comparison of frustules containing no Ge (44) with that of frustules containing 0.36 wt% Ge (45) along cultivation time

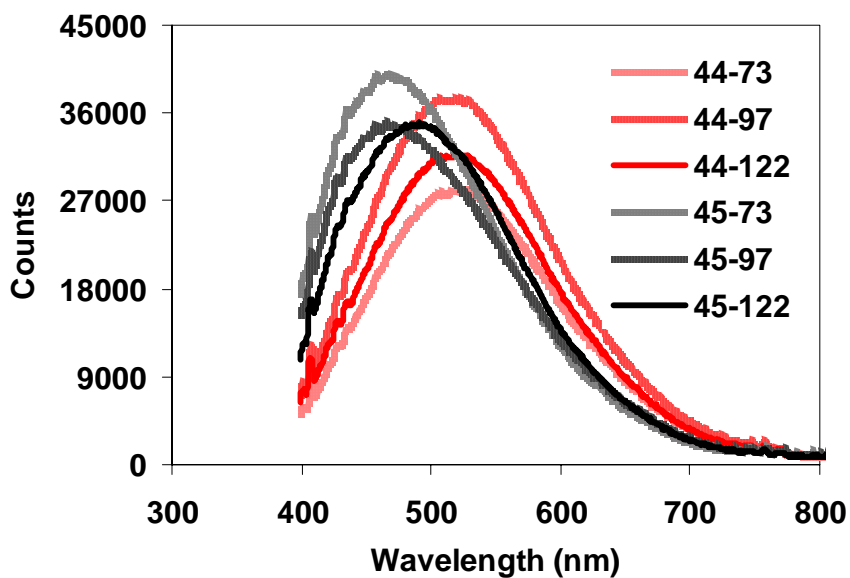


**Figure C.4** Photoluminescence spectra comparison of frustules containing no Ge (44) with that of frustules containing 0.36 wt% Ge (45) along cultivation time

*PL Spectra of frustules with different amount of incorporated Ge*

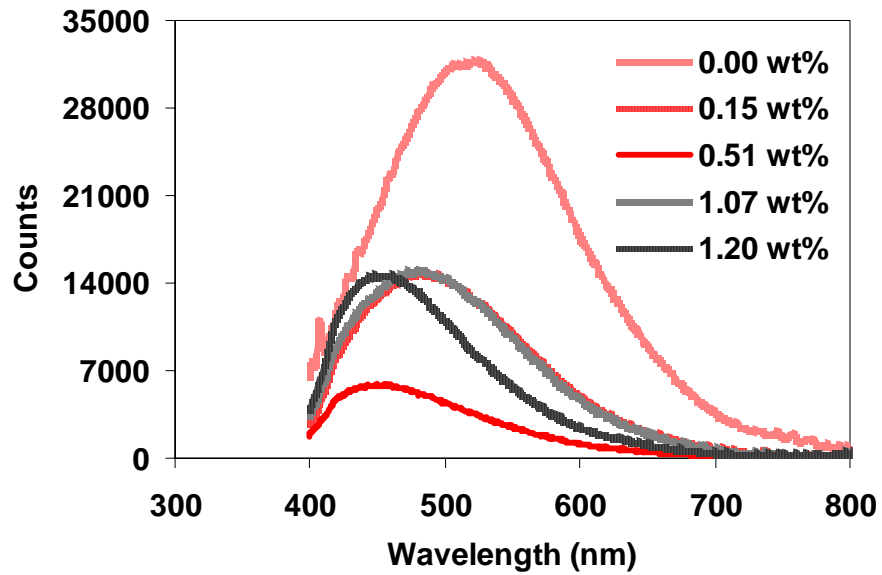


**Figure C.5** Photoluminescence spectra comparison of different Ge-incorporated frustules collected at the end of stage II (120 hours of cultivation)